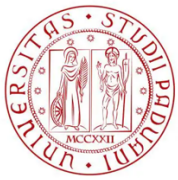

UNIVERSITÀ DEGLI STUDI DI PADOVA

UNIVERSITÀ DEGLI STUDI DI PADOVA

DIPARTIMENTO DI INGEGNERIA INDUSTRIALE

CORSO DI LAUREA MAGISTRALE IN CHEMICAL AND PROCESS ENGINEERING

Tesi di Laurea Magistrale in

Chemical and Process Engineering

Data-driven modeling approach to investigate the tableting properties of three powder blends for pharmaceutical product development

Relatore: Prof. Massimiliano Barolo

Correlatrice: Ing. Paula Barbosa

Laureanda: LINDA GAIANI

ANNO ACCADEMICO 2023-2024

Abstract

The manufacturing process of pharmaceutical tablets involves feeding a powder formulation into a die followed by compaction using rigid punches. The die filling step is part of a larger tableting process which is usually performed using the multiple station rotary press and it has a major impact on the quality, uniformity and mechanical properties of the tablets produced. In this study, the effect of the main compression settings of the rotary press on the final tablet quality is analyzed for three different blends by exploiting multivariate statistical techniques, with a particular focus on weight consistency and uniformity, which are the most important quality parameters in die filling. It results that, while some settings have the same effect on all the considered blends (e.g., feed frame speed in increasing mean weight or overfill in decreasing weight variability), some others affect each blend in different ways. This may be related to the properties of the powder itself, in particular its flowability, which are known to be related to the operating conditions of the rotary press in determining die filling performance. In particular, it has been found that tablets made from more flowable powders are characterized by lower weight variability. The effect of the feed frame on the lubrication state of the blends is also evaluated, as its mechanical action can cause particle friction and over lubrication, resulting in lower tablet strength and slower dissolution. By comparing the data collected on the compactor simulator for both powder samples and samples with known lubrication, it is concluded that the feed frame only has a meaningful effect on powder lubrication above a certain feed frame speed.

This thesis is the result of a collaboration between the Process Engineering & Analytics team of GSK (Stevenage; UK) and the CAPE-Lab group at the University of Padova.

Table of Contents

Introduction

Powder compaction is widely used in the manufacture of tablets, the most common solid dosage form in the pharmaceutical industry. It involves placing the powder in a die (known as the die-fill stage) and then compressing it under high pressure to form the tablet. This stage is part of a larger tableting process, usually carried out in multi-station rotary presses, to produce high volumes of uniform weight, shape and size tablets. In particular, the efficiency in die filling has been found to be fundamental to achieve consistent weight, hardness and dosage of active pharmaceutical ingredient (API) in each tablet (Zakhvatayeva, 2018). Several studies have demonstrated how die filling is influenced by the combination of several factors, going from the operating conditions chosen at the rotary press to the flow properties of the powders. In fact, powders characterized by greater mean particle size, air permeability, air sensitivity and flow function coefficient are known to be characterized by better die filling (Mills and Sinka, 2013; Zakhvatayeva, 2018), but operating conditions can also have a major impact on the process. In particular, the effect of the feed frame used to distribute the powder over the dies of the rotary press plays a crucial role in determining die filling performance and maintaining specifications on mean weight and weight variability (Ketterhagen, 2015). Furthermore, the mechanical action of the feed frame may impact the powder blend causing particle attrition or over-lubrication, which could lead to reduced tablet strength and slow dissolution.

The objective of this Thesis is to identify which are the compression settings of the rotary tablet press that most influence tablet properties, in particular mean weight and weight variability. This will be done by evaluating experimental data collected at the multi-station rotary press by the partner company for three powder blends. In addition, the effect of the feed frame speed on the lubrication state of the powder is evaluated for one of the previous blends, using data collected on a compactor simulator. The latter is a means of simulating the action of the rotary press using a fraction of the material that would be required by the rotary press, with significant time and materials savings. The results obtained are finally related to the flow properties of the powder blends, analyzed thanks to the availability of flow function and wall friction tests carried out on the blends under study.

The Thesis is structured in four chapters. Chapter 1 introduces to elementary design features and working mechanism of typical rotary tablet presses, focusing on the contributions of material properties and process parameters to the flow behavior during die filling, including an explanation on the use of compactor simulator in alternative to rotary press. Chapter 2 provides detailed information on the equipment used for data collection, including the Fette 1200i tablet press, the Phoenix compactor simulator and the Brookfield tester. A description of the materials

used and the structure of the data sets is also included. The mathematical methods used for data analysis are then discussed in Chapter 3, which provides an overview of the fundamentals of multivariate analysis techniques and the theoretical knowledge necessary to discuss the results reported in Chapter 4. In this chapter, starting with a preliminary analysis that takes into account all the tablet characteristics collected, the focus is put on the weight data in particular and in the compression settings that are mostly affecting it. Moreover, a method for assessing the increase in the lubrication extent coefficient by exploiting data collected at the compactor simulator is proposed. The final step is to relate the blend behavior in the rotary press to the flow properties of the free powder blends themselves, to see how flow can explain different effects of compression settings on the powder blends during the compaction process.

Chapter 1
Rotary die filling system for pharmaceutical powders

Die filling is a critical step in the compaction process used in the manufacture of pharmaceutical tablets. This chapter examines elementary design features and working mechanism of typical rotary tablet presses, focusing on the contributions of material properties and process parameters to the flow behavior during die filling, on which the mass and content uniformity of tablets and the production throughput depend. The use of the compactor simulator as an alternative to the rotary press is then investigated, along with the advantages and limitations of such a choice. Finally, an overview is given of flow indices used to describe material properties and their correlation with die filling performance.

1.1 Introduction to die filling process

In the pharmaceutical production of tablets, powdered or granular materials are measured and transferred into a die cavity, in which they are successively compressed. The die filling process has a major impact on the quality, uniformity and mechanical properties of the tablets produced, so ensuring its accuracy is essential to achieve consistent weight, hardness and dosage of active pharmaceutical ingredient (API) in each tablet (Zakhvatayeva, 2018). The die filling step is part of a larger tableting process, including compression, ejection and coating, which is usually performed using the multiple station rotary press. Proper control of several factors, including the flow properties of the powder, the speed of the tablet press, the geometry of the die cavity, and environmental conditions such as humidity, is fundamental to guarantee the efficiency of the die filling, as will be seen below.

1.1.1 The multiple station tablet rotary press

The rotary press is a high-speed machine employed in pharmaceutical industry to compress powders and granular materials into tablets with uniform size, shape and weight. Moreover, modern rotary tablet presses often incorporates automated monitoring and data acquisition to maintain quality control and optimize production (https://www.ipharmachine.com). This

machine is provided with multiple tooling stations, consisting of a die with an upper and lower punch, that rotate continuously around a central turret, allowing for the simultaneous production of multiple tablets with each revolution. The portions of the turret head that hold the upper and lower punches are called *upper* and *lower turrets*, while the one holding the dies is the *die table* (see Fig. 1.1).

Figure 1.1. *Rotary tablet press turret with 36 tooling stations (https://www.researchgate.net/tablet_dosage_forms).*

The dies are sealed from below by a bottom punch. This ensures that a precise amount of powder enters and fills the die with the correct adjustment, and it also assists in the compression and ejection process. The upper punch, on the other hand, ensures that the required amount of compression force is applied to the powder, producing a tablet of the desired shape and size. As the head rotates, the punches are moved up and down by fixed cam tracks, which control the filling, compression and ejection process. The capacity of the rotary press is determined by the rotation speed of the turret and the number of stations of the press. A schematic representation of the overall working mechanism of the tablet rotary press is reported in Fig.1.2, showing that each station passes through some subsequent stages (https://www.ipharmachine.com):

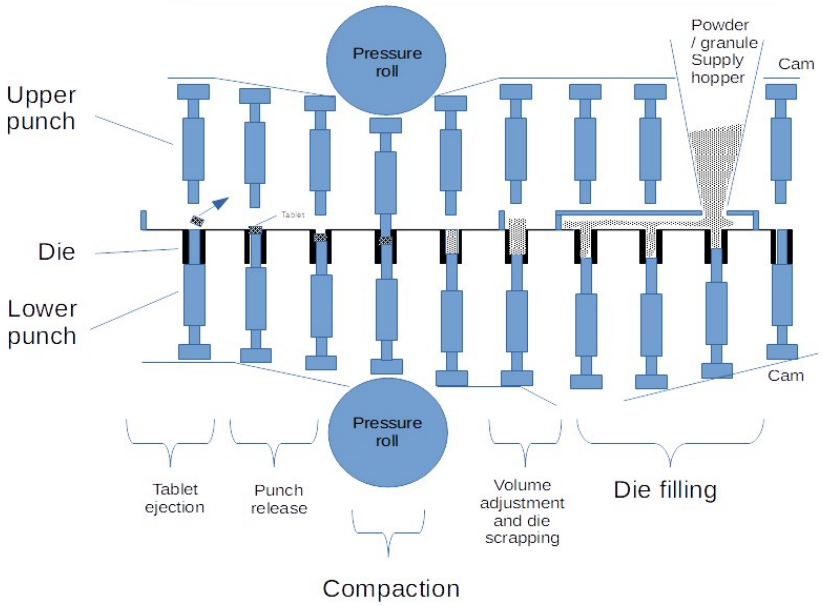

Figure 1.2. *Representation of a rotary tablet press including all subsequent stages through which the die passes (https://powderprocess.net).*

- Powder die filling (Fig.1.3(a)): the powder or granulated material is stored in the hopper and fed into the die cavities via a force-feeding system called feed frame. The feed frame ensures a consistent flow of powder into the dies, which is crucial for maintaining uniform tablet weight and dosage, preventing overfilling or uneven distribution. Further details about the function of feed frame in the compression process are reported below.
- Metering (Fig.1.3(b)): After the fill stage, a weight control unit modifies the lower punch track to ensure that as the punch rises the correct amount of powder remains inside the die and a scraper removes eventually the excess product.
- Compaction (Fig.1.3(c)): it is the phase in which compression and consolidation of the powder occurs at high force, applied by both the upper and lower punches on the die. In order to produce more homogenous tablets, a precompression process can be employed to carry out deaeration. In fact, if air is still present during the effective compression of the powder, its expansion at the end of compaction force application can cause capping. Precompression rollers are usually smaller than the compression ones and apply a lower compression force.

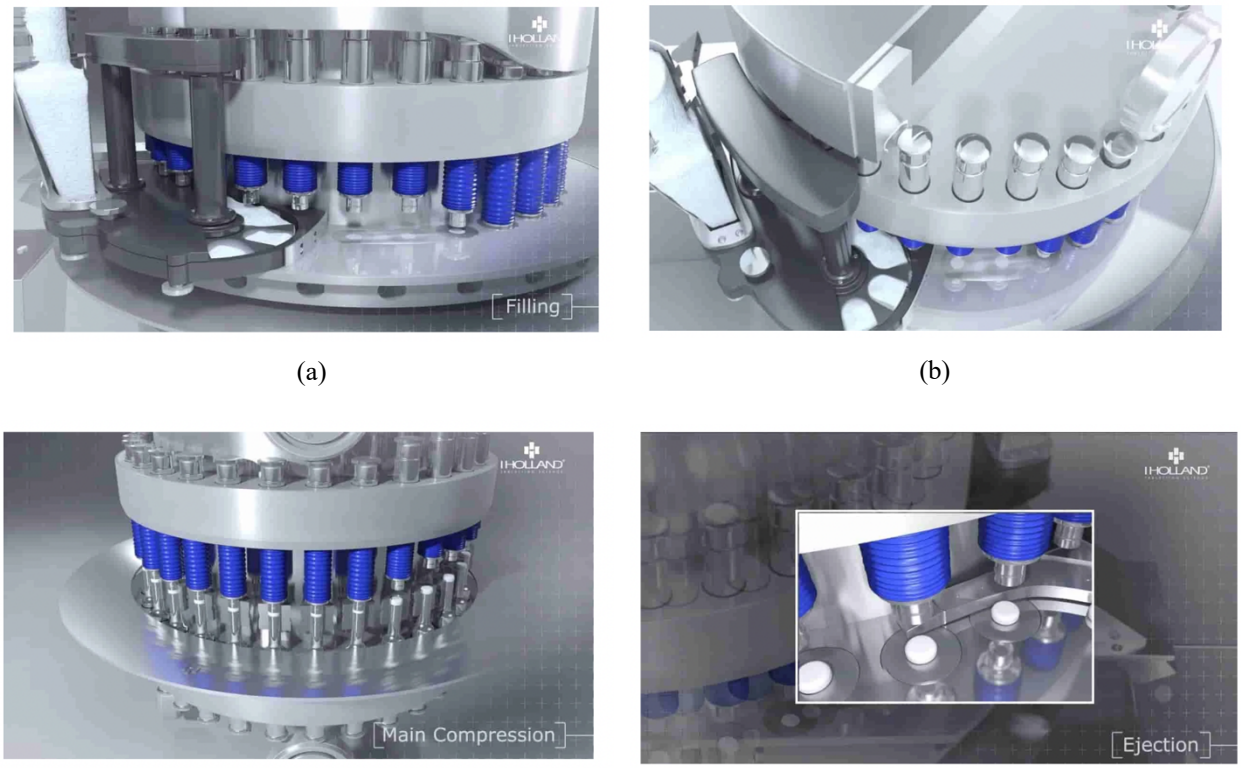

(a) (b)

(c) (d)

Figure 1.3. *Main stages of tablet production in rotary tablet press, specifically: (a) die filling, (b) metering, (c) compression and (d) ejection (https://www.ipharmachine.com).*

- Tablet ejection (Fig.1.3(d)): The lower punch is raised to remove the tablet, which is then collected for further processing as packaging. This stage requires force to break the adhesion between the compact surface and the die wall. Radial die wall forces and die wall friction can cause uneven stresses on the tablets, leading to capping or lamination. This risk can be avoided by using lubricants that minimize the stress patterns to which the tablets are subjected. After ejection from the die, the take-off blade deflects the tablets down the discharge chute, where they are finally collected.

1.2 The effect of powder flowability on tableting process

Weight consistency and uniformity are the most important parameters in die filling, and are strongly influenced by the powder properties, especially its flowability. The latter is known to be determined by the inter-relationship between powder properties, such as cohesion, particle size and morphology, and process conditions (Zakhvatayeva, 2018). For this reason, many studies have been carried out to assess the extent to which powder flow is a function of these.

1.2.1 The shoe-die system

Powder flow during die filling has largely been studied using a model shoe die system, which mimics the die filling process in the rotary tablet press and identifies the types of flow that occur during this process. An example of a shoe-die system is shown in Figure 1.4, where it can be seen that a rectangular moving shoe containing the powder translates over the opening of a stationary die and progressively fills it.

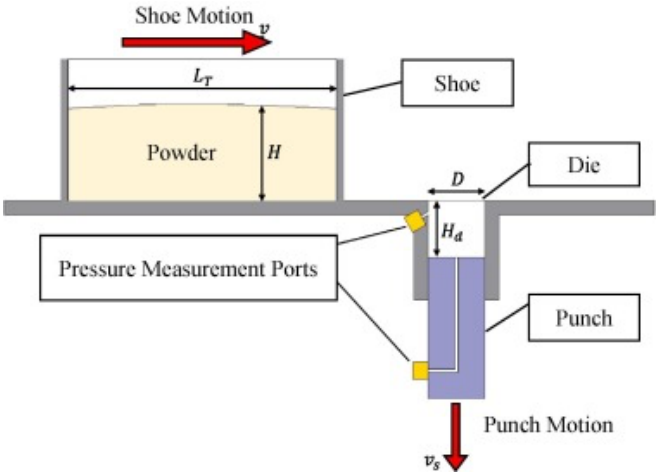

Figure 1.4. *Example of shoe-die system used to investigate the types of powder flows originating during the die fill process (Baserinia, 2019).*

Wu and Cocks (2004) identified two types of flow that contribute to the filling in this system:

- Nose flow: it occurs at lower shoe velocity and it is the most efficient in filling the die completely, since it allows the air entrapped between powder particles to escape more readily. The name is derived from the nose-shaped profile that the powder assumes as it moves towards the back of the shoe when the latter accelerates.
- Bulk flow: it predominates at higher die filling velocities, as the shoe completely covers the die during the powder discharge. In this case, the material continues to detach from the bulk of the powder and falls into the die.

It can be deduced that velocity of die filling (i.e. the velocity of the shoe with respect to the stationary die) plays an important role in determining the amount of powder deposited in the die. In general, it was noted that the slower the filling velocity and the higher the fill density (Wu and Cocks, 2004; Mills and Sinka, 2013). In addition to this, the presence of nose flow or bulk flow during die fill was also found to vary depending on whether gravity or suction filling was used. While in Figure 1.5(a) it is possible to see what the nose flow and bulk flow are in gravity filling, as the powder is discharged from the shoe by gravity alone, Figure 1.5(b) introduces the suction filling mechanism. In suction fill, the die opening is initially covered by the suction punch, while the successive downward motion of the punch creates a suction effect which facilitates powder flow into the die.

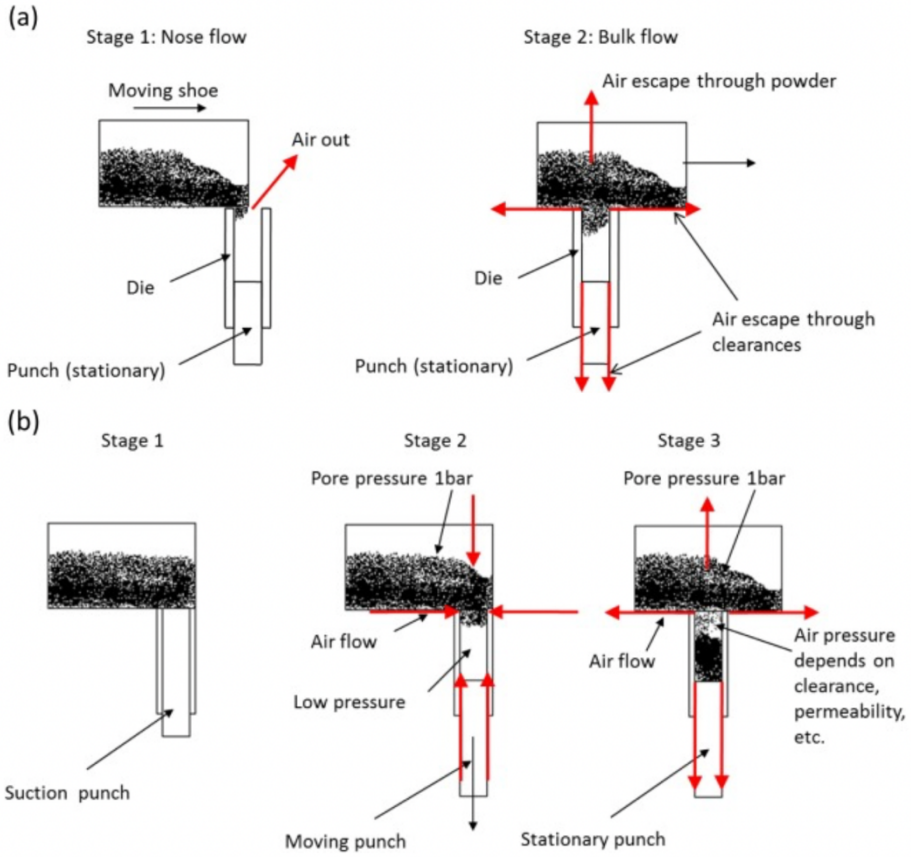

Figure 1.5. *Types of flow originating in a shoe-die system for (a) gravity filling and (b) suction filling (Baserinia, 2019).*

At this stage, air can enter the die through the powder bed and clearances in the system. When the suction movement is complete, the powder is discharged into the die by gravity and the air pressure in the die begins to rise, preventing further powder flow. At this point, similar to gravity filling, the air in the die can only escape through the powder bed and clearances (Baserinia, 2019). It was noted by Wills and Sinka (2013) that in case of suction filling no nose flow mechanism was present, since the entire die opening is exposed to powder before the punch travels downward, and that compared to gravity filling, suction one is much more efficient. Specifically, to evaluate the efficiency of the die filling process, two parameters can be introduced: the fill ratio and the critical velocity. The fill ratio is defined as:

$$\delta = \frac{m}{M} \tag{1.1}$$

where m is the mass of powder in the die at given fill velocity and M is the mass of powder in a fully filled die (Zakhvatayeva, 2018). When the filling velocity is above the so-called critical velocity, the die remains incompletely filled ($\delta < 1$), and the fill ratio becomes function of the die filling velocity v and the critical velocity v_c as:

$$\delta = \left(\frac{v_c}{v}\right)^n \quad (v > v_c) \tag{1.2}$$

where n is a material-dependent parameter. The critical velocity was found to be significantly increased by suction filling mechanism, allowing to use higher die filling velocity during the tableting process and consequently to increase the throughput without damaging the weight consistency and uniformity expected by the process (Zakhvatayeva, 2018). Specifically, the improvement in die filling by suction mechanism was noted to be more relevant for smaller particles, since larger ones, with better permeability, allow air to escape more easily and are so less affected by suction.

1.2.2 Powder properties and die filling relationship

The effect of powder properties on die filling performance has been extensively investigated and the key findings are reported below. Mills and Sinka (2013) found out a strong correlation between critical velocity and particle size; they demonstrated that finer particles generally exhibit higher cohesion and intermittent die flowing behavior, for that an intermittent flow of powder detach from the shoe and falls into the die. Together with mean particle size, critical velocity is also affected by other powder characteristics, such as air permeability and sensitivity (Zakhvatayeva, 2018). Air permeability quantifies how easily air can pass through a powder bed and it is measured in terms of pressure drop across the powder bed. A low air permeability value results in intermittent flow and compromised filling, and this can be caused by fine

particles: higher fines content results in more compacted powder beds and lower air permeation. Differently, air sensitivity index is calculated as:

$$\xi = A_r \phi_r \tag{1.3}$$

where ϕ_r is the normalized particle density, calculated as the ratio between the solid true density (ρ_s) and the air density (ρ_a), while A_r is the Archimedes number, describing the number of particles flowing in air:

$$A_r = \frac{\rho_a(\rho_s - \rho_a) g {d_p}^3}{\eta^2} \tag{1.4}$$

with d_p=particle diameter, g=gravitational acceleration and η=air viscosity. A higher air sensitivity index corresponds to a powder which is less air sensitive. From the studies of Zakhvatayeva (2018), made on seven commonly used pharmaceutical powders tested on a die filling process in a rotary press, it is obtained that critical filling velocity increases with both air permeability and air sensitivity indices. This confirms that denser and coarser particles perform better in die filling. In addition to this, critical filling velocity was found to increase with the specific energy of the powder, measuring the resistance of particles moving relative to each other in an unconfined state. Finally, the effect on flow function and cohesion on die filling has been assessed, proofing that the process improves for higher flow function and lower cohesion. These two powder parameters can be determined by means of a rotational shear cell test, but for their full definition and collection process refer to §1.5.

The discussion so far has focused mainly on the effect of powder properties on the tableting process, but it has already been said that operating conditions can also have a major impact on the process. In particular, the effect of the feed frame used to distribute the powder over the dies of the rotary press plays a crucial role in determining die filling performance.

1.3 The effect of the feed frame on tablet properties

The feed frame, or powder feeder, plays an important role in the rotary press tablet manufacturing process, as it is the last piece of equipment through which the powder flows before it is compressed into a tablet, after which the tablet mass and contents are fixed (Ketterhagen, 2015). Given that there are specifications for the mean and range (or variability) of both the tablet mass and the mass of the active pharmaceutical ingredient (API) within the tablets, it is important to maintain consistent powder fill weights in the tablet dies and to avoid any segregation of the powder blend in the process. In addition, the mechanical action of the feed frame may impact the powder blend causing particle attrition or over-lubrication which could reduce tablet strength and slow dissolution. For these reasons, a deep understanding of

powder flow in the tablet press feed frame for varying process conditions is crucial for controlling appropriately the tablet final quality. Figure 1.6 shows the action of the feed frame paddle wheel in filling the die. Powder is discharged from a hopper and distributed within the die by the paddle wheel of the feed frame, whose shape, direction of rotation and speed all influence the particle flow patterns and residence time distributions. Different mechanisms act simultaneously in a feed frame (Sierra-Vega, 2019):

- gravity feeding: the powder falls from the hopper to feed frame, and then to the dies.
- forced feeding: the rotation of the feed frame paddle wheels force the powder into dies.
- suction fill: it takes place for the downward movement of the lower punch, that creates a partial vacuum driving the powder to the dies.
- centrifugal forces, originated by the rotational movement of the die disc and the paddle wheels.
- overhead pressure due to the pressure exerted on the powder in the feeder and die by the weight of the powder.

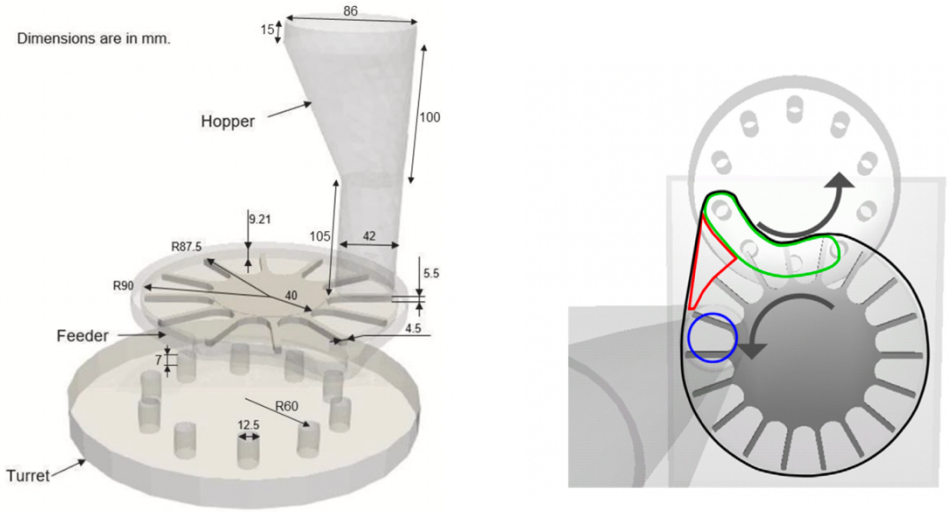

Figure 1.6. *Schematic representation of (a) a tablet-press feeder system (Mahto et al., 2024), (b)feed frame and die turret with the fill point in blue, the die filling region in green and a possible dead zone in which the paddle wheel does not sweep in red (Ketterhagen, 2015).*

A non-uniform die filling may significantly affect the compression force, and consequently, the physicochemical properties of the tablets, such as density and porosity, tensile strength and hardness, dissolution rate, weight and drug content (Sierra-Vega, 2019). It must be noted that mass and mass variability are important quality attributes for a tableting process, and while weight mass can be set by adjusting some main press settings, the weight variability, expressed in terms of relative standard deviation (RSD), is not a value that can be directly set. For this reason, any investigation of how press settings and powder characteristics, such as flowability,

affect weight RSD are crucial for modulating it. The study of Mendez et al. (2012) found out that mean die fill weight increased and the fill weight RSD generally decreased for blend powders subjected to increased feed frame paddle wheel speed. Furthermore, the powder flow properties seemed to improve, and the fill weight RSD to decrease, by increasing the number of paddle wheel blade passes. Ketterhagen (2015) adds that the reduction in weight RSD at higher feed frame speeds is valid regardless of the direction of rotation chosen for the paddle wheel. Despite of this, it was also noted that a small increase in weight RSD can verify with the transition from a low particle solid fraction in the die filling region at low speeds to a large solid fraction at large paddle wheel speeds. All these findings have been taken into account in the work developed in this Thesis and appropriate analyses have been carried out to assess whether they are borne out by the available experimental data.

1.3.1 Lubrication extent coefficient

It has been said that the speed of the feed frame has a significant effect on the powder mixture passing through it, including its state of lubrication. Tablet formulations are typically lubricated by blending the powder with a lubricant, such as magnesium stearate, that aids manufacturability by reducing die-wall friction, increasing the powder bulk density, and reducing powder adhesion to the metal components of the process equipment (Wang et al., 2010). However, the over-mixing inside the feed frame, given by the prolonged exposure of the powder to excessive shear strain, could be detrimental for the final tablet by increasing its hydrophobicity, reducing dissolubility and tablet tensile strength. The over lubrication state has been investigated for years, and it is actually attributed to both process parameters and formulation features. In particular, Kushner and Moore (2010) developed a semi-empirical model to estimate the tablet tensile strength as a function of two formulation dependent terms, in which the extent of lubrication generated in a bin blender is calculated as:

$$k_{bb} = V_b^{\frac{1}{3}} F_{headspace} r \tag{1.5}$$

where V_b is the bin volume, $F_{\text{headspace}}$ is the fractional headspace in the bin and r the number of bin revolutions. According to Eq. 1.1, the lubrication extent of the powder, measured in [dm], is expected to depend mainly on the volume of the blender, the blending time, the mass and the bulk density of the powder charged in the blender. This model was further extended by Blackwood (2012) to estimate the extent of lubrication provided by the action of the tablet press feed frame:

$$k_{ff} = v_{tip} \tau \tag{1.6}$$

with v_{tip}= tip speed of the paddle wheel and τ=mean particle residence time in the feed frame. The above mentioned terms are calculated as:

$$v_{tip} = \pi D_{FF} FF_s \tag{1.7}$$

$$\tau = \frac{m_{hold}}{m_{throughput}} = \frac{\rho_{blend} V_{FF}}{m_{throughput}} \tag{1.8}$$

where D_{FF} is the feed frame diameter, FF_{s} is the feed frame speed in [rpm], V_{FF} is the feed frame volume and $m_{\text{throughput}}$ the mass of tablets produced per unit time. The sum of k_{bb} and k_{ff} gives the total extent of lubrication developed during the manufacturing process, assuming that there are no other unit operations causing increase in lubrication. From the model defined by Blackwood (2012), it can be deduced that the coefficient of lubrication extent should increase linearly with the feed frame speed, and this will be assessed in this study.

1.4 Compactor simulator

Rotary presses are widely used for tablet manufacturing in pharmaceutical industry, but current techniques used for the implementation of this unit operation are still based on material-and time-expensive procedures. In fact, to evaluate if roller compaction is a convenient option for manufacturing, conventional scale equipment must be used, and this can be unfeasible in early development stages in which only low amounts of material (especially APIs) are available (Zinchuk, 2004). Using a laboratory scale compactor simulator is a mean of simulating the rotary press action (Fig.1.7), predicting the effects that critical parameters such as roll speed, pressure and radius have on the properties of compressed powder using a fraction of material required by conventional roller compaction equipment.

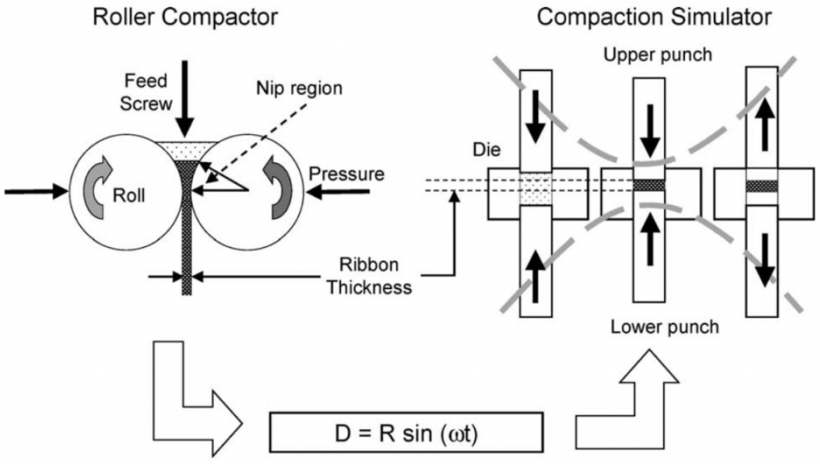

Figure 1.7. *Simulating a roller compactor using a compaction simulator , where D is displacement, R is roll radius, ω is roll rotation frequency, t is time (Zinchuk (2004)).*

This is done by means of a mathematical expression based on the sine function, used to model the movement of a tangential point on the circumference of the roll compactor:

$$Displacement = R\,sin(\omega t) \tag{1.9}$$

where R is the radius of the roller, ω is the roller rotation rate and t is time. The model allows to control the upper and lower punch displacement profiles of the compaction simulator. The powder is initially charged in the die of the compactor simulator. At $t = 0$, the punches move towards each other, compressing the powder at the same strain rate as in the real roller compaction process. The point at which the punches (or roller points) reach their minimum separation is correlated to the peak of the sine function, which can be used to target the thickness of the simulated tablets. When the punches reach their minimum separation, they retract to decompress the tablet before it is ejected by the movement of the lower punch. To quantitatively evaluate the simulation, Zinchuk et al., (2004) used tablet SF and the tensile strength profiles for comparing roll compaction and compactor simulator processes, with microcrystalline cellulose used as powder material. The results showed that tablets with similar SFs exhibit good agreement in tensile strength comparison, indicating that the method is valid for evaluating roll compaction behavior. The capability of the compactor simulator to mimic the rotary press compaction will be assessed in this Thesis, too, by exploiting the solid fraction and tensile strength profiles for tablets obtained with the two unit operations. It must be noted that compactor simulator is not able to account for some roll compaction aspects, since it employs a batch process to imitate a continuous one. Specifically, it does not account for roller compaction variables associated with continuous operation such as powder feed mechanisms, the nature of the shear forces experienced by the powder or the transition from the slip to no-slip region of compaction. Despite of this, the compactor simulator remains a useful and representative tool allowing for control of critical variables like roll speed, separation, pressure and radius (Beccaro, 2023).

1.5 Powder flowability

One of the most critical properties of powders in pharmaceutical manufacturing is their ability to flow freely in operating units designed to achieve solid dosage forms. In fact, they must have sufficient flowability to be transported by gravity or to fill die cavities in a consistent manner, even at high throughputs. There are several flow characterization techniques used to quantify the flowability of a powder, but one of the most commonly employed by industry is the rotational shear cell flow test. Below is a description of the main flow indices obtained from the above test, which were then used as a reference in this thesis.

1.5.1 The flow function

The flow function coefficient (*ffc*) is widely used in pharmaceutical development as reference index for powder flow assessment, often in a comparative fashion (Leung, 2017). It represents the powder's ability to flow under a consolidating stress and it is found as:

$$ffc = \frac{\sigma_1}{\sigma_c} \tag{1.10}$$

where σ_1 is the major principal stress that consolidates the powder and σ_c is the stress at which the compacted powder will begin to flow or yield without confinement. The rotational shear cell test derives *ffc* operating on the basis of the Mohr circles, which consist on a graphical representation of the stress states within a powder material after that a pre-consolidation stress has been applied. To understand how Mohr circles are derived, it is useful to refer to the monoaxial compression test for explanation (Schulze, 2021). Imagining that a normal stress σ_v is applied to a powder sample, a horizontal stress σ_h originates on the sample (Fig. 1.8(a)).

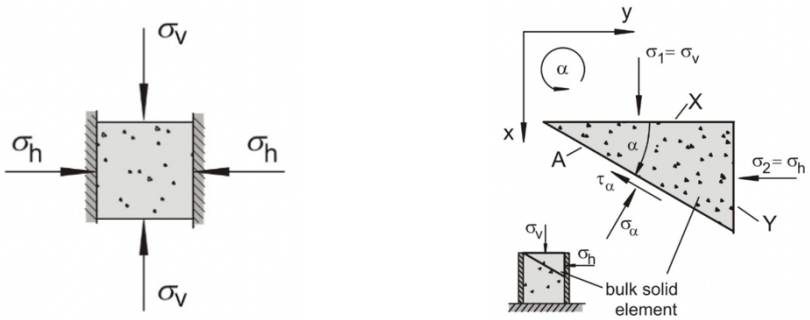

Figure 1.8. *(a) Element of a bulk solid with application of a normal stress σ_v from which a horizontal stress σ_h originates and (b)volume element with triangular cross section of the bulk solid subjected to normal stress (Schulze, 2021) .*

It results that different stresses can originate in different cutting planes of the sample, and through equilibrium of forces it is possible to find which are the shear stress (τ_α) and the normal stress (σ_α) acting on a bulk solid plane inclined of a certain angle α (Fig.1.8(b)):

$$\sigma_\alpha = \frac{\sigma_v+\sigma_h}{2} + \frac{\sigma_v-\sigma_h}{2}\cos(2\alpha) \tag{1.11}$$

$$\tau_\alpha = \frac{\sigma_v-\sigma_h}{2}\sin(2\alpha) \tag{1.12}$$

The pair of values $(\sigma_\alpha, \tau_\alpha)$, which can be calculated for each angle α, can be plotted in a shear-normal stress diagram and they form a circle in it, which is called "Mohr stress circle", representing the stresses on all cutting planes at arbitrary inclination angles α, i.e., in all possible cutting planes within a bulk solid element. Applying different normal loads to the powder, sample, it is subjected to several shear stresses and a Mohr circle for each pre-set load is

obtained. The tangent line to the Mohr circle corresponding to the yield points of the powder under various stresses is drawn, namely the yield locus, and σ_1 is found as the maximum normal stress on the Mohr circle that touches the yield locus without crossing it. Differently, σ_c is determined by constructing a Mohr circle that is tangent to the yield locus and passes through the origin (zero normal and shear stress), representing the stress state where the powder would yield if unconfined (Fig.1.9). Another important parameter that can be found by means of the Mohr circles is the cohesion, which is the intercept of the yield locus on the shear stress (τ) axis when the normal stress (σ) is zero. It represents the intrinsic shear strength of a material when no normal stress is applied on it. Once that σ_1 and σ_c are known, *ffc* can be found.

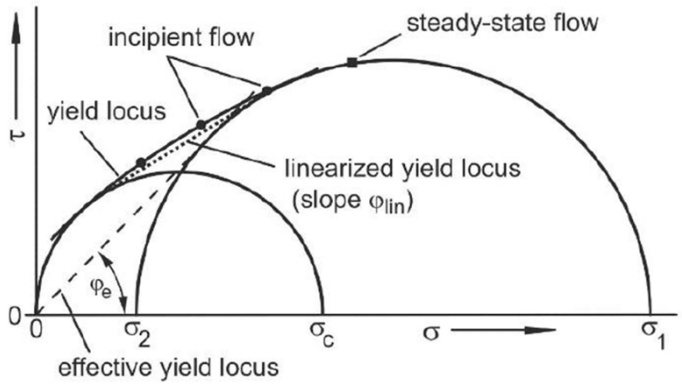

Figure 1.9. *Schematic representation of yield locus, σ_1 and σ_c found through Mohr circles built on a pre-consolidation load applied to a powder sample (Manokaran, 2024).*

The larger *ff*c is, i.e., the smaller the ratio of σ_c over σ_1 , the better a bulk solid flows. The diagram in Fig.1.10 clearly shows that *ff*c in most cases increases with σ_1, for that one obtains a different value of flowability for each consolidation stress applied. Since flowability results to be dependent on consolidation stress, it is not possible to express in absolute way the flowability by means of a single numerical value, but *ffc* can be efficiently used for powder comparisons.

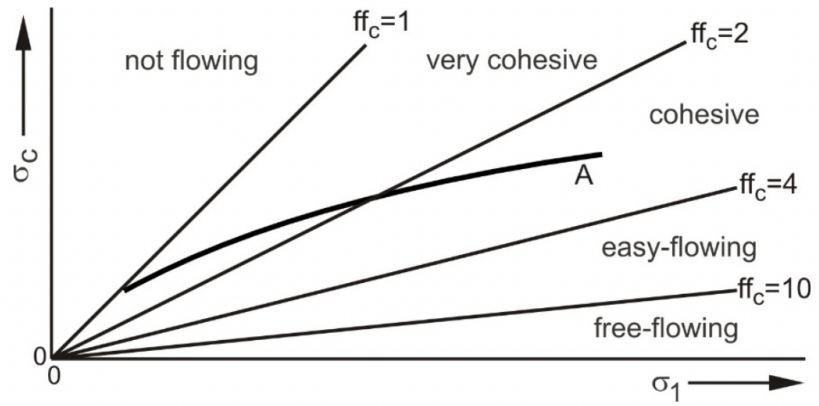

Figure 1.10. *Flow function for a bulk solid A and constant reference flowability lines (Schulze, 2021).*

1.5.2 The wall friction

Wall friction is the friction between a bulk solid and a solid surface, such as the walls of a silo or hopper. The determination of wall friction or wall friction angle is important for the design of equipment where the bulk solid has to flow over a solid surface (Schulze, 2021). The principle of wall friction test can be easily explained by Fig. 1.11. A bulk solid is subjected to a vertical normal stress, and the stress acting between the solid and the wall surface is called σ_w.

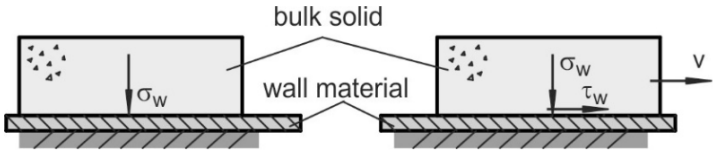

Figure 1.11. *Basic principle of wall friction test, in which a normal stress is applied to a powder sample and the relative shear stress developed on it is measured (Schulze,2021).*

The bulk solid starts to shift over the wall surface with a certain velocity, and the shear stress acting between bulk solid and the wall surface is measured. For each applied normal stress, a correspondent constant wall shear stress τ_w can be found. By conducting the experiment applying different normal stresses, all pairs of σ_w and τ_w are plotted together and joining the points it is possible to find a wall yield locus (Fig.1.12), describing the wall shear stress necessary to shift a bulk solid continuously across a wall surface under a certain wall normal stress (Schulze, 2021).

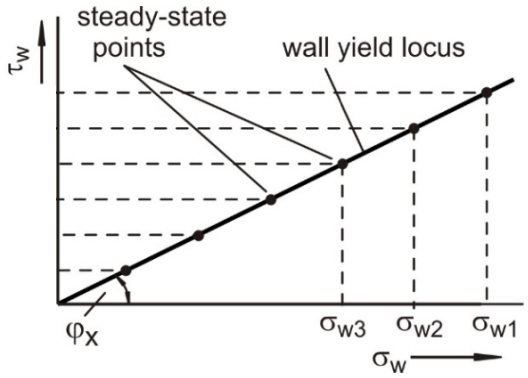

Figure 1.12. *Basic principle of wall friction test, in which a normal stress is applied to a powder sample and the relative shear stress developed on it is measured (Schulze,2021).*

At this point, the wall friction angle φ_x , which is the slope of the line passing through the origin of the σ_w, τ_w diagram and a point of the wall yield locus, is used to assess the wall friction. The larger it is and the greater is wall friction. In addition to this, also the bulk density of the powder

is measured during the wall friction test, before and after stress application, in order to obtain the bulk density curve of the material. In general, a free-flowing material will be incompressible, so it will show only a small increase in density with stress. In contrast, a very cohesive, poorly flowing bulk solid will show a large increase in bulk density with increasing stress. In this study, the powder bulk density determined during the wall friction test is used to calculate another meaningful index of the flowability of different powder formulations, the compressibility index (as will be explained in more detail in section §4.5.2); this last, together with the flow function coefficients and the wall friction angles, will provide a complete description of the flowability of the tested samples.

1.6 The answers sought in this Thesis

As previously described, the final properties of tablets produced in the rotary press are influenced by the inter-relationship between the compression settings chosen and the characteristics of the free powder. With this in mind, the aim of this Thesis is to answer the following questions:

- Is it possible to identify which compression settings have the greatest influence on tablet properties, with particular emphasis on mean weight and weight variability? Is the effect of the compression settings the same for all the blends studied or is it blend specific?
- With regard to the effect of the feed frame, can it be shown that its speed is one of the main factors influencing the final tablet quality? Are the statements in the literature regarding its ability to reduce weight variability and increase the lubrication state of powders consistent with the behavior observed for the blends under investigation?
- Is it possible to verify the appropriateness of the semi-empirical model proposed by Kushner and Moore (2010) and extended by Blackwood (2012) to estimate the state of lubrication of the powder subjected to a given feed frame speed?
- Does the composition of the blend affect the final properties of the tablet? In what way?
- Can flow function tests and wall friction tests carried out on the powder blends be used to assess the effect of the feed frame on the original powder flowability and to understand how the intrinsic powder properties are related to the blend behavior in the rotary press?

Chapter 2

Materials, equipment and datasets

This chapter provides a comprehensive presentation of the pharmaceutical powder mixtures used for the experiments, together with a detailed description of the equipment used for data collection, including the Fette 1200i tablet press, the Phoenix compactor simulator and the Brookfield tester machine. The data collection procedure is explained in detail, as the results are crucial to understanding the subsequent analysis approach. Finally, the dataset structures are presented, examining compression settings, measured and calculated product quality attributes contained within them.

2.1 Powder mixtures

The aim of this study is investigating the relationships existing between compression settings and tablet properties after compaction for three pharmaceutical placebo powder blends or formulations, whose components and related compositions are reported in Table 2.1. It must be noted that even if no API is present, lactose monohydrate is added as surrogate of it with the aim of imitating its behavior.

Table 2.1. *Placebo formulations with related materials and compositions.*

Materials	**Function**	**Formula Qty (mass %) in formulation/batch/blend**		
		Blend 1	**Blend 2**	**Blend 3**
Lactose monohydrate 200M	Diluent	23.02	5	22.34
Avicel	Diluent	24.99	22.74	58.66
Lactose anhydrous	Diluent	47.99	68.26	15
Croscarmellose sodium	Disintegrant	3	3	3
Magnesium stereate	Lubricant	1	1	1
Total		100	100	100

Placebo formulations, i.e., not containing any APIs, are of paramount importance for clinical studies, since they are made to match the physical properties of a real drug, like shape, size and color, but they do not have any therapeutical effects on the body. In this way, they allow to improving drug development at a lower cost and saving most valuable resources. They can be

constituted by several types of excipients, that are inert or active substances generally added in formulations for aiding in processing of drug delivery system during manufacture, to protect and enhance stability of the product and to assist in maintaining integrity during use and storage. As it can be seen in Table 2.1, excipients can have different functions in a formulation: diluent, disintegrant, lubricant, binders, etc. Some of the main features of the ones employed in this work are following presented, and related SEM images are reported in Fig. 2.1:

- Lactose monohydrate 200M: it is a milled powder of α-lactose monohydrate, combining good compaction, blending properties and storage stability. Fine in nature and with relatively high surface area, it is mechanically milled at different degrees of particle size allowing pharmaceutical companies to choose the grade best fitting for their study. It is commonly used as excipient in pharmaceutical drug development.
- Avicel: it is a purified, partially depolymerized alpha-cellulose excipient made by acid hydrolysis of specialty wood pulp, commonly used as binder in pharmaceutical formulations. It is a type of microcrystalline cellulose (MCC), which generally flows and compresses extremely well, properties that gives this material a variety of applications in many fields. MCC is commonly available in different sizes, and Avicel is the one characterized by a nominal mean particle size of 100 μm, providing it a good flowability and making it suitable for direct compaction, being it resistant to a wide range of compaction pressures and to organic and non-organic contaminants (Yu, 2013).

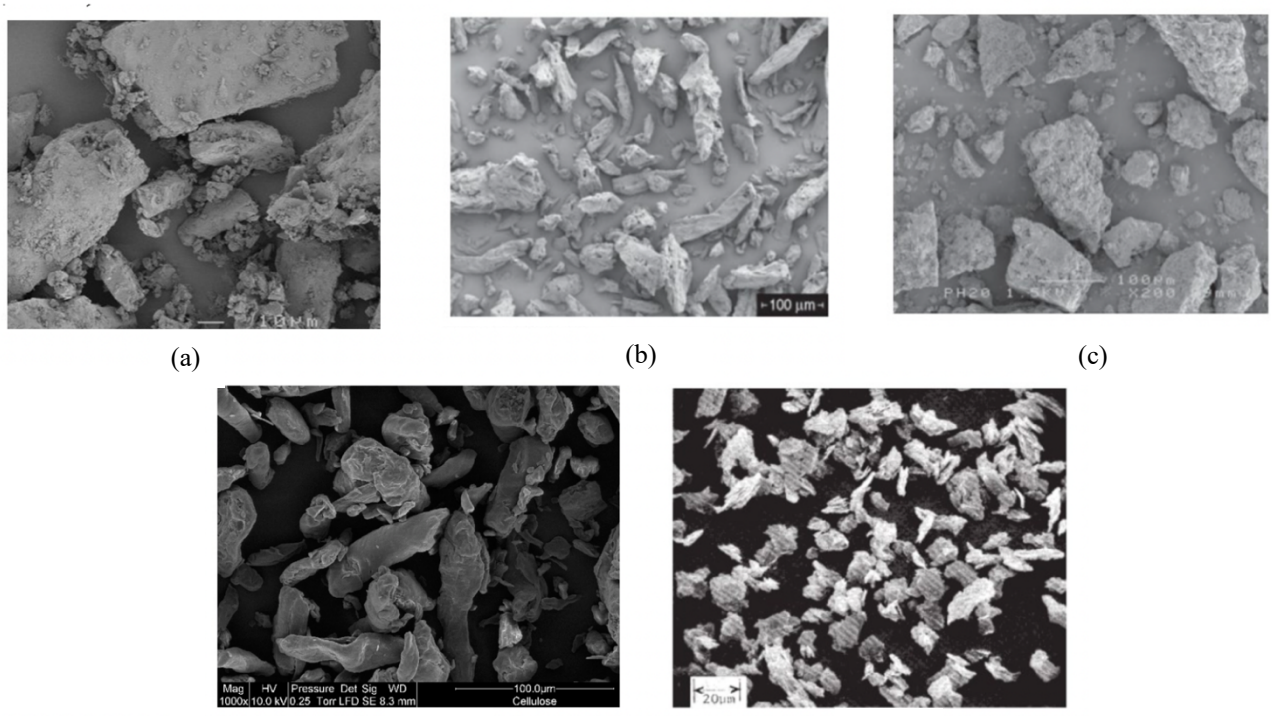

Figure 2.1. *SEM images of (a) Lactose monohydrate 200M, (b) Avicel, (c) Lactose anhydrous Supertab (d) Croscarmellose sodium and (e) Magnesium stereate (Rowe et al. 2009; https://dfepharma.com/excipients/pharmatose-200m; https://www.researchgate.net/figure/SEM-picture-of-croscarmellose-sodium-particles).*

- Lactose anhydrous Supertab: it is a disaccharide sugar used as filler, diluent and bulking agent in a wide variety of pharmaceutical tablets, capsules, powders and other preparations. It is characterized by a low level of crystalline water, resulting very suitable for formulations with sensitive moisture APIs.
- Croscarmellose sodium: is an internally cross-linked sodium carboxymethyl cellulose, which is insoluble, hydrophilic and extremely absorbent, giving it excellent swelling properties and high water absorption capacity. It is commonly used as disintegrant in pharmaceutical manufacturing, providing an efficient disintegration at low levels of use.
- Magnesium stearate (MgSt): This is a salt formed by the combination of stearate molecules with magnesium ions. It has historically been implemented at low percentages in pharmaceutical tableting as a lubricant to aid in ejection from tablet punches and it is used also to improve flowability when blended to lactose powder. MgSt also slows down the absorption and dissolution time of the tablet.

For all three blends, lots of 100 kg are firstly manufactured, then processed in two sublots of 50 kg each due to limitations of bin size. The first blending phase occurs in a IBC blender, where all ingredients are added orderly to the formulation (the same as Table 2.1), except for magnesium stearate, at certain blending speed and time. MgSt is successively added to the formulation at the same speed but reduced blending time. At this point the formulation is ready to go to compression in Fette 1200i machine. After this phase, samples are collected via polyethylene bottle.
A summarizing scheme of the main steps involved in the formulation preparation is reported in Fig.2.2.

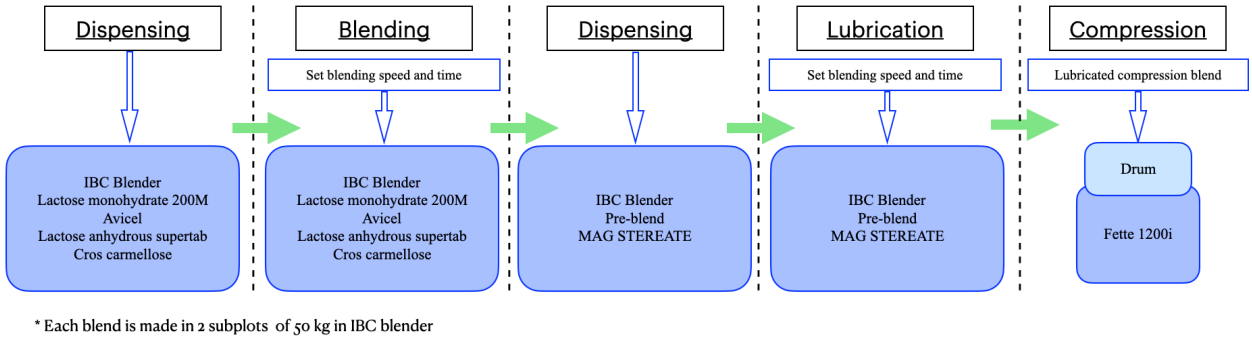

Figure 2.2. *Process flow of material transfer for manufacture, from blending of excipients to compression phase with operating conditions.*

2.2 Equipment

It was anticipated that the work of this Thesis is based on data belonging to different datasets, collected by the partner company by using different equipment, settings and procedures. Regarding the equipment, GSK commercial dataset is based on the use of Fette 1200i tablet press, a high-performance machine widely employed for pharmaceutical manufacturing. Compactor simulator data, differently, are obtained through the Phoenix, an advanced and sophisticated tool replicating the process of compacting powder into tablets generally operated by compacting tablet presses. Main features of both are going to be presented here following, together with the ones of the Brookfield powder flow tester, used for shear cell data collection.

2.2.1 Fette 1200i tablet press

Rotary tablet presses are essential machines in the pharmaceutical industry, designed for the mass production of tablets. They operate by continuously rotating a die table, allowing multiple compression stations to simultaneously fill, compress and eject tablets. They enable an efficient and consistent production of large quantities of tablets, ensuring uniformity in weight, hardness and shape. Their use is crucial for manufacturing of a wide range of products, meeting the industry's stringent standards for quality and precision.
For the aims of this work, the Fette 1200i is employed (Fig.2.3), a high-performance rotary tablet press designed for efficiency, precision and reliability in mass production. It stands out for its ability to produce large quantities of tablets consistently and with high precision and it is particularly suitable for pharmaceutical applications where tablet uniformity, quality and production speed are critical. This machine is often used to produce prescription drugs, over-the-counter medications and nutritional supplements (https://www.fette-compacting.com).

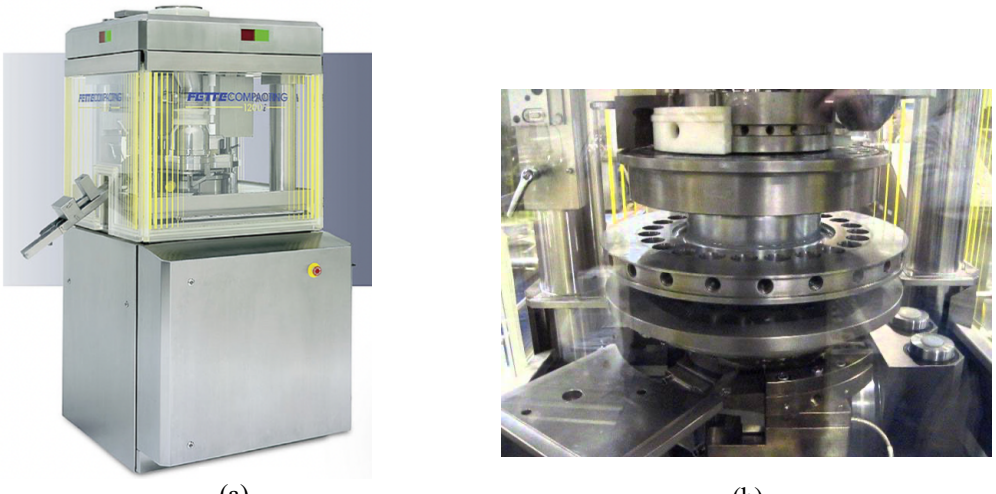

(a) (b)

Figure 2.3. *Fette 1200i rotary tablet press (a) with internal die table visualization (b)* (https://www.fette-compacting.com).

The machine operates according to the rotary tablet press working principles, here briefly reported (for details, refer to §1.1.1):

- *Powder filling*: a feeder system is providing pharmaceutical powder into the die cavities of the press table. The powder must be accurately dosed to ensure uniform tablet weight and consistency among tablets produced.
- *Compression*: The press starts rotating, bringing progressively all the die cavities under a set of punches (upper and lower), which exert a force on the powder compressing it into a solid tablet.
- *Tablet ejection*: After the compression phase, the lower punch pushes the newly formed tablet out of the die cavity, which is then recovered by a conveyor or a handling system.

Fette 1200i, as a rotary press, can perform these steps in a continuous cycle. Its die table rotates, allowing for simultaneous filling, compression and ejection at different stages around the press head. In this way, it ensures a high output producing thousands of tablets per hour, guaranteeing at the same time a precise control over tablet parameters. Its versatility makes it suitable for a wide range of tablet sizes and shapes, making it adaptable for different product requirements.

2.2.2 Phoenix compactor simulator

Phoenix is a highly instrumented single-station compression machine designed to simulate the operation of industrial tablet compaction machines, enhancing understanding of machine settings and process optimization without the need for large amounts of product.
This type of equipment is commonly used for training, allowing users to simulate various aspects of tablet production, including powder feeding, compression force adjustments, ejection phase closely mimicking real-world operations (https://www.korsch.com).

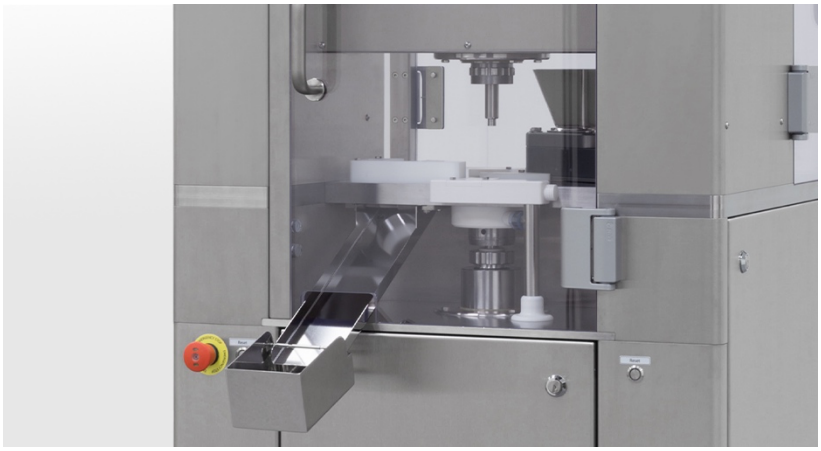

Figure 2.4. *Compactor simulator equipped with a single station for compression (https://tabletingtechnology.com).*

For this specific study, Phoenix is employed only for blend 3 analysis, with the aim of using the collected data to evaluate firstly if compaction simulator mimics well the tablet rotary press, and successively for an estimation of the lubrication extent coefficient value acquired by the blend after subjection to different feed frame speeds. Details about data collection procedure are reported in the following sections.

2.2.3 Brookfield powder flow tester (PFT)

For the aims of this study it is fundamental to characterize powder flow properties and flow behavior, understanding how they are related to operating conditions chosen during compression in determining final tablets qualities. This is done by Brookfield PFT, a precision instrument able to measure, display and print out flow results at specified compaction loads (https://www.brookfieldengineering.com). There are several powder flow properties that PFT can measure to categorize flowability, but the most recognized indication of powder flowability is the unconfined failure strength when viewed as a function of the consolidating stress, known as the flow function. Wall friction, internal friction, and bulk density are also commonly used to relate measurements to flow behavior.

Figure 2.5. *Brookfield powder flow tester (PFT) with powder sample in an annular shell cell going to be compressed by a compression lid vertically downward into it (https://store.brookfieldengineering.com/pft-powder-flow-tester).*

The main working mechanism of PFT consists of driving a compression lid vertically downward into a powder sample contained in an annular shear cell (Fig.2.5). The powder sample has a defined volume and its weight is measured before the start of the test. The compaction stress applied to the powder is controlled by a calibrated beam load cell. The test properly starts with the annular shear cell rotated at a defined speed, while the torque resistance of the powder in the shear cell moving against the powder in the stationary lid is measured by a calibrated reaction torque sensor (https://store.brookfieldengineering.com/pft-powder-flow-

tester). The geometries of the lid, shear cell, rotational speed of the cell, and the compressive loads applied to the powder all contribute to the calculations which determine the "flowability" of the powder.

2.3 Data collection procedure

The purpose of this study is to verify the impact of various parameters and materials attributes on final tablet properties, especially tablet weight variability. For this reason, a design of experiments (DOE) was conducted, examining the impact of five main factors on tablets properties by using Fette 1200i tablet press. The factors to be explored are listed, with the applicable ranges in the table below (Table 2.2). Runs 1 to 5 were collected to manufacture round concave tablets, while runs 8 to 12 to produce oval tablets. In addition to them, also additional runs were performed when leftover powder was available, but not reported here since not reliable for the aims of the study.

Table 2.2. *DOE specifications for data collection in Dataset 1 and Dataset 2.*

Run	**Fill cam** (8mm,10mm,12mm,14 mm)	**Fill depth** (mm)	**Overfill** (% fill cam)	**Feed frame speed** (rpm)
Run design for round concave tooling (9 mm)				
1	10	7	30	15
2	10	9	10	15
3	10	8	20	30
4	10	7	30	45
5	10	9	10	45
Run design for oval tooling (15.5 mm × 8.5 mm)				
8	14	11	20	15
9	14	13	7	15
10	14	12	15	30
11	14	11	20	45
12	14	13	7	45

A brief overview of what these compression settings represent is here reported:

- Fill cam: it is part of the tablet press mechanical system, with the primary function of controlling the lower punch position within each die cavity, determining the amount of powder that is filled into it.
- Fill depth: it refers to the depth of the cavity that is filled with powder, determining the volume of the material that will be compressed for obtaining the final tablet and influencing consequently weight, size and density of the tablet.

- Overfill: it can be described as the offset between fill cam and fill depth, ensuring weight consistency even in presence of powder flows variations or redistributions within the die cavity.
- Feed frame speed: it has a critical role in determining how efficiently powder is distributed inside die cavities, having a significant effect on final tablets properties. For further details about feed frame and related speed see §1.3.

Samples used for this study are exclusively the ones collected at steady state, after a time of 0, 5 and 10 min from the beginning of each run.

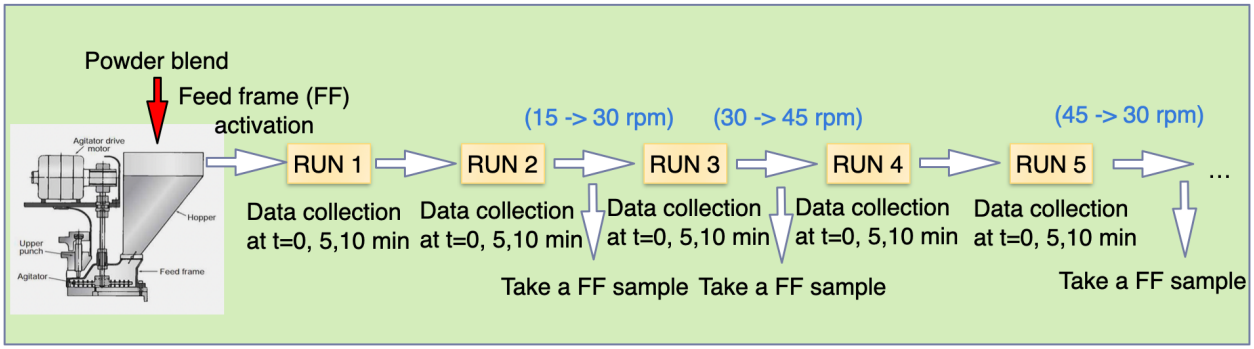

Figure 2.6. *Data collection procedure synthetic flow for Dataset 1 and Dataset 2.*

It can be noted from Fig 2.6 that some feed frame samples, consisting in powder samples remaining in the feed frame, were then collected after runs 2, 3 and 5. These will be useful later on, for lubrication extent coefficient estimation purposes with compactor simulator.

2.3.1 Dataset 1: GSK commercial dataset

In this dataset, only data from runs 2, 3 and 5 are reported for each blend, as these are considered experimentally significant for an evaluation of the effect of the main compression settings on the final tablet properties. Together with the settings seen in §2.3, compression force is also varied for the data collection, since it is known from Pellett et al. (2018) to influence some tablets properties such as thickness, hardness and dissolution time.

Time related data (at 0, 5 and 10 min) are reported only for an applied compression force of 13 kN, while other few data, independently from time dimension, are also collected at 6.5, 9.5 and 16 kN. Ten replicates (tablets) data are present for each time instant at 13 kN, for a total of thirty replicates available at this compression force, while for the other force values ten replicates are totally performed. While for blend 1 and 2 rotor speed is maintained constant in all runs considered by this dataset, in blend 3 it is also varied (from 41 to 49 rpm) in run 2 and 3 and consequently considered among compression settings in the successive analysis of this Thesis work. A summarizing scheme of data structure for GSK commercial dataset is reported below

(Fig 2.7). At this point, an overview of which tablets properties are considered and reported in the dataset is provided in Table 2.3, with a successive focus in volume and tensile strength calculation.

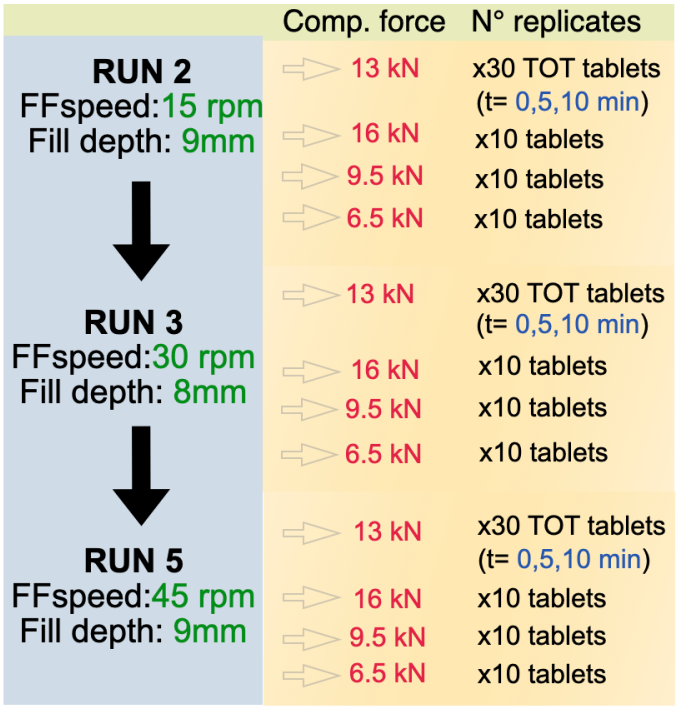

Figure 2.7. *General data structure representation for Dataset 1 valid for all blends, considering that for blend 3 two "RUN 2" and two "RUN 3" exist, one at 41 and one at 49 rpm rotor speed.*

At this point, an overview of which tablets properties are considered and reported in the dataset is provided in Table 2.3, with a successive focus in volume and tensile strength calculation.

Table 2.3. *Tablets properties (measured and calculated) taken into account in Dataset 1.*

	Units of measure
Weight	mg
Thickness	mm
Hardness	kp
Tensile strength	MPa
Width	mm
Volume	mm^3
Density	g/cm^3
Solid fraction	[-]

2.3.1.1 Volume

Tablet volume reported in the dataset is calculated as a function of the so-called *cap* volume (V_c), including the top and bottom of the tablet, and the *wall thickness region* volume (V_w):

$$V = 2V_c + V_W \tag{2.1}$$

where $V_c = \frac{\pi h}{6}(3a^2 + h^2)$, with a=base radius of the cap and h=cap depth, while $V_W = \pi r^2 W$, with r=tablet radius and W=tablet wall thickness (see Fig. 2.8).

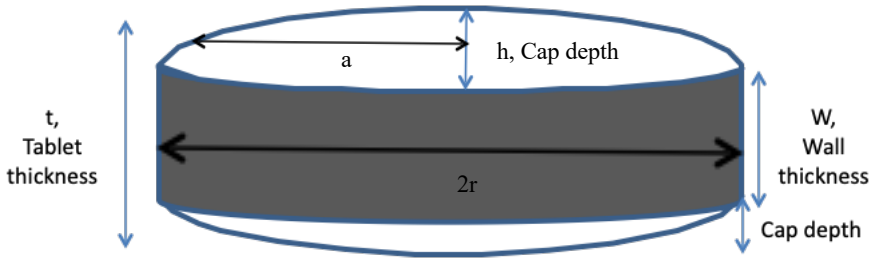

Figure 2.8. *Details on terms significance for calculation of tablet volume.*

2.3.1.2 Tensile strength

Tensile strength of a tablet is a crucial measure of its mechanical integrity and robustness, as it ensures the tablet is strong enough to be able to withstand treatments successive to compression, such as film coating, packaging, transportation and use, but also weak enough to break in the human body and release its content (Pitt et al., 2013). While hardness test takes into account only the compressive force required to fracture a specimen across its diameter, tensile strength considers also the dimension and the shape of the compact, allowing ready comparisons to be made between samples of different shapes and size. It can be influenced by several factors as formulation, compression force and powder properties, and it is often used as a quality control parameter in pharmaceutical manufacturing to assess if the tablets meet the required mechanical standards. The tensile strength can be assessed by means of the following equation (Pitt and Newton, 1988) for round tablets only:

$$TS = \frac{10P}{\pi D^2}\left(2.84\frac{t}{D} - 0.126\frac{t}{W} + 3.15\frac{W}{D} + 0.01\right)^{-1} \tag{2.2}$$

where P is the breaking force (N), D is the tablet diameter (mm), t is the tablet thickness (mm) and W is the wall region thickness.

2.3.1.3 Solid fraction

This is a key intermediate product attribute in tablets formulation and manufacturing as it influences several tablets physical properties, like hardness, mechanical strength, disintegration and dissolution rate. Solid fraction (SF) is defined as the portion of tablet volume occupied by solid material, as opposed to the volume occupied by voids (pores or air space). It can be calculated as the ratio between the tablet density (ρ_{tablet}), and the powder true density (ρ_s), where the latter is the density of the solid material alone:

$$\rho_{tablet} = \frac{tablet\ mass}{total\ volume\ (solid+interstitial\ voids)} = \frac{m_s}{2V_C+V_W} \tag{2.3}$$

$$\rho_s = \frac{tablet\ mass}{tablet\ solid\ volume} = \frac{m_s}{V_s} \tag{2.4}$$

$$SF = \frac{\rho_{tablet}}{\rho_s} = \frac{m_s}{\rho_{s\times(V_W+2V_C)}} = 1 - porosity \tag{2.5}$$

From the work of Stranzinger et al. (2021) it is known that, while the true density is a characteristic of the powder itself, the tablet density is highly affected by material processing in a unit operation; this is why it is crucial to understand how compression settings affect it in order to obtain appropriate tablet solid fractions. A higher solid fraction is usually correlated to a tablet which is denser and harder, as more of its volume is occupied by solid material, affecting consequently tablet tensile strength and its ability to withstand handling without breaking.

2.3.2 Dataset 2: weight dataset

Referring to the same compression settings and data collection procedure seen in §2.3, weight dataset includes exclusively tablet weight data for three different time instants (0, 5 and 10 minutes) along several runs for each blend. Thus, differently from the previous dataset in which only runs 2, 3 and 5 were considered, additional runs data are reported, considering for each run the data time evolution and adopting a fixed compression force. For each time instant, sixty tablet weights are collected, with the aim of investigating specifically weight variability between runs and within runs for the different formulations (Fig. 2.9).

Runs included in this dataset are here listed:

- For blend 1: run 1, 2, 3, 4, 5 and 10 .
- For blend 2: run 1, 2, 3, 4, 5, 8 and 9.
- For blend 3: run 1, 1A, 2, 2A, 3, 3A, 4 and 5.

RUN 1			
Time [min]	t=0	t=5	t=10
Weight data [mg]	$\times 60\ replicates$	$\times 60\ replicates$	$\times 60\ replicates$
RUN 2			
Time [min]	t=0	t=5	t=10
Weight data [mg]	$\times 60\ replicates$	$\times 60\ replicates$	$\times 60\ replicates$
RUN N			
Time [min]	t=0	t=5	t=10
Weight data [mg]	$\times 60\ replicates$	$\times 60\ replicates$	$\times 60\ replicates$

Figure 2.9. *Dataset 2 structure: sixty tablet weights are reported at each time instant for the single run.*

Note that for blend 1 and 2, runs producing oval tablets are introduced (see Table 2.2), allowing one to evaluate how larger variations of compression settings like fill depth and rotor speed are affecting final weight of the tablets. With regard to the latter, the runs for oval tablet production are set at 15 rpm, as opposed to the 40 rpm used for runs 1-7. For blend 3, only 9 mm round tablet runs are selected, but the variation in rotor speed is also taken into account as it is set at both 41 and 49 rpm for runs 1 to 3. In some cases, and specifically indicated, additional runs data which are not present in the dataset but available in supplementary material are included in the Thesis work for comparison purposes.

2.4 Dataset 3: Compactor simulator dataset

As explained in §2.3, three feed frame samples of blend 3 are collected between one run and another in order to be studied at the compactor simulator. This is done firstly to evaluate if the latter is able to mimic well the compression process at the rotary press, bringing the advantages of low material consumption and high process flexibility. Compactor simulator employs highly controlled punch displacement profiles to deliver a range of compression forces to the powder, in this case going from 6.5 to 16 kN, as well as in the rotary press (see §2.3.1). Tablets properties are measured for five tablets at each compression force level considered, and successively compared to the rotary press ones. In conjunction with the above mentioned samples, also the lubricated commercial blend 3, not yet subjected to feed frame sample, and four new realized blends are studied at the simulator under the same explained conditions. The new blends have the same composition as blend 3 and are obtained in a blender with V=500 mL for different blending times, varying in this way their extent of lubrication k (see Table 2.4).

Table 2.4. *Blending conditions and lubrication extent of new lubricated blends realized for compactor simulator profiles analysis.*

	Lubrication extent k [dm]
New sample 1	60
New sample 2	300
New sample 3	600
New sample 4	1000

Once these known-k blends are subjected to the compactor simulator, the correspondent tablets properties are analyzed and compared to the feed frame samples ones, with the aim of investigating the over lubrication state provided to the powder by the feed frame presence. Further details about are provided later on.

2.5 Shear cell flow data

The flow of powders in process equipment is a complex and challenging area of study, as it can change significantly during a process depending on the operating conditions and consequently affect the quality of the final product. In the absence of a unified framework for describing powder flow behavior, the collection of experimental data and the use of empirical correlations are fundamental to gaining adequate knowledge of the powders under investigation. To this end, a flow function and a wall friction test are carried out on powder samples of blends 1, 2 and 3 before and after subjecting them to a feed frame.

2.5.1 Flow function test

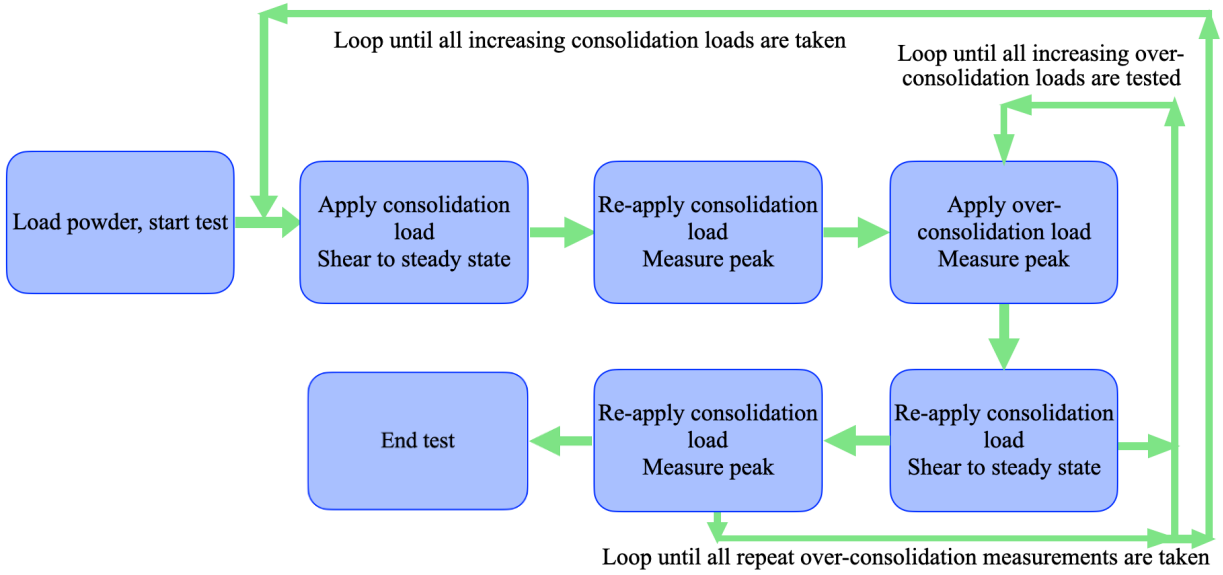

Fig. 2.10. *Flow function test algorithm followed in Brookfield PFT.*

For the flow function test, Small Vane Lid 304 S/S (5 cc, 5-in. dia.) and Small Trough (38 cc, 5-in. dia.) are used as PFT equipment, with an axial speed of 1mm/sec and torsional speed of 1 rev/hr. Five initial consolidation stresses are tested (1.06, 1.69, 2.66, 4.20,6.63 kPa) for each sample, using geometric spacing between each stress and applying three over-consolidation stresses at each stress. A brief scheme of flow function test algorithm employed is reported in Fig. 2.10. As the data contained in this dataset are collected automatically after the above conditions have been set, specific details of the shear cell data collection procedure are beyond the scope of this study, but further information can be found in the work of Schulze (2021). As a result of each flow function test, a summary table is provided showing the most useful data for the purposes of this flowability analysis. For each of the five initial consolidation stresses, a corresponding major principal consolidation stress and unconfined yield strength are given, which can be plotted together to give the powder flow function value. Details of cohesion, density and effective angle of internal friction are also provided.

2.5.2 Wall friction test

For running the wall friction test, seven stresses are tested for each powder sample by using two displacement levels evenly spaced. The lid used in the Brookfield PFT is the Small Wall 304 S/S, 2B Finish (5-in. dia.), while the trough employed is the Small Trough (38 cc, 5-in. dia.), with an axial speed of 1mm/sec and a torsional speed of 1 rev/hr.

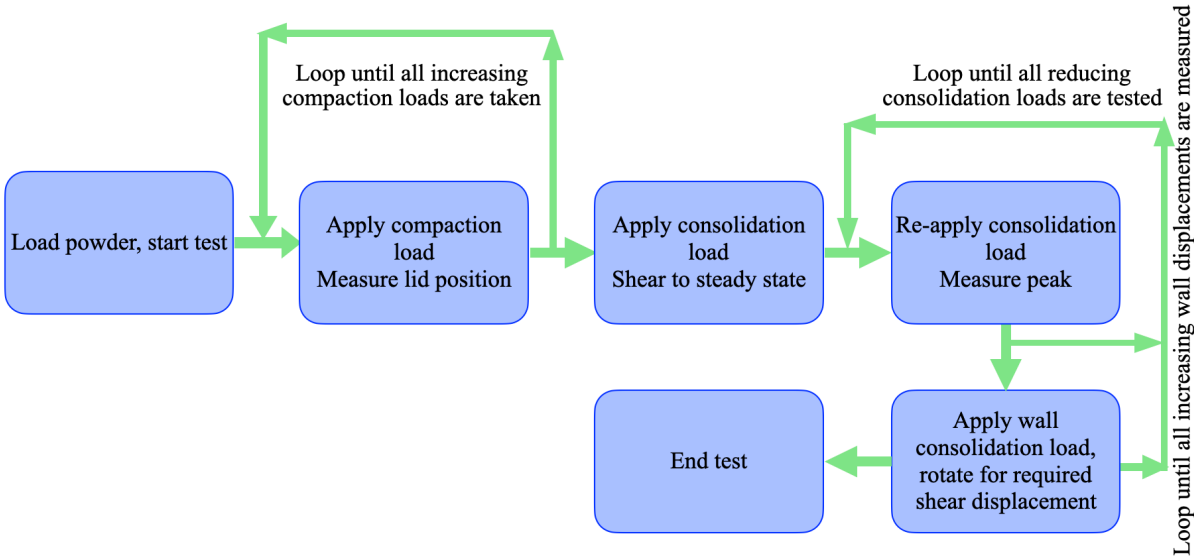

Fig. 2.11. *Wall friction test algorithm followed in Brookfield PFT.*

A brief scheme of flow function test algorithm employed is reported in Fig. 2.11. The wall friction angles obtained for each stress applied, which represent the sliding angles under normal flow for a given bulk solid against a wall surface, describe the resistance present between the

powder and the stainless steel wall of the equipment used. In addition, the data obtained on the initial bulk density of the powder, consisting of the freely settled bulk density of the powder and the maximum density recorded after shear compaction, are used to determine the compressibility index and the Hausner ratio of the samples tested, providing a clear and representative way of describing and comparing the flowability of the powders studied.

Chapter 3

Mathematical background

Machine learning methods are largely employed in pharmaceutical industry for evaluating data, discovering patterns and trends that allow to make appropriate decision to improve production and product quality (Vamathevan et al., 2019). One of the most popular, used in this study for preliminary data analysis, is principal component analysis (PCA), an unsupervised methodology consisting in a dimensionality reduction exploited to manage large data sets, identifying at the same time main relationships among variables. Partial least-squares (PLS) models are then described, since they allow to identify main predictors (variables) determining a desired response, giving information about which settings are more appropriate to modify in order to reach a target. Analysis of variance (ANOVA) is finally presented, as it will be used for evaluating qualitatively the actual impact of some factors on a response of interest, namely tablet weight in this study. The quantitative evaluation is instead provided through response surface methodology.

3.1 Quality-by-design implementation through latent-variable models

Nowadays, the use of systematic and science-based approaches has a key role for supporting pharmaceutical development and manufacturing activities, contributing to the practical implementation of the quality-by-design paradigms. Ohage et al. (2016) highlight that, according to QbD, the proactive design of pharmaceutical manufacturing process and controls must be enhanced to consistently deliver the intended performance of the product, through an extensive mechanistic understanding of the relations between the product quality and the parameters that can have an impact on it. Latent-variable (LV) models can be used for that, resulting to be useful in any product development phase for a deeper understanding of product and process design, process improvement and optimization and control. They are designed to identify significant correlations among real data to describe the behavior of a system in a reduced number of variables (called LVs), which account for the systematic part of the variability of the data. Tomba et al. (2013) suggest that these models are effective also when a limited amount of samples is available, so that they are particularly suitable with product and process development in companies, like pharmaceutical ones, which are often not “data-rich” organizations.

Among the most common LV models employed, PCA and PLS are used in this study, allowing one, after an appropriate dataset organization, to identify the main driving forces acting on a system and providing a clear and deep understanding of the analyzed processes. In the following, a detailed description of the above-mentioned models is provided.

3.1.1 Principal component analysis (PCA)

This is one of the most successful multivariate statistical techniques used for exploring dominant information patterns in the data. As described by Tomba et al. (2013), it consists on finding the directions of maximum variability of the data, transforming correlated original variables (online process measurements, raw material characteristics, product features, etc.) into sets of linearly uncorrelated variables called *principal components (*PCs*)*. Harvey and Handson (2022) explain that PCA is essentially a process of rotating the original set of V axes, which correspond to the V variables we measured, until we find a new axis that explains as much of the total variance as possible. This becomes the first PC axis. We then project the data onto the $V- 1$ dimensional surface that is perpendicular to this axis and repeat this process of rotation and projection until the original V axes are replaced with a new set of A PC axes. The first PC is the one explaining the major part of the variability, while each successive one, found through iterative extraction procedures or alternatively by exploiting appropriate algorithms, does not correlate with the previous ones and expresses the remaining part of the variability. The representation of the original observations in a low-dimensional space, typically 2-5 PCs, gives a convenient overview of the data available with a minimum loss of information, describing the main driving forces of the system under study. An example of PCA working mechanism is provided in Fig. 3.1.

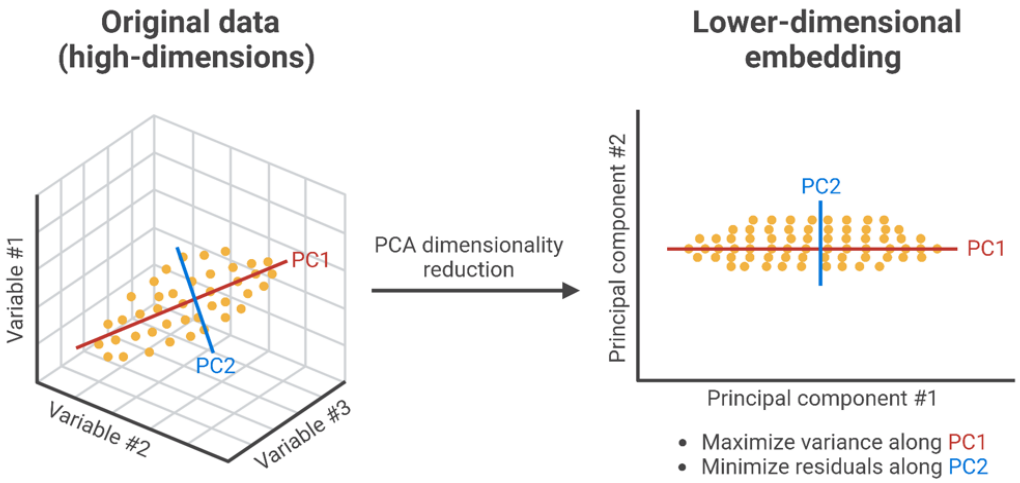

Figure 3.1. *Principal component analysis transformation of the original variables space in a low-dimensional space of artificial variables (https://learnche.org/pid/latent-variable-modelling/principal-component-analysis)*

Mathematically, PCA finds the directions of maximum variability of the data matrix **X**, with *N* rows and *V* columns ($N \times V$), maximizing the covariance matrix of the process variables. Wise and Gallagher (1996) discuss the theoretical derivation of PCA, starting from the definition of the covariance matrix:

$$\mathbf{cov(X)} = \frac{\mathbf{X^T X}}{\boldsymbol{N-1}} \tag{3.1}$$

The original matrix **X**, containing the variables whose correlations must be investigated, is expressed by the PCA model as:

$$\mathbf{X = TP^T + E} = \sum_{a=1}^{A} \mathbf{t_a p_a}^{\mathbf{T}} + \mathbf{E} \ , \tag{3.2}$$

where **T** is the score matrix $N \times A$ containing the projection of the *N* observations in the *A*-dimensional space defined by the *A*-principal components (where $A \leq \min\{N, V\}$), **P** is the matrix $V \times A$ of the loadings and **E** is the residual matrix, accounting for the reconstruction error of **X**. Note that for any pair $\mathbf{t_a}, \mathbf{p_a}$, $\mathbf{Xp_a} = \mathbf{t_a}$, since the score vector is a linear combination of the original **X** data defined by $\mathbf{p_a}$. From the study of Wise and Gallagher (1996) it can be derived that the analytical solution of the above mentioned maximization problem is the same as the one of the eigenvector problem, since $\mathbf{p_a}$ vectors are eigenvectors of the covariance matrix, i.e. for each $\mathbf{p_a}$:

$$\boldsymbol{cov}(\mathbf{X})\mathbf{p_a} = \lambda_a \mathbf{p_a} \ , \tag{3.3}$$

where λ_a is the eigenvalue associated with the eigenvector $\mathbf{p_a}$ and provides an indirect measure of the variance explained by the product $\mathbf{t_a p_a}^{\mathbf{T}}$. This means that the optimal linear projection for which the variance of the projected data is maximized is now defined by the eigenvectors of the data covariance matrix **X** corresponding to the largest eigenvalues and that will be consequently chosen as PCs. Solving the eigenvector problem is one of the most popular and widely used methods for finding principal components for PCA model construction, but there are many other useful approaches such as singular value decomposition, iterative and probabilistic methods that can be exploited for it. Once the principal components have been identified, the number (*A*) of them to be selected to build the model is usually determined through cross-validation or rules of thumb (Mardia et al., 1979; Valle et al., 1999). If we now provide a geometric interpretation of PCA, it can be said that the scores define the location of the original samples in the coordinates of the newly discovered principal component axes, while loadings give an indication of the location of the principal component axes with respect to the original axes. As can be seen in Fig. 3.2, each principal component is defined by the cosine of its angle of rotation with respect to each of the original axis. Once identified the angle of rotation

of the PC to the axis for variable 1 and 2, the cosine of the angle correspond to a loading which describes how a variable contributes to the principal component.

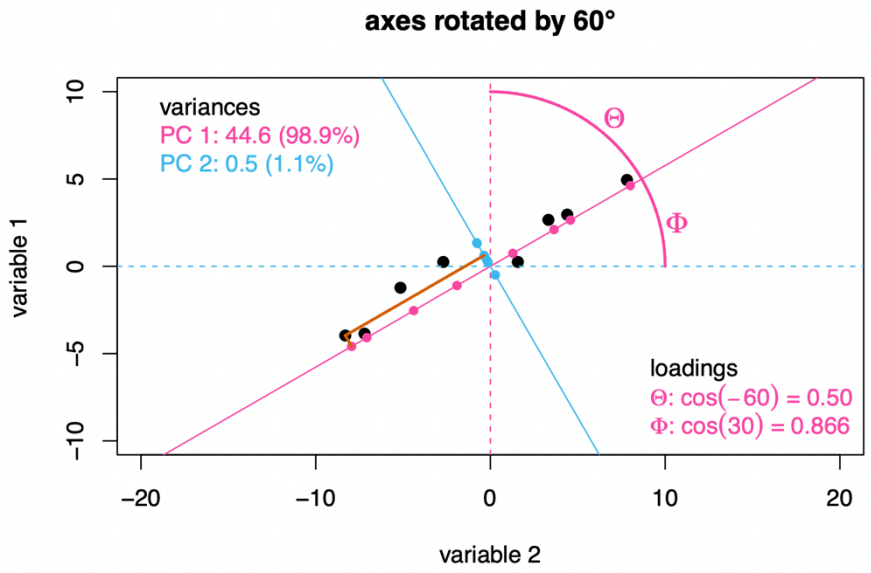

Figure 3.2. *Representation of the relationship existing between original variables and first principal component through the loadings (Harvey and Handson, 2022).*

Loading vectors, describing the direction of the principal components in relation to the original variables, express the correlations among variables for the percentage of variability explained by the considered PC. The sign of a loading determines how a variable contributes to the principal component: a positive loading indicates that an increase of a variable is correlated with an increase of all the other variables that can be found in the positive side of the loading plot, while the same variable decreases for an increase of the variables that can be found in the negative part of the loading plot. On the other hand, the score vectors, indicating the direction of the principal components in relation to the observations, describe similarity among the observations in the new latent variable space.

3.1.2 Projection on latent structures (PLS)

PLS is a linear multivariate statistical method combining the advantages of integrating principal component analysis and linear regression analysis. Abdi (2007) suggest that it is particularly useful when it is needed to predict a set of dependent variables from a large set of independent variables (predictors), because it reduces the variables, used to predict, to a smaller set of predictors, which are actually included in the regression.
It relates in this way two data matrices:

- **X** $[N\ observations \times V\ variables]$, including settings and process variables

- **Y** $[N\ observations \times M\ variables]$, which are quality/response variables,

by exploiting the ability of multivariate projection methods to analyze noisy and collinear data identifying the directions of maximum variability of **X** that best predict **Y**.
It has a large variety of applications, like estimation and prediction as soft sensing, process monitoring, design and transfer of process and products on different scales and production sites, process and product optimization, response surface modelling in DOE and instrument calibration (Facco, 2024).
As well as in PCA, **X** matrix is decomposed as described in Eq. 3.2, but in addition also **Y** matrix is similarly decomposed:

$$\mathbf{Y} = \mathbf{U}\mathbf{Q}^{\mathbf{T}} + \mathbf{F} = \sum_{\mathbf{a=1}}^{\mathbf{A}} \mathbf{u_a}\mathbf{q_a}^{\mathbf{T}} + \mathbf{F} \tag{3.4}$$

where **U**, **Q** and **F** are respectively the scores, loadings and residuals matrices of **Y**. The decomposition problem is solved through appropriate algorithms. For further information about, it is suggested to refer to the work of Geladi et al. (1986). Dunn (2023) clearly explains that differently from PCA, PLS works not only in catching the directions of maximum variability of **X**, but on the transformation of **X** data in order to maximize the covariance of its latent variables with **Y** dataset (Fig.3.3).

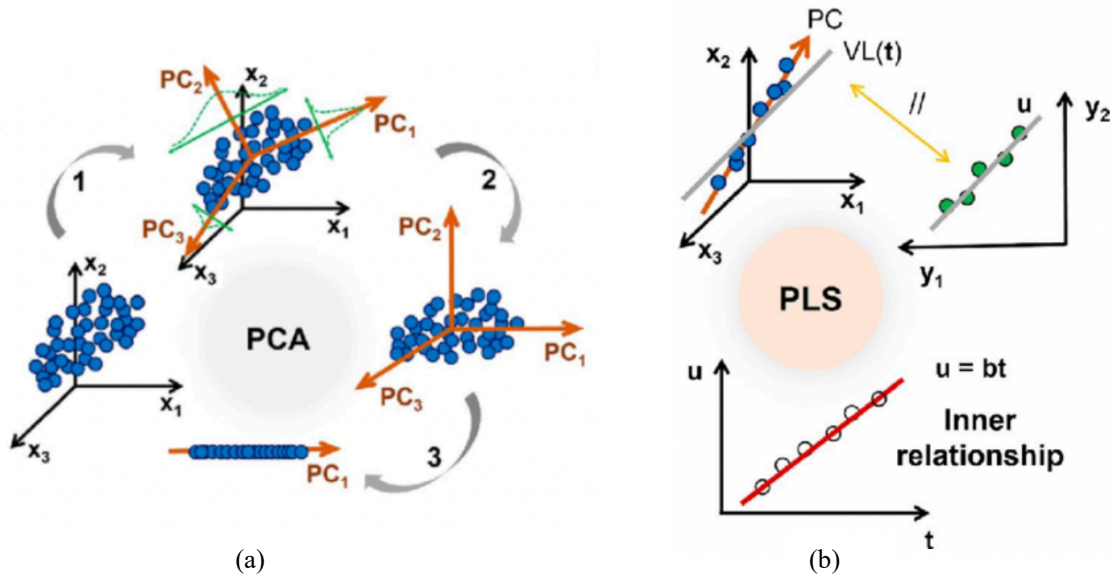

(a) (b)

Figure 3.3. *In (a): 1) PCA with estimate of PCs, 2) subsequent representation of the new space and 3) projection of real data on it; in (b) PLS graphical representation maximizing the correlation between X and Y ((Santos et al.,2023).*

As anticipated in Fig. 3.3, PLS model finds regression coefficients that define the linear relation among the score space of **X** matrix (**t**) and the one of **Y** matrix (**u**), explaining the relationship between independent and dependent variables in the new latent space:

$$\mathbf{u} = \mathbf{bt} \tag{3.5}$$

Non-linear versions of PLS are sometimes needed and they can be built changing the above-mentioned equation. PLS defines a new vector space, that is a subspace of the previous one, in which original data are represented. Loading, score and residual matrices contain all the information to draw this new space with its own observations and quantities. Scores in PLS are interpreted as PCA ones, allowing one to recognize similarities and differences among observations through the identification of clusters, outliers and patterns in the line plot of scores. But differently from PCA, where loadings are the main descriptors of correlations among variables, in PLS it is more appropriate to refer to the weights (**W**), which represent the coefficients of the linear combination of **X** determining the scores (**T**), as shown in Eq. 3.6 and 3.7, and needed to make these last orthogonal to each other (Geladi et al.,1986):

$$\mathbf{T} = \mathbf{X}\mathbf{W}^{*} \tag{3.6}$$

$$\mathbf{W}^{*} = \mathbf{W}(\mathbf{P}^{\mathbf{T}}\mathbf{W})^{-\mathbf{1}} \tag{3.7}$$

Plotting the weights is very powerful because they allow to superimpose the loadings plots for the **X** and **Y** space simultaneously. In this way, we do not only see the relationship between the **X** variables, but also their relationship between the **Y** variables (Dunn, 2023). We usually prefer to refer to **W*** rather than **W** when investigating the relationships in a PLS model, since **W*** directly expresses the relationship between the score vectors **t** and the original matrix **X**, whereas **W** relates **t** to the deflated data resulting from the iterative procedure of the Nipals algorithm for PLS model construction, making the interpretation of the scores difficult. For further investigation about the differences between **P**, **W** and **W***, Dunn (2023) study is recommended.

3.1.3 Data pretreatment

Before proceeding with PCA or PLS, it is often necessary to operate a data pretreatment in order to avoid that the variability extracted by the models is affected by the different scales of data collected. In this study, before each PCA or PLS model construction, variables are weighted in the same way by applying autoscaling, consisting of two subsequent steps as explained by Gallagher and Shaver (2015):

- mean-centering: mean of each column *V* of matrix **X** is subtracted by all terms of the same column, in order to avoid that the LV models identify as significant directions of variability in the data the differences among variable mean values.

- scaling to unit variance: each column of **X** matrix is divided by its standard deviation, essential to make the analysis independent of the units of the variables.

It is clarified that the most appropriate methodology for data pretreatment can vary depending on the data and the type of application of the study. In this case, the above-mentioned procedure is sufficient in order to treat efficiently data available. After autoscaling, it is possible to build the most informative model depending on the purposes of the analysis, investigating the correlations among variables from the loadings based on auto-scaled data.

3.2 Data unfolding techniques for dynamic analysis of data

As discussed in Chapter 2, tablets data are collected at different time instants (0, 5 and 10 min), meaning that the structure of the data corresponds to a three-dimensional array or cube, including the run observations *I*, variables *J* and time interval *K*. In order to model these data and capture their dynamic time dependence, it is necessary to unfold the data array into a two-dimensional matrix. PCA or PLS can be then applied to these matrices and model them to explain the maximum variance or covariance with the fewest possible number of latent variables. Chai et al. (2013) specify that each method of unfolding provides a different matrix with a different structure and a different dimension with respect to the original one, but the batch-wise unfolding technique (or better, in this case, the run wise unfolding one) is the most applied one, since it allows to express the run dynamics referring to the mean time trajectory of variables. Data are unfolded into a two-dimensional structure, maintaining the run direction and unfolding the variable and time ones (Fig. 3.4). In this way, each row contains the information about a single run, capturing the variable correlations both within time and time-to-time; both cross-correlated and self-correlated relationships in process data are so expressed.

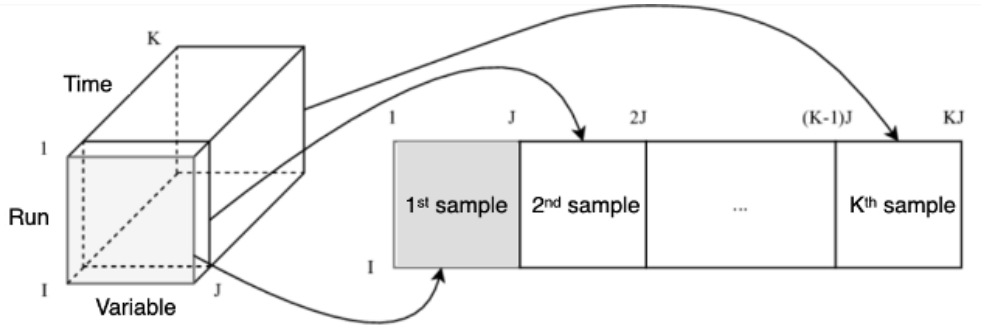

Figure 3.4. *Run wise unfolding procedure used to reduce matrix dimension for PCA and PLS analysis.*

Applying PCA or PLS to this unfolded matrix is therefore modeling the time-varying behavior of the runs as a locally linear dynamic model with all the variables at every sample time, as investigated by Chai et al. (2013). The models built after this unfolding contain data dynamic

information in the loading plot, which express the time trajectories of each variable and determine their importance on data variability. The score plot, as well as seen before, continues to describe the relationship among observations (replicates of runs), since each point in it represent a synthesis of all variables time trajectories of each run for the entire time considered.

3.3 Analysis of variance (ANOVA)

Analysis of variance is a statistical method used to simultaneously compare means of several data groups to determine if the observed difference are due to chance or if actual distinctions are present (Smalheiser, 2017). This is done by comparing variability recorded by applying different treatments/levels of some main factors (variability between treatments) and variability of repeated measures at the same treatment (variability within treatments). ANOVA can handle multiple factors, varied on different levels, providing a robust way to identify their relationships with each other and with dependent variables of interest.

3.3.1 The ANOVA table

The fundamental ANOVA identity is made of two contributions that provide the total variability:

$$SST = SS_{treatment} + SS_{error} \tag{3.8}$$

where *SST* is the total sum of squares, $SS_{treatment}$ is the sum of square of the difference between treatment averages and grand average and SS_{error} is the sum of squares of differences of observations within treatments from the treatment average (the random error).

In mathematical form, Eq. 3.8 can be rewritten as:

$$\sum_{i=1}^{a}\sum_{j=1}^{n}(y_{ij}-\bar{y}_{..})^2 = n\sum_{i=1}^{a}(\bar{y}_{i.}-\bar{y}_{..})^2 + \sum_{i=1}^{a}\sum_{j=1}^{n}(y_{ij}-\bar{y}_{i.})^2 \tag{3.9}$$

with:

- y_{ij}: single observation j under the i-th treatment
- $\bar{y}_{i.}$:average of the observations under the i-th treatment
- $\bar{y}_{..}$:grand average of all observations
- n :total number of observations for treatment i
- a: total number of treatments

The comparison of the mean squares of the above-mentioned sum of squares (obtained by dividing them for the respective degrees of freedom) through an F-test is used to determine if actual difference among treatment means is present. The output of the test is an ANOVA table (an example is given in Table 3.1) showing how the sums of squares are distributed according to the source of variation, and hence the mean sum of squares (Brereton, 2018). For each factor examined, an F-test value and a corresponding *p-value* are reported. The latter can be used as an indication of whether or not the null hypothesis of the F-test (equality of treatment means) should be rejected. As an indication, a significance level of 0.05 is chosen, as values of $p \leq 0.05$ indicate that the null hypothesis should be rejected, i.e. that a factor does have an effect on the response.

Table 3.1. *Example of ANOVA table providing sum of squares (SS), mean squares (MS), degrees of freedom (DF) and F statistic values for a single factor evaluation.*

	SS	**DF**	**MS**	**F-value**	**P-value**
Treatment	SStreatment	a-1	MST=SST/(a-1)	MST/MSE	$> or \leq 0.05$
Error	SSerror	N-a	MSE=SSE/(N-a)		
Total	SST	N-1			

It is important to note that ANOVA provides qualitative information about the relationship between a factor and a variable of interest, determining only whether or not the latter is properly dependent on it. The quantitative way in which a factor influences the response must be further assessed by the use of response surfaces.

3.4 Response surface design

Response surface methodology (RSM) is a collection of statistical and mathematical techniques useful for developing, improving, and optimizing processes. It also has important applications in the design, development, and formulation of new products, as well as in the improvement of existing product designs. It exploits quantitative data from appropriate experimental designs to explore the space of the process or independent variables developing an appropriate approximating relationship between independent variables and a response of interest, dependent on them. Data collection procedure is crucial for a robust statistical analysis and meaningful insights on the variable relationships within the experimental domain. A meticulous and systematic data acquisition, performed through planned experimental runs and precise collection of the corresponding responses, allows to capture accurately the interactions between process variables and response variables. The relationships between them are represented in a graphical way as response surfaces, which have three main purposes (Raymond and Montgomery, 2016; Özkal et al., 2005):

- to determine how process variables affect the response.
- to determine the inter-relationships among different process variables.
- to describe the combined effect of all process variables on the response.

The response function *f*, expressing the dependence of the response (η) on the independent variables (x_1 and x_2 for example) considered, is usually approximated by using low-order polynomials, like first order (Eq. 3.10) or second order (Eq. 3.11) ones:

$$\eta = \beta_0 + \beta_1 x_1 + \beta_2 x_2 + \beta_{12} x_1 x_2 \tag{3.10}$$

$$\eta = \beta_0 + \beta_1 x_1 + \beta_2 x_2 + \beta_{11} {x_1}^2 + \beta_{22} {x_2}^2 + \beta_{12} x_1 x_2 \tag{3.11}$$

where the final term of both equations describes the interaction between the test variables x_1 and x_2. It must be noted that adding an interaction term introduces a curvature on the response surface (Fig. 3.5). When the curvature in the true response surfaces is strong, as it happens in most real cases, first order model is not appropriate to use, and the second order one is required.

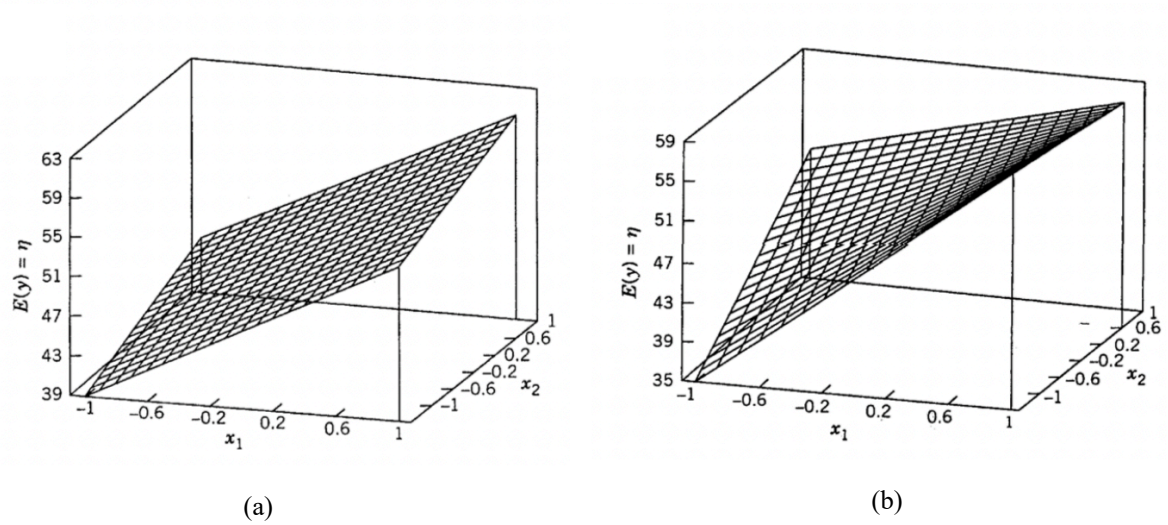

(a) (b)

Figure 3.5. *Response surface (a) for a first order model including only main effects and (b) for a first order model with interaction term (b) (https://online.stat.psu.edu/stat503/lesson/11).*

Second order models are very flexible and suitable for use when response optimization is required, as they approximate well the narrow region of the design space where curvature is present. Another useful graphical tool often used to present the results of response surface design is the contour plot, a two-dimensional view in which all points that have the same response are connected to produce contour lines of constant responses. The contour plot is closely related to the shape of the response surface because it is actually a graphical representation of it, holding constant the *z*-slices (i.e. contours) and drawing lines to connect

the coordinates at which a chosen *z*-value occurs. An example of a contour plot related to the response surface found by RSM is shown in Figure 3.6.

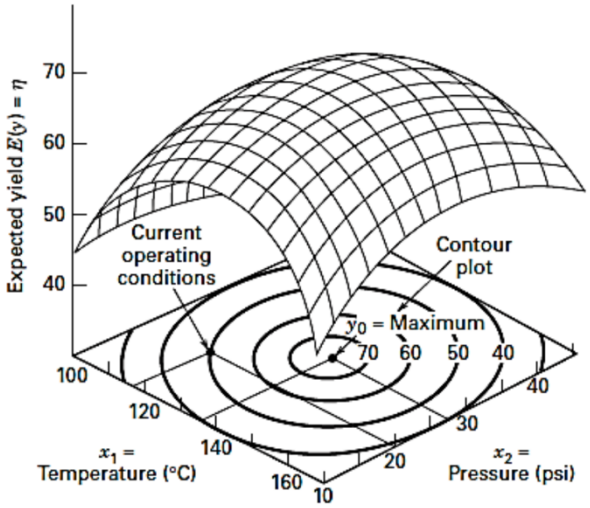

Figure 3.6. *Contour plot of a response surface (https://jaeronline.com.-Response-Surface-Methodology)*

RSMs are constantly evolving and have a wide range of applications, capable of handling complex systems and providing the knowledge to optimize them. In fact, mapping a response surface over a particular region of interest not only allows the relationships between multiple factors and a response variable to be understood, but also allows changes in a response variable to be predicted in advance by adjusting some key factors. Furthermore, knowledge of this relationship allows the appropriate selection of operating conditions to meet specifications and requirements.

Chapter 4

Results and discussion

The compression settings used in a rotary press have a strong influence on the final tablet quality. For this reason multivariate statistical analysis is used to capture such correlations. Starting with a preliminary analysis that takes into account all the tablet characteristics collected, the focus is on the structure of the weight data in particular. It is also known that the effect of the feed frame speed affects the lubrication state of the powder (Ketterhagen, 2015), and a method for assessing the increase in the lubrication extent coefficient is proposed. Finally, the previous findings are related to the flow properties of the powders considered.

4.1 Tablets properties exploratory analysis

The first step is to understand how the final tablet properties are related to the main compression settings used in Dataset 1. The settings in the dataset are namely fill depth, feed frame speed and main compression force. To do this, a PCA model is built for each blend using an appropriate matrix that takes into account all replicates collected at each time point in each run. It is recalled from §2.3.1 that for blends 1 and 2 the dataset contains data from sixty tablets for run 2, sixty for run 3 and sixty for run 5, which include ten replicates per run time at 13 kN and ten replicates for each other main compression force applied. The total number of observations considered is 180, which will be the number of rows in the matrix. In contrast, for blend 3, the number of observations increases, up to 299, because additional replicates are made, which also vary the rotor speed. The diagnosis of the PCA models built is reported in Table 4.1, while the process variables and tablet properties whose relationship must be investigated are described in Tables 4.2 and 4.3.

Table 4.1. *Diagnostics of the PCA models built on Dataset 1.*

	Matrix dimension [NxV]	N° of PCs	Explained variance
Blend 1	180×11	3	98.0 %
Blend 2	180×11	3	99.2 %
Blend 3	299×12	4	98.7 %

Table 4.2. *Compression settings and tablet properties from Dataset 1 used as variables to perform PCA for blend 1 and 2.*

N.	Variable
1	Fill depth [mm]
2	Feed frame speed [rpm]
3	Main compression force [kN]
4	Weight [mg]
5	Thickness [mm]
6	Hardness [kp]
7	Tensile strength [MPa]
8	Width [mm]
9	Volume [mm^3]
10	Density [g/cm^3]
11	Solid fraction [-]

Table 4.3. *Compression settings and tablet properties from Dataset 1 used as variables to perform PCA for blend 3.*

N.	Variable
1	Fill depth [mm]
2	Rotor speed [rpm]
3	Feed frame speed [rpm]
4	Main compression force [kN]
5	Weight [mg]
6	Thickness [mm]
7	Hardness [kp]
8	Tensile strength [MPa]
9	Width [mm]
10	Volume [mm^3]
11	Density [g/cm^3]
12	Solid fraction [-]

The score plots, providing an indication of the behavior similarities among the observations considered, suggest that feed frame speed and compaction force applied are the main reasons of variability between the collected tablet properties. In fact, it can be seen from Fig. 4.1 that for all blends four clusters of observations can be distinguished at each level of feed frame speed, corresponding to different compaction forces used to run the tableting process. It can be also noted that for all blends the runs performed at 15 and 30 rpm feed frame speed and 13 and 16 kN compression force are always found together in the positive part of the first PC, meaning that their behavior is similar and described by the correspondent loading plot. On the other hand, PC 2 describes mainly the differences between clusters at 30 and 45 rpm for blend 2 and blend 3, while for blend 1 it is more representative of the differences between clusters at 15 and 45 rpm. One other notable thing is that while all clusters of observations at 45 rpm are described

by the positive part of PC 2 for blend 2 and 3, for blend 1 the cluster at 13 kN is the only one in the positive part of PC 2, behaving in an opposite way with respect to the others at 45 rpm. In addition to this, the above mentioned cluster is also more dispersed with respect to the other blend clusters at 45 rpm, meaning that in blend 1 at highest feed frame speed there is the highest replicates variability.

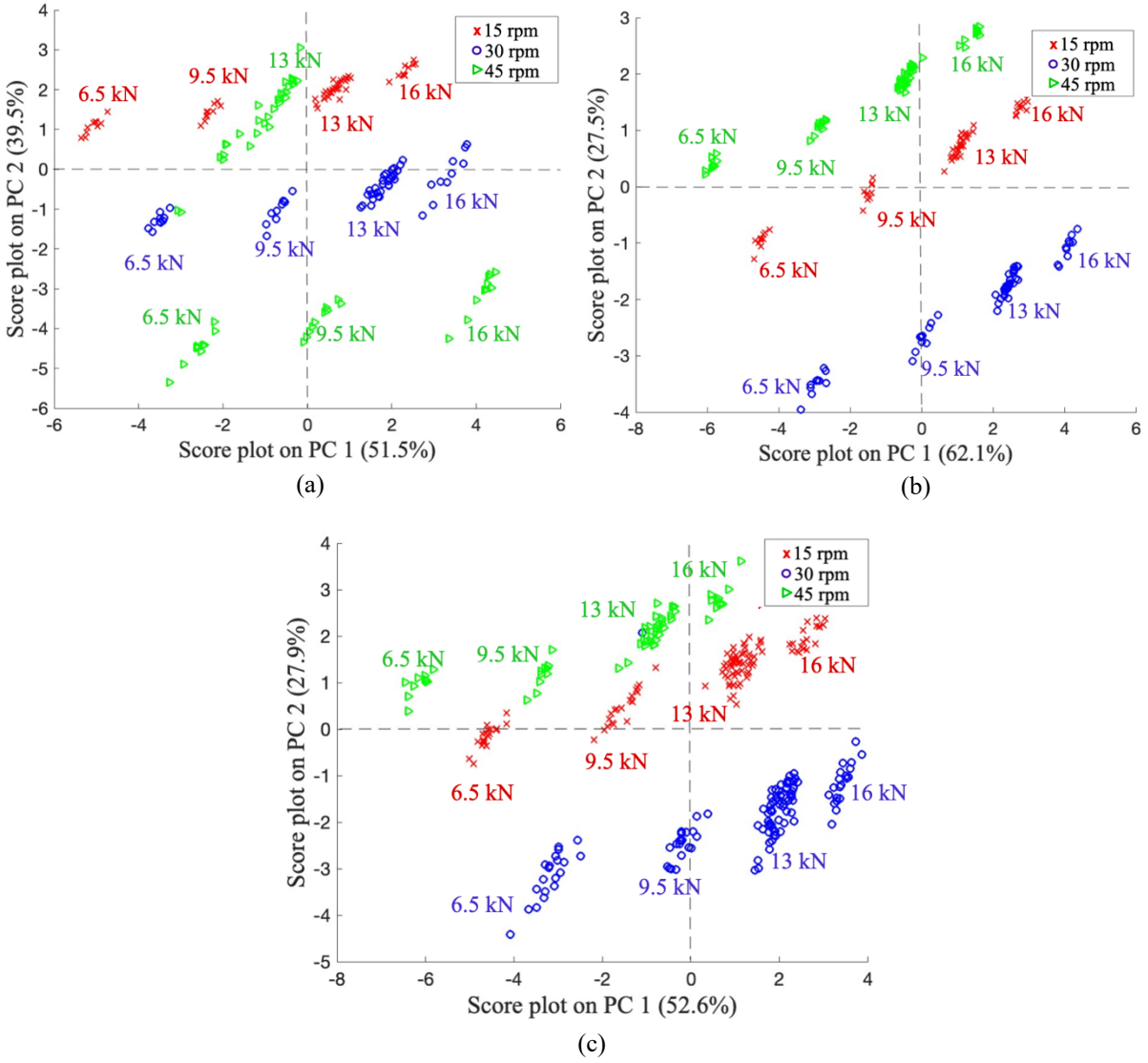

Figure 4.1. *Score plot built on Dataset 1 including data of all compaction forces applied for (a) blend 1, (b) blend 2 and (c) blend 3.*

Observing the loading plots on the first two PCs, explaining most of the variability, common findings among blends are derived (Table 4.2 for variables identification). Starting from blend 1 and 2, there seem to be two main correlations between the variables studied:

- force-volume based relationship: fill depth, weight, thickness, width and volume change together and in an opposite way with respect to main compression force, hardness, tensile strength and solid fraction (Fig. 4.2(a) and 4.3(a)).
- weight-fill depth relationship: weight is increased by fill depth, also when feed frame speed is lower (Fig. 4.2(b) and Fig.4.3(b)).

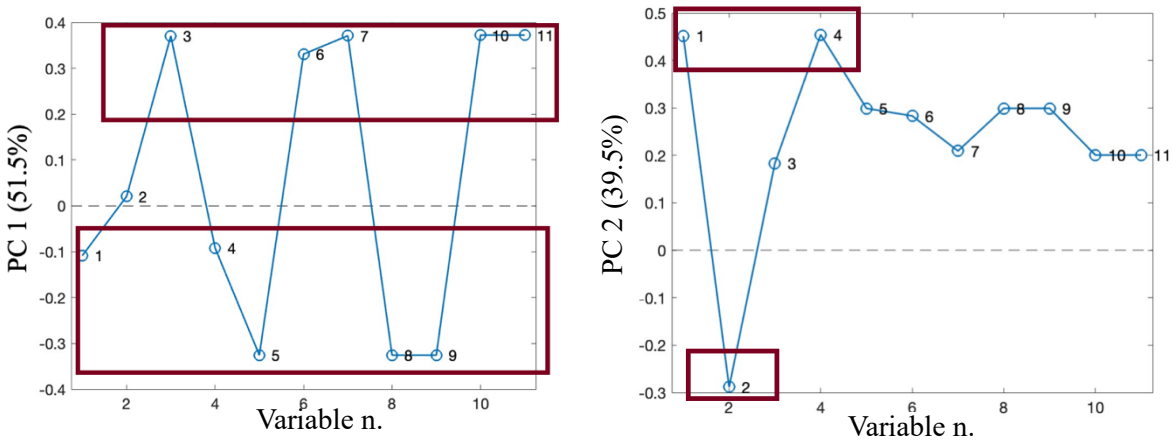

(a) (b)

Figure 4.2. *Loading plot on (a) PC 1 and (b) PC 2 of the PCA model built on Dataset 1 for blend 1.*

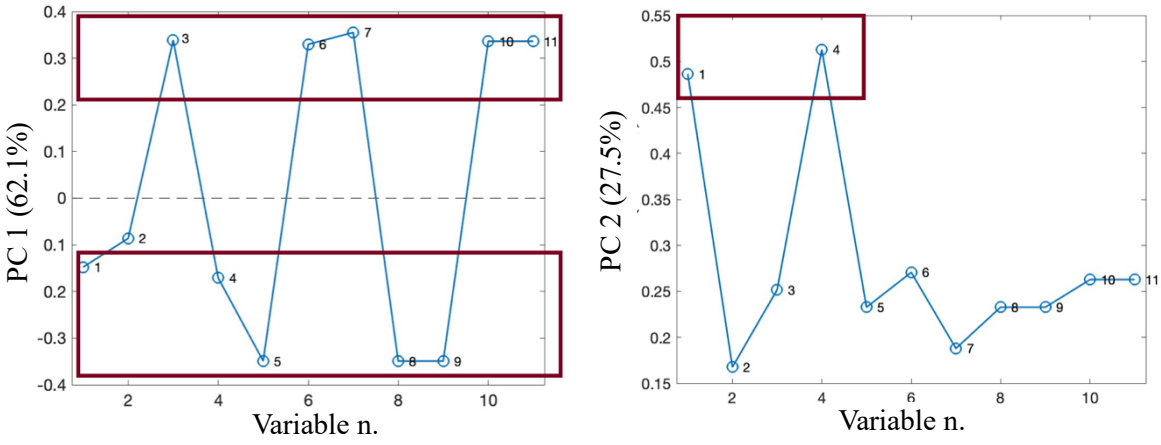

(a) (b)

Figure 4.3. *Loading plot on (a) PC 1 and (b) PC 2 of the PCA model built on Dataset 1 for blend 2.*

For blend 3, an additional compression setting has to be considered, as for this blend the rotor speed is also varied to find its effect on the tablet properties (see Table 4.3 for variable identification).

The main relationships (force-volume based and weight-fill depth ones) found for blends 1 and 2 are valid also for blend 3 (Fig. 4.4). The additional information provided here is that rotor speed has not an actual influence on general correlations found between variables neither in PC 1 nor PC 2 loading plots. It can be concluded that, for the 90% variability expressed by the model for blend 1 and 3 and 80% for blend 2, variables of the two above-mentioned groups

vary together, for that greater fill cam corresponds to greater weight, thickness, width and volume, while greater compression force results in greater hardness and tensile strength. In addition to this, the 50% variability of data suggests that when weight, thickness, width and volume are greater, hardness and tensile strength are smaller.

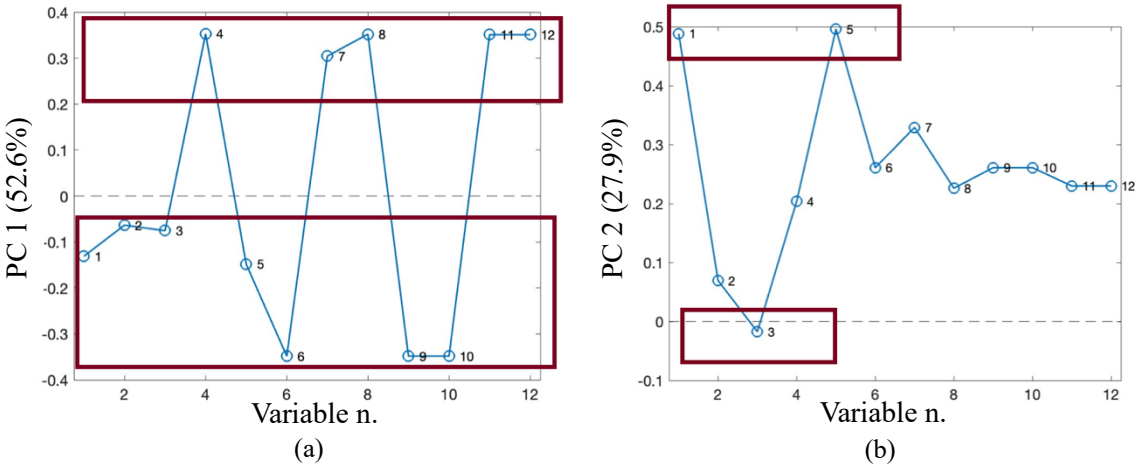

Figure 4.4. *Loading plot on (a) PC 1 and (b) PC 2 of the PCA model built on Dataset 1 for blend 3.*

Furthermore, rotor speed doesn't seem to affect significantly tablets properties relationships, at least for blend 3. These are preliminary considerations on tablets properties relationships between each other and with compression settings, valid in general for all blends. It is now appropriate to go deeper into the topic by considering each blend behavior separately. It should also be remembered that the data on tablets were collected at different times for each set of compression settings; therefore, the subsequent models to be built will also take into account the dynamic time dependence of the data, in order to evaluate whether the time evolution is significant in determining the tablet properties.

4.2 Time dependence of tablet properties

Tablets properties are collected for each run at three different time instants (every 0, 5 and 10 minutes), assuming for each of them steady state conditions.
The dynamic dependency of tablet properties will be assessed to understand if there are consistent changes in them as time progresses.

4.2.1 Weight and compression force trend in time

The speed of the feed frame plays an important role in determining the weight during the compaction process, as it is responsible for the uniform distribution of the powder in the die cavities. A first assessment of the effect of feed frame speed on mean weight and compression force trend can be made by comparing two runs, 2 and 5, in which all compression settings are

identical except for the feed frame speed. It must be specified that weight appearing in the following plots is a mean weight calculated above all weight data available for each time instant in Dataset 1.

4.2.1.1 Blend 1

Even though a greater weight should be achieved with a higher feed frame speed (Mendez et al.(2010)), it can be seen from Figure 4.5 that at t=0 the weight is smaller than expected at 45 rpm, while after 5 min it increases and remains approximately constant until the end. At the same time, the main compression force increases after time 0 and then remains constant. This increase may be due to the inability of the machine to reach a steady state and therefore the steady state compression force, and this may be due to flowability problems of the powder, as will be seen in section §4.5.

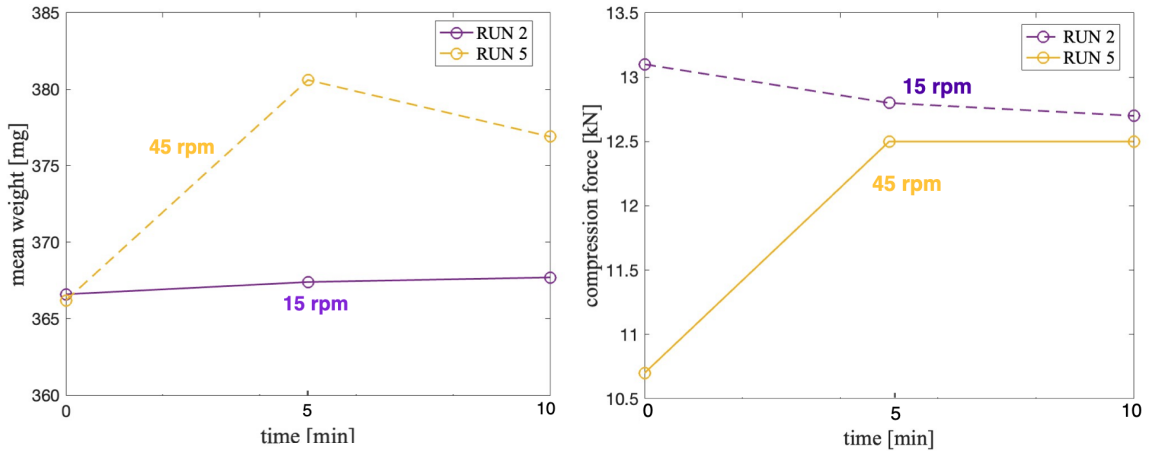

(a) (b)

Figure 4.5. *(a) Weight and (b) compression force profiles over time in Dataset 1 at feed frame speed of 15 rpm (run 2) and 45 rpm (run 5) for blend 1.*

4.2.1.2 Blend 2

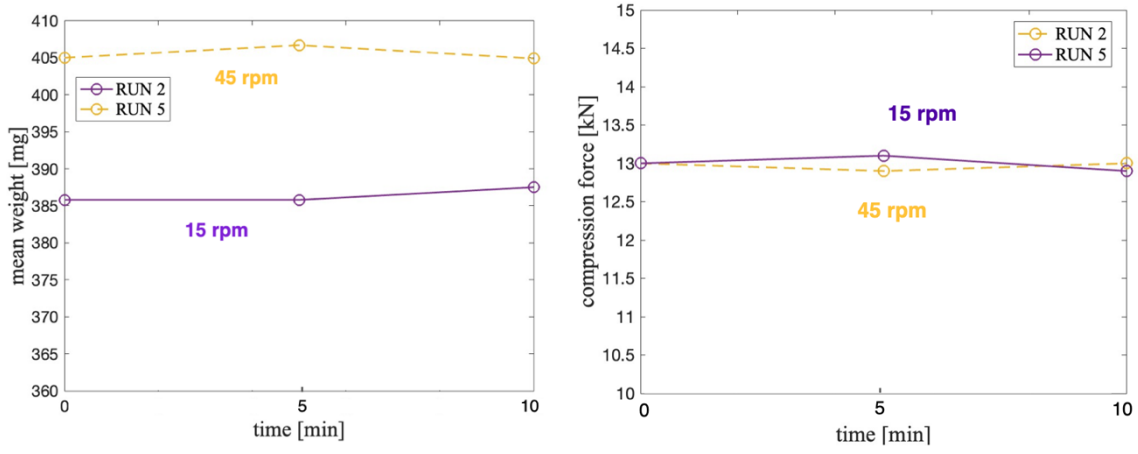

(a) (b)

Figure 4.6. *(a) Weight and (b) compression force profiles over time in Dataset 1 at feed frame speed of 15 rpm (run 2) and 45 rpm (run 5) for blend 2.*

For this compound, the weight is greater at the higher feed frame speed from the beginning of the run and remains approximately constant throughout (Fig. 4.6(a)). The compression force also remains constant (Fig.4.6(b)), confirming that blend 2 has good flowability even at the higher feed frame speed considered, as confirmed in §4.5.

4.2.1.3 Blend 3

Run 2 and 2A are performed with the same compression settings except for rotor speed (49

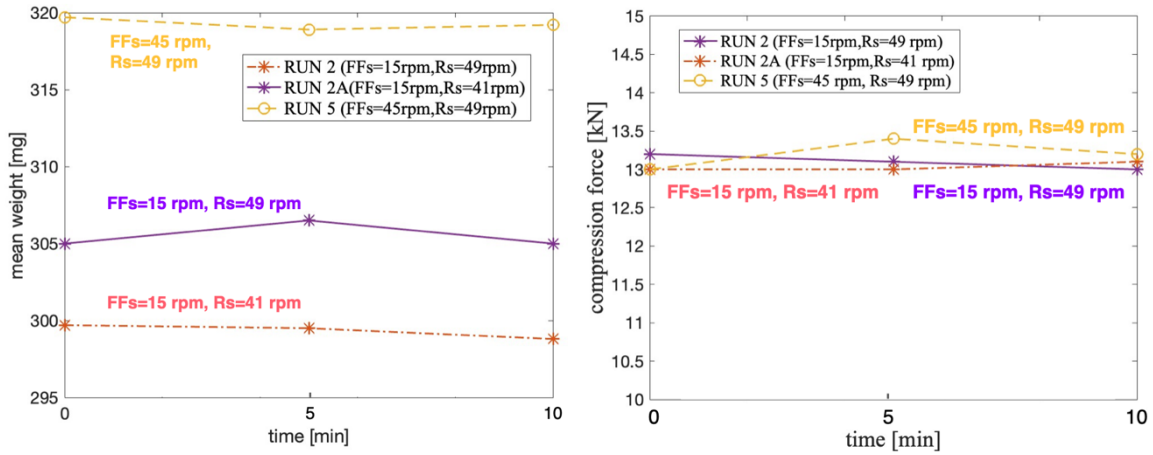

(a) (b)

Figure 4.7. *(a) Weight and (b) compression force profiles over time in Dataset 1 at feed frame speed of 15 rpm (run 2) and 45 rpm (run 5) for blend 3.*

and 41 rpm respectively), an additional setting varied in this blend to evaluate its impact on tablets properties, too. It can be seen that weight is smaller at higher rotor speed maintaining a constant feed frame speed (Fig. 4.7(a)).

The compression force is constant in time (Fig. 4.7(b)), meaning that for this blend, as for blend 2, flowability is good for all settings conditions considered and is not varying as consequence of feed frame speed.

By a first preliminary analysis on these time profiles, it can be concluded that blend 1 is the only one that exhibits an abnormal behavior, even if only at high feed frame speed.

4.2.2 Data dynamic analysis

To assess the dynamic time dependence of the data, a multivariate analysis technique, specifically PCA, is used to assess whether correlations between compression settings and tablet properties change over time. This is only done for the data collected at 13 kN compression force, as this is the only data for which the time evolution was taken into account in the data collection procedure for Dataset 1.

For the purpose of this study, it is necessary to construct an appropriate matrix. First of all, the original matrix dimension is reduced according to a run wise unfolding strategy, as explained

in §3.2. It is wanted to assess the dynamic dependence of data, but it must be taken into account that there is not a real relationship between tablet replicates produced at time 0 with the ones produced at time 5 or 10. For this reason, fictitious run replicates are created combining each original replicate row at t=0 with all the rows of the other groups (t=5 and t=10) for runs 2, 3 and 5, considerably increasing the matrix dimension with respect to the one in §4.1 for PCA modeling. An example of row combinations for a single run (run 2 in this case) is shown in Figure 4.8. With ten replicates available at each time point, a matrix of 1000 rows (10×10×10) is obtained for each run by combining them all. Considering that there are three runs available for each blend, a matrix of dimension 3000×36 is obtained for blends 1 and 2 and a matrix of 5000×36 is obtained for blend 3, for which additional data are available because a change in rotor speed was also taken into account in the data collection phase (from 41 to 49 rpm).

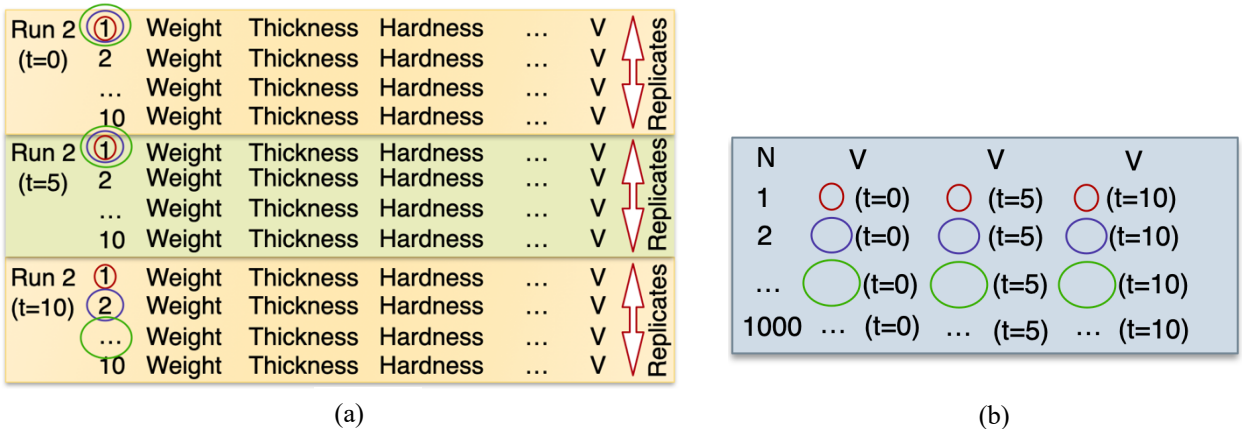

Figure 4.8. *(a) Fictitious combination procedure of run replicates for PCA model construction and (b) example of matrix configuration after RWU and replicates combination for a single run.*

The columns of the matrix, alias the variables included in the study (*V* in Fig. 4.8) are the following (Table 4.4):

Table 4.4. *Compression settings and tablets properties included in the PCA model built on Dataset 1 at 13 kN for dynamic data analysis.*

N.	Variable
1	Feed frame speed [rpm]
2	Main compression force [kN]
3	Rotor speed [rpm]
4	Fill depth [mm]
5	Weight [mg]
6	Thickness [mm]
7	Hardness [kp]
8	Tensile strength [MPa]
9	Width [mm]
10	Volume [mm^3]
11	Density [g/cm^3]
12	Solid fraction [-]

In Table 4.5 model structure and correspondent PCs selected with related explained variance are reported. Successively, only data related to PC 1 and PC 2 will be considered since they are the ones explaining most of the variability.

Table 4.5. *Diagnostics of the PCA models built on the Dataset 1 at 13 kN for dynamic data analysis.*

	Matrix dimension [NxV]	N° of PCs	Explained variance
Blend 1	3000 × 36	3	87.3 %
Blend 2	3000 × 36	3	85.7 %
Blend 3	5000 × 36	4	86.8 %

The similarity of the behavior between the tablet replicates collected for runs 2, 3 and 5 for each blend is first assessed by means of the score plot (Fig. 4.9). Indeed, it is known that observations that are close to each other in this plot are similar to each other.

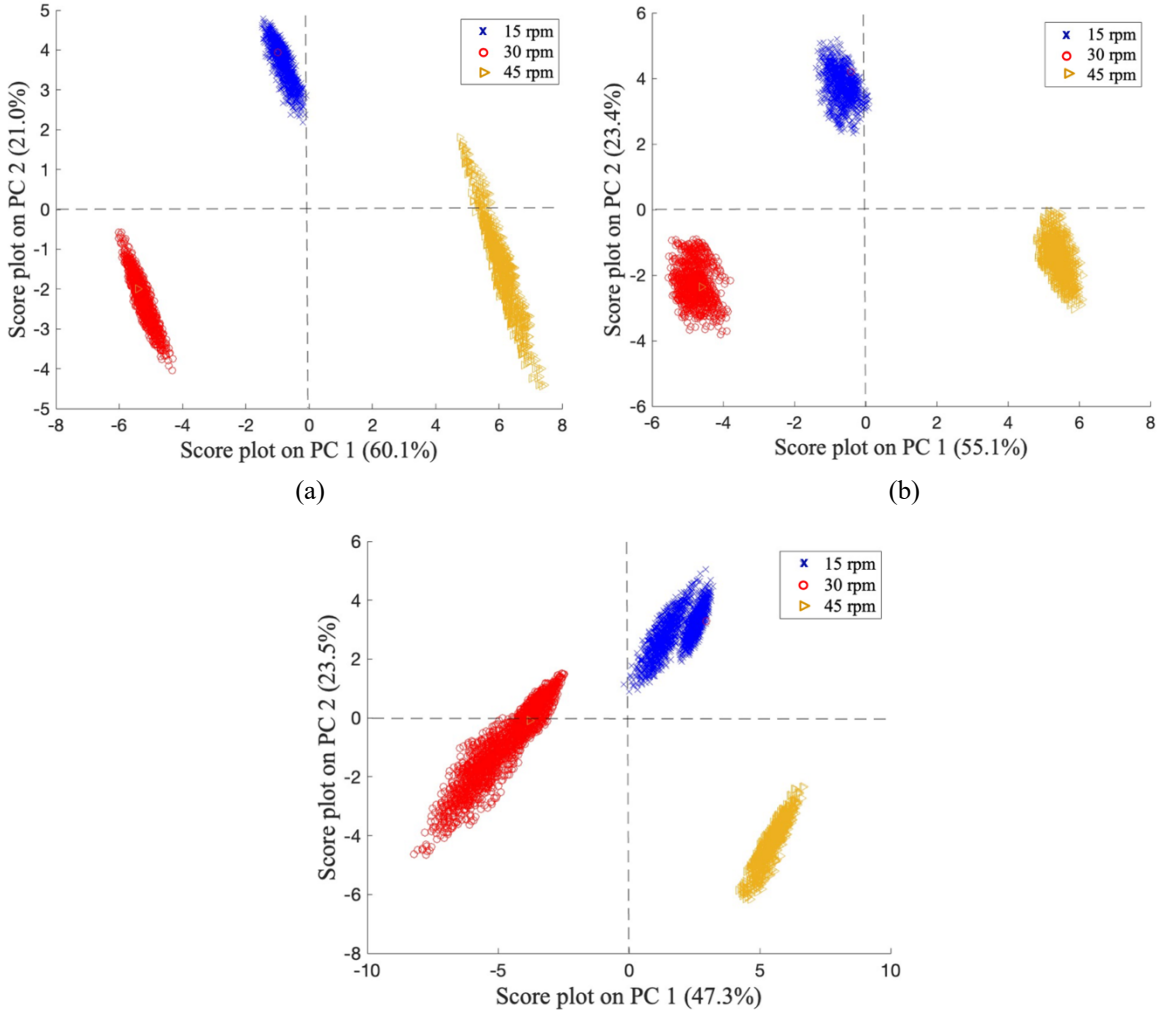

Figure 4.9. *Score plot reporting similarities between tablet replicates in (a) blend 1, (b) blend 2 and (c) blend 3 for the PCA model built on Dataset 1 with RWU and replicates combination strategy.*

In each blend three clusters of observations with similar behavior can be identified (Fig. 4.9), noting that the main cause of variability between them is given by the feed frame speed. It can also be seen that in blend 2 the clusters are more compact, whereas in blend 1 and 3 they are characterized by a greater spread across the score space, which means that the variability within runs is greater at a fixed feed frame speed. This translates in reduction of properties uniformity between tablets produced at the same compression settings, making it more difficult to achieve adequate CQA in all tablets. It is therefore useful to investigate the reasons for such an increase in variability between replicates at a constant feed frame speed, such as 45 rpm in blend 1, where it is considerable. Observing more in detail the score plot for blend 3 at 15 and 30 rpm (Fig. 4.10), obtained with the same model used for Fig. 4.9, it can be noted that higher rotor speed increases runs variability at the same feed frame speed conditions.

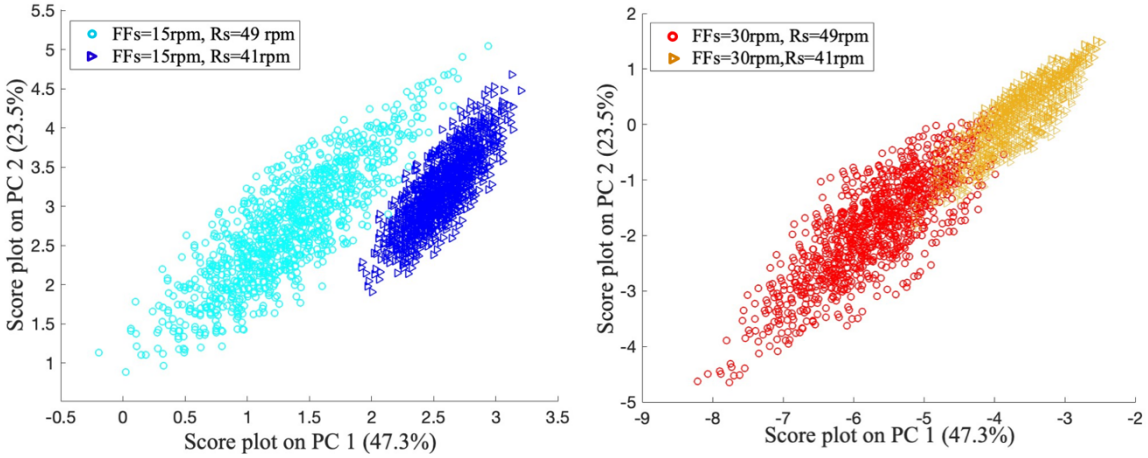

Figure 4.10. *Focus on the score plot for blend 3 compressed at (a) 15rpm and (b) 30 rpm feed frame speed and different rotor speed obtained from PCA model built on Dataset 1 with RWU and replicates combination strategy.*

It can be concluded that the speed itself, of both the feed frame and the rotor, has an effect on tablet quality: greater speed leads to greater variability. In order to better understand what happens in blends at fixed feed frame speed, which is the main source of variability, the matrices previously used are re-organized so that each contains tablet replicates data not for the individual blend but instead for the individual feed frame speed. An example of the new matrix structure is shown in Table 4.6. This configuration gives a 4000×36 matrix for FFspeed=15 rpm and 30 rpm, whereas a 3000×36 matrix dimension is obtained for FFs=45 rpm as only rotor speed at 49 rpm is used for blend 3 at 45 rpm. In Table 4.7 is it possible to observe the diagnostic of the PCA models built with the new configuration.

Table 4.6. *Matrix configuration for PCA application using RWU and replicates combination strategy on Dataset 1 at fixed feed frame speed, including observations for all blends.*

	FF speed	Rotor speed	Variables	Variables	Variables
			Replicate 1 (t=0)	Replicate 1 (t=5)	Replicate 1 (t=5)
Blend 1	15	41	Replicate…(t=0)	Replicate…(t=5)	Replicate…(t=5)
			Replicate 1000 (t=0)	Replicate 1000 (t=5)	Replicate 1000 (t=5)
			Replicate 1 (t=0)	Replicate 1 (t=5)	Replicate 1 (t=5)
Blend 2	15	41	Replicate…(t=0)	Replicate…(t=5)	Replicate…(t=5)
			Replicate 1000 (t=0)	Replicate 1000 (t=5)	Replicate 1000 (t=5)
			Replicate 1 (t=0)	Replicate 1 (t=5)	Replicate 1 (t=5)
Blend 3	15	41	Replicate…(t=0)	Replicate…(t=5)	Replicate…(t=5)
			Replicate 1000 (t=0)	Replicate 1000 (t=5)	Replicate 1000 (t=5)
			Replicate 1 (t=0)	Replicate 1 (t=5)	Replicate 1 (t=5)
Blend 3	15	49	Replicate…(t=0)	Replicate…(t=5)	Replicate…(t=5)
			Replicate 1000 (t=0)	Replicate 1000 (t=5)	Replicate 1000 (t=5)

Table 4.7. *Diagnostic of the PCA models built on Dataset 1 including in each matrix all data of all blends at fixed feed frame speed.*

	Matrix dimension [NxV]	PCs selected	Explained variance
FFspeed=15rpm	4000 × 36	2	81.7 %
FFspeed=30rpm	4000 × 36	2	77.8 %
FFspeed=45rpm	3000 × 36	2	86.4 %

The differences in blends behavior at fixed feed frame speed can be evaluated by using the score plot in Fig. 4.11. It can be seen that blend 1 and 2 behave very similarly at lower feed frame speed, while they adopt a different behavior for the highest one. At the same time, blend 3 behaves in an opposite way with respect to the other blends for all the feed frame speeds considered.

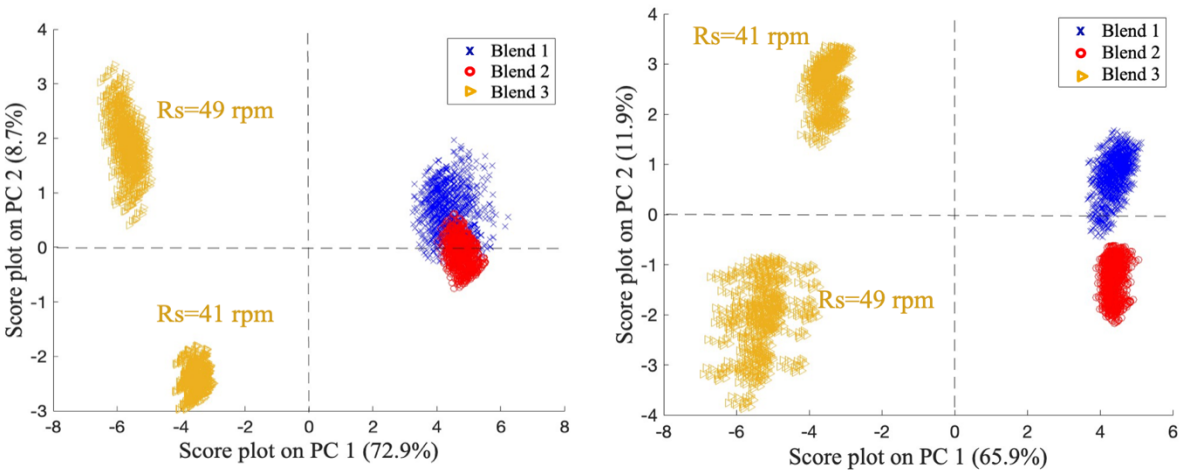

(a) (b)

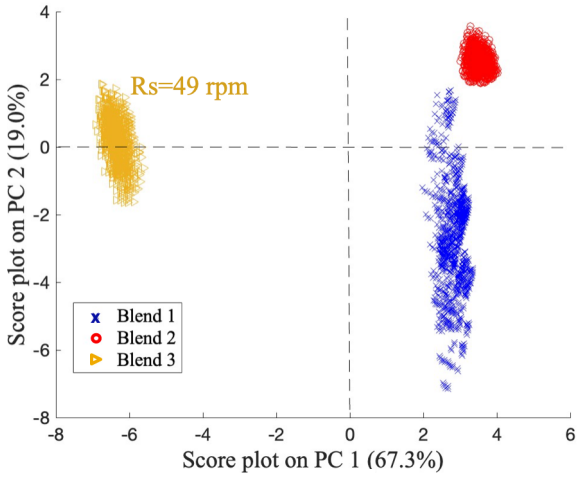

(c)

Figure 4.11. *Score plot resulting from PCA application on the matrix described in Table 4.6 reporting tablet replicates similarities at (a) 15 rpm, (b) 30 rpm and (c) 45 rpm.*

The main cause of variability is expressed by the first PC, indicating that blend 1 and 2 are similar while blend 3 has an opposite trend. For blend 3, two different rotor speed are tested: it results that, for both 15 and 30 rpm, rotor speed affects blend 3 variability increasing it (while this is not known for the other blends). It can be noted also that blend 1 variability is large at high FFspeed, and the reasons for that are described mainly by the second PC of the model.
The loading plots are thus analyzed to capture the relationships between the variables of interest.

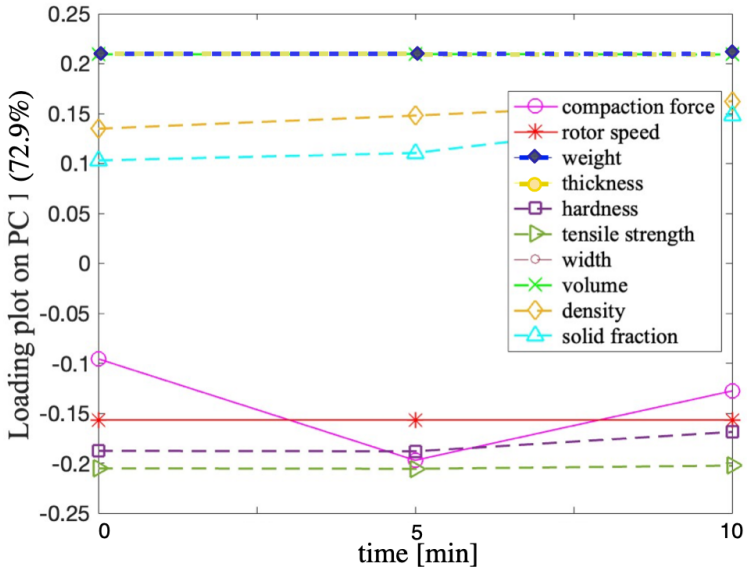

Figure 4.12. *Loading plot on the first PC for 15 rpm feed frame speed from PCA model built on Dataset 1 using RWU and replicates combination strategy at fixed feed frame speed.*

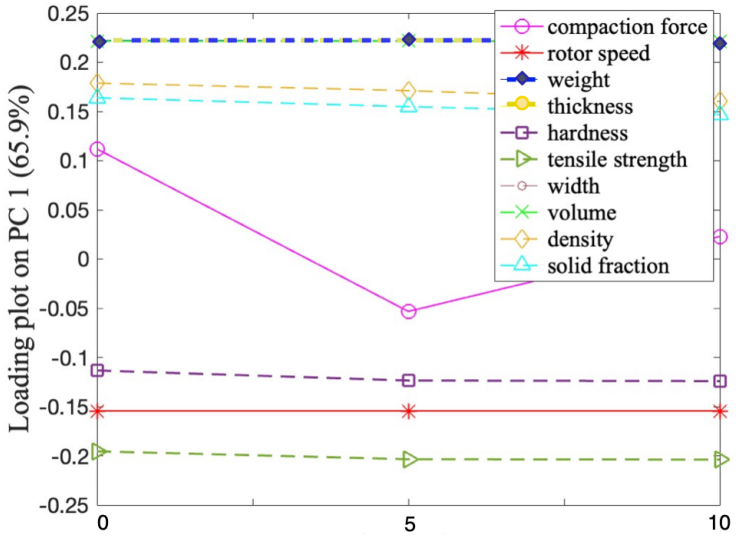

Figure 4.13. *Loading plot on the first PC for 30 rpm feed frame speed from PCA model built on Dataset 1 using RWU and replicates combination strategy at fixed feed frame speed.*

The solid line refers to compression settings, while the dashed one refers to measured and calculated variables. For both 15 and 30 rpm, two groups of variables that vary together can be identified (Fig. 4.12 and Fig. 4.13): compression force, hardness and tensile strength on one side, and weight, thickness, width and volume on the other. Considering that blend 1 and 2 are in the positive part of the score plot, while blend 3 in the negative one, it can be also concluded that blend 1 and 2 have greater weight, thickness, width and volume and lower hardness and tensile strength with respect to blend 3.

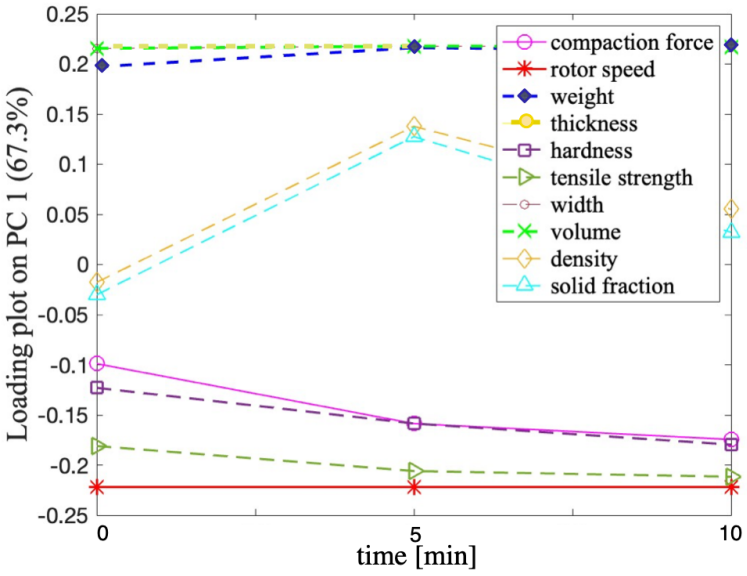

Figure 4.14. *Loading plot on the first PC for 45 rpm feed frame speed from PCA model built on Dataset 1 using RWU and replicates combination strategy at fixed feed frame speed.*

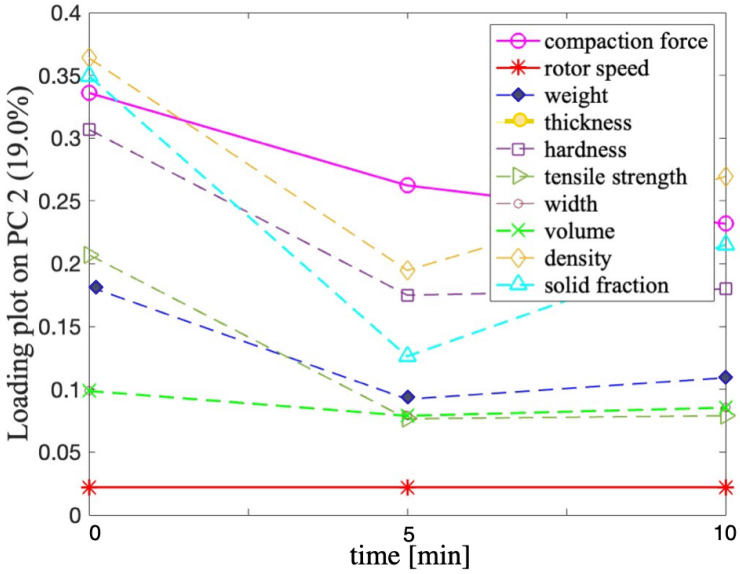

Figure 4.15. *Loading plot on the second PC for 45 rpm feed frame speed from PCA model built on Dataset 1 using RWU and replicates combination strategy at fixed feed frame speed.*

Regarding the 45rpm case, the loading plot for PC 2 is also considered because it explains 19% variability, more than doubled with respect to the previous models. The first loading plot (Fig. 4.14) confirms that two groups of variables are still recognizable at 45 rpm, while the second one (Fig. 4.15) highlights that an increase in compression force goes together with an increase in solid fraction especially at the beginning of the run. Even if it would be expected that compression force remains constant during the run, the above analysis demonstrates that it is changing during time, especially in some runs (like run 5 for blend 1).Remembering that PC 2 is describing the high amount of variability in blend 1 at 45 rpm, it is possible to say that the relationship between compression force and solid fraction is causing such an increase in run variability. It must be generally noted that variables are not changing their relationship in time, so no dynamic time dependence between data seems not to be present. The conclusion that can be derived from all the loading plots studied is that time evolution is not significant with respect to the relative relationship between the variables.

4.2.3 Additional considerations on tablet replicates variability

The study of the loading plots obtained by PCA modeling with the initial matrix configuration, whose diagnostic is described in Table 4.5, considering each blend separately, can be useful to derive some additional information about the relationships between variables in each single blend. In particular, the loading plots on the second PC are reported, since they describe the variability within clusters for a fixed feed frame speed. It can be seen from Fig. 4.16 that there are stable and common relationships between some variables for all blends, most importantly the increase in hardness and tensile strength with a decrease of feed frame and rotor speed, even

if it must be remembered that this refers to only 20% of the variability. However, common relationships between blends are not significant in explaining why the shape of one blend cluster differs from that of another blend at the same feed frame speed. The only relationship that is changing for different blends is the compression force - solid fraction one, even if the loading plots are not emphasizing in all blends the importance of this relation with respect to others. Given this, it can be said that the variability within clusters can be attributed to the relationship that exists between compression force and solid fraction with respect to the other variables. The loading plots of blends 1 and 2 provide significant information about the relationships between these two variables: in blend 1, the main compression force does not seem to have adequate control over the solid fraction, whereas in blend 2 they vary strictly together. The relationship between compression settings and powder characteristics will be further discussed (§4.3.4 and §4.5), but it is anticipated that the sudden variations of solid fraction in the different blends could be related to the different physical properties of the blends themselves, concluding that a more flowable powder, such as blend 2, allows for an easier control of the tablets solid fraction.

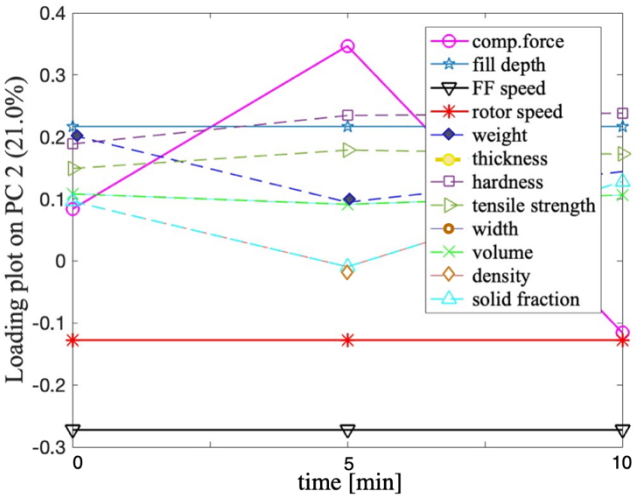

(a)

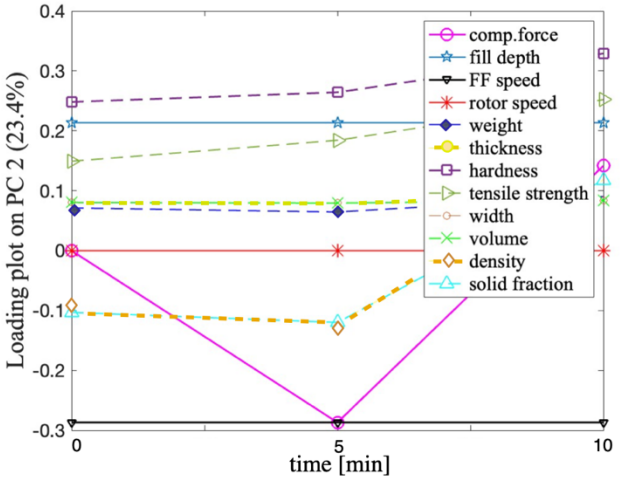

(b)

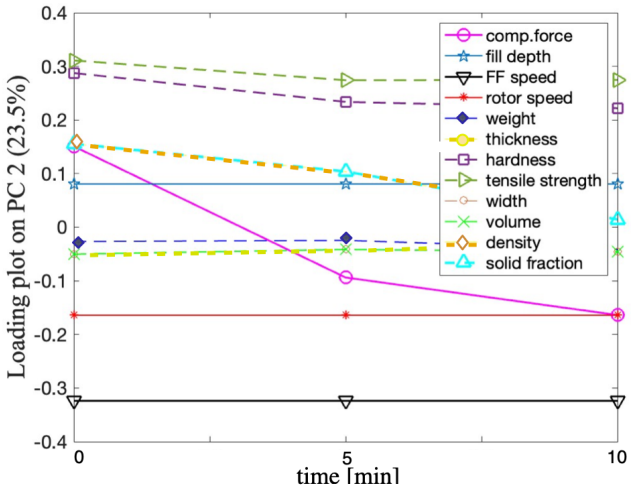

(c)

Figure 4.16. *Loading plot on the second PC obtained by PCA modeling of Dataset 1 using RWU and replicates combination strategy for (a) blend 1, (b) blend 2 and (c) blend 3*

4.3 Weight data structure

Die filling is known to be a critical step in the tableting process and influences several quality characteristics of the final product. It is responsible for the weight uniformity of the tablets, which is a critical quality attribute to be monitored to ensure an appropriate drug dosage and that the same amount of API is contained in each tablet produced.

The following study focuses on understanding which are the significant factors determining tablet weight variability within the design space studied.

4.3.1 Mean weight and weight variability definition

The mass and content uniformity of tablets depend on both process variables and powder properties, and they must be guaranteed after the compression process. In the following study, both of these tablet properties are going to be analyzed. More specifically, mean weight is used to describe the average weight achieved for particular compression settings (and therefore for a particular run), while weight variability, expressed as weight relative standard deviation, describes the variability in weight characteristics between tablets obtained at the same compression settings within the specific run. In fact, it is necessary to ensure that the same quantity of powder, and in particular of API, is present in the tablets produced in a run, so that the CQA of the tablets are uniform. In each run, mean weight and weight variability are obtained for each time instant as follows:

$$Mean\ weight\ [mg] = \frac{\sum_{i=1}^{N} w_i}{N} \tag{4.1}$$

where N=total (60) tablet replicates at a specific time instant and w_i= tablet weight [mg] in the single observation, while the relative standard deviation is calculated as:

$$Weight\ RSD\ [\%] = \frac{\sqrt{\frac{1}{N}\sum_{i=1}^{N}(w_i - mean\ weight)^2}}{mean\ weight} \times 100 \tag{4.2}$$

4.3.2 Runs time profile of mean weight and weight variability

It has already been shown that mean weight increases with feed frame speed, fill depth and fill cam, while it tends to decrease for higher overfill and rotor speed. In addition, from the mean weight and compaction force profiles over time for the three blends in Dataset 1 described in §4.2.1, it is possible to deduce that weight variations are also related to those of the compaction force.

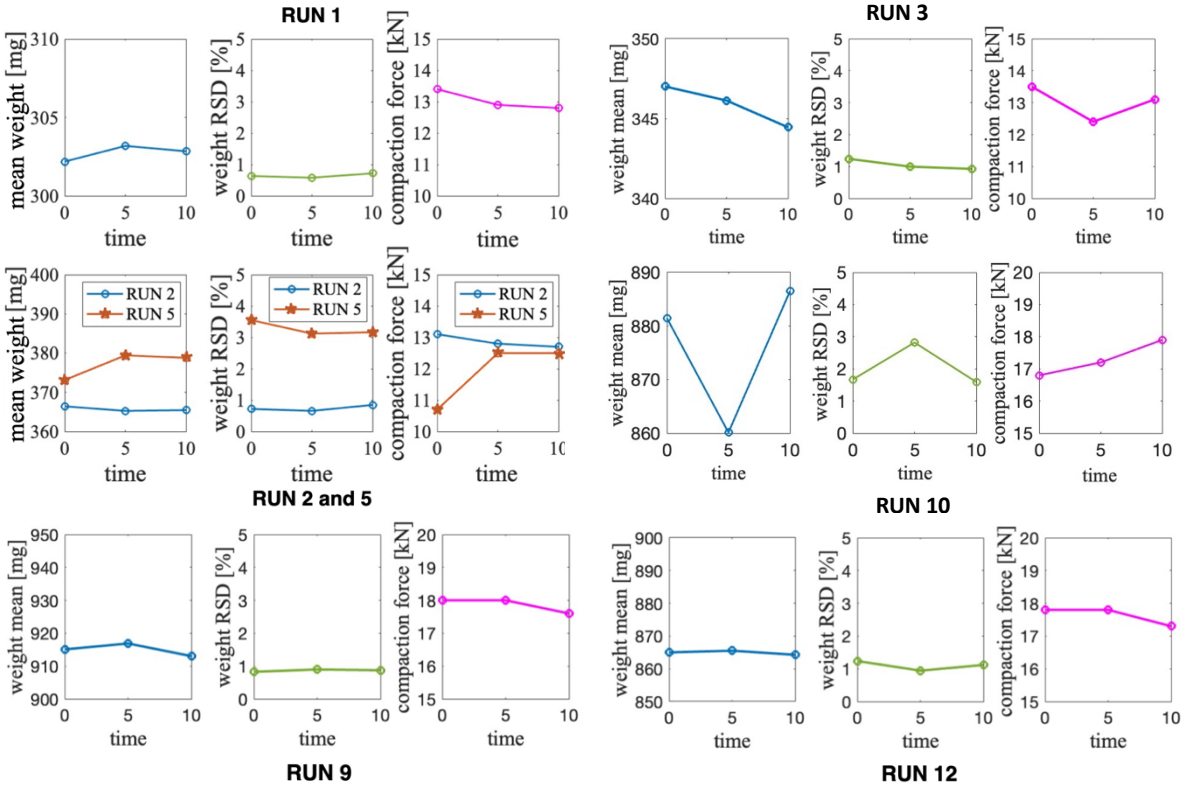

Figure 4.17. *Mean weight (mg), weight variability in terms of RSD (%) and compression force (kN) time profiles for runs of blend 1 taken from Dataset 2.*

It is known from the work of Mendez et al. (2010) that a higher feed frame speed should reduce the tablet weight variability and therefore the variability between tablets obtained at the same compression setting, but this does not correspond to reality in some cases, as can be seen from the time profiles obtained by Dataset 2 and reported in Fig. 4.17. For example, in blend 1 (Fig. 4.17), high weight variability is recorded at the highest feed frame speed (run 5). Furthermore, run 10 setting conditions, with the highest fill cam and fill depth, in blend 1 make more difficult to achieve weight uniformity. Run 9 and 12 are added to the analysis to compare their behavior with run 10, and it can be seen that in both of them weight is uniform along time and the related variability is low. It can be concluded that the increase in variability recorded for run 10 is run-specific, and it does not depend on the increase of target weight imposed.

Blend 2 has a constant mean weight in time and low weight variability for all compression settings considered; additionally, runs at lower fill depth give lower weight variability, independently of the feed frame speed value, as can be seen from Fig. 4.18(a) and Fig. 4.18(b). In this blend the increase in feed frame speed is beneficial in reducing weight variability.

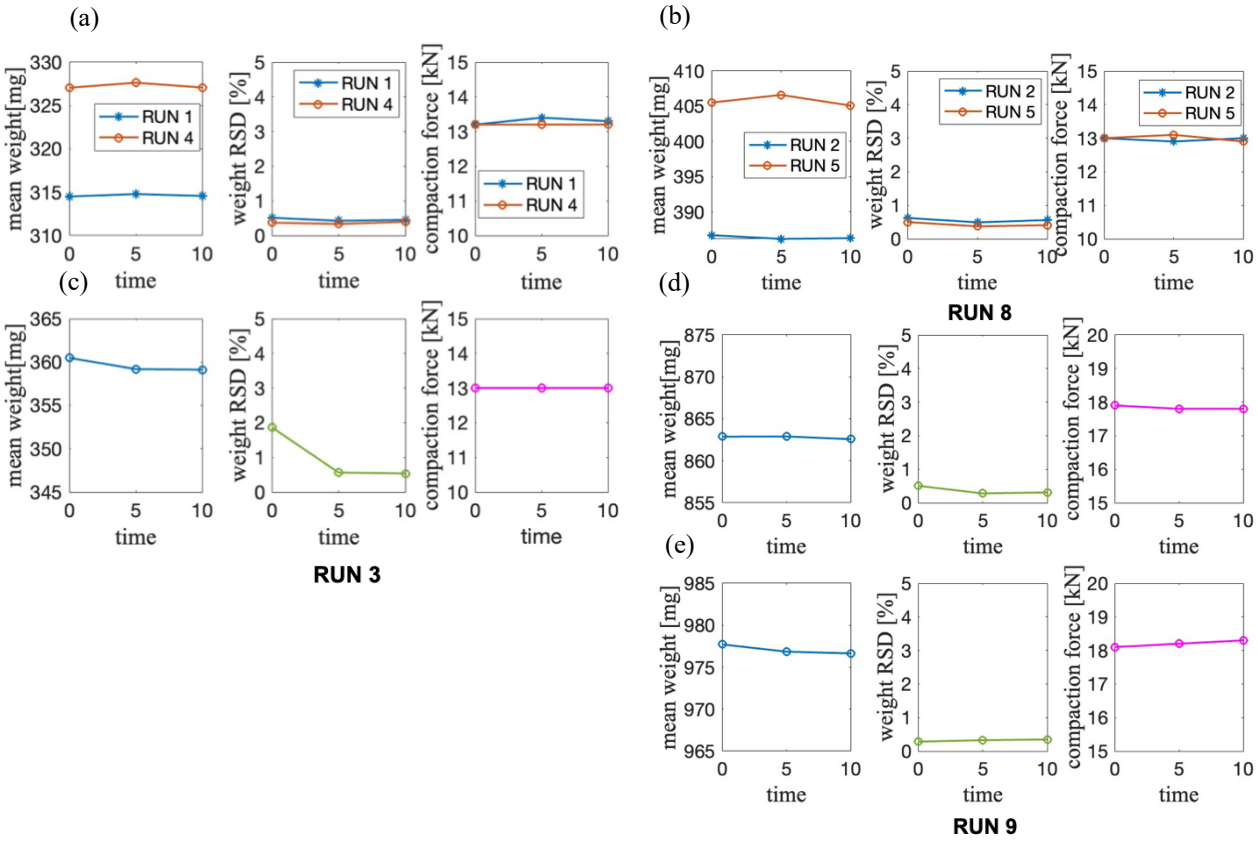

Figure 4.18. *Mean weight (mg), weight variability in terms of RSD (%) and compression force (kN) time profiles for (a) runs 1/4, (b) runs 2/5, (c) run 3, (d) run 8 and (e)run 9 of blend 3 taken from Dataset 2.*

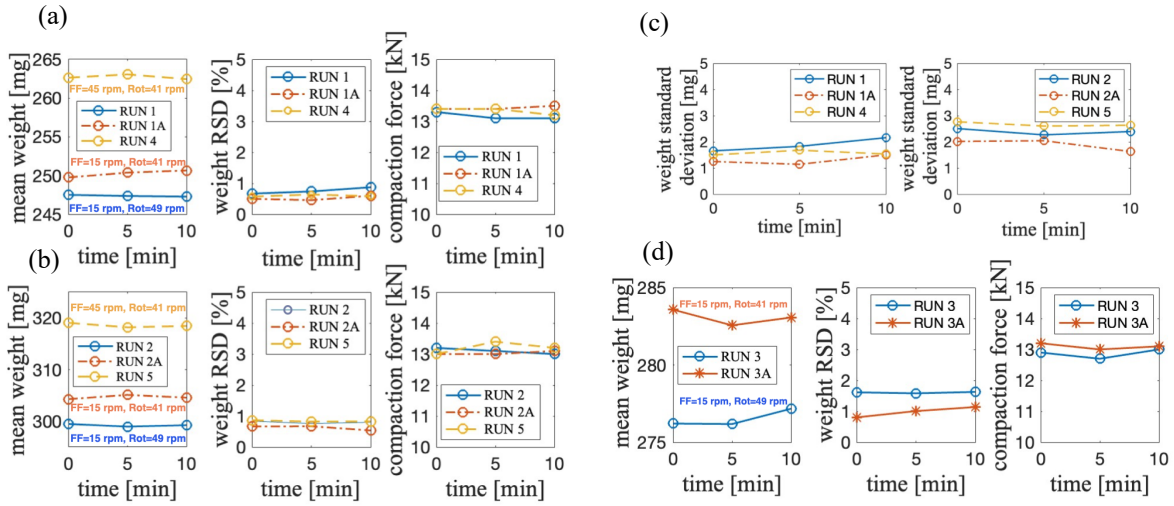

Figure 4.19. *Mean weight (mg), weight variability in terms of RSD (%) and compression force (kN) time profiles for (a) runs 1/1A/4, (b) runs 2/2A/5, (d) runs 3/3A with (d) comparison of weight standard deviation profiles of runs 1/1A/4 and 2/2A/5 of blend 3 taken from Dataset 2.*

In blend 3, again, increasing the feed frame speed causes a negligible increase in weight variability (run 2-5 and run 1A-4 profiles in Fig. 4.19). An additional information given by these runs is that higher rotor speed affects negatively weight variability, as can be seen by comparing run 1-1A, 2-2A and 3-3A. Moreover, it can be noted (Fig. 4.19(c)) that runs with lower fill depth, as runs 1 and 4, are characterized by slightly lower weight variability with respect to runs at higher fill depth, as runs 2 and 5. It is evident that process parameters have an influence on the weight uniformity of tablets, more or less relevant depending on the blend considered, and that such relationships need to be further investigated.

4.3.3 Composition and settings affecting weight properties

It has already been noted how the effect of some compression settings on weight can vary for different blends. At this point, it seems reasonable to investigate whether there is a relationship between the weight properties and the blend composition itself, in order to understand which powder ingredients are mostly correlated to mean weight and variability. Although it is known that general assumptions are critical, this type of study is useful to better investigate the effect of composition on tablet properties for the specific blends studied. With this aim, a PCA model is built by using Dataset 2, calculating a mean weight and weight relative standard deviation with the 60 observations collected at each time instant. A unique matrix of dimensions 62×10 is constructed, containing all the blends within it, but still distinguishable one from each other for the variations in the composition variables included in the columns (Table 4.10). Each row is representative of the mean weight and weight variability for a single time instant of a single run; considering all time instants of all runs reported in Dataset 2, 62 rows are obtained. A PCA

model is constructed with 3 PCs explaining 79.4% of the variability. The variables included are the ones reported in Table 4.8, comprehending compression settings, composition and weight properties.

Table 4.8. *Variable list used to build the PCA model to evaluate weight properties dependence on blend composition.*

N.	*Variable*
1	Mean weight [mg]
2	Weight variability (RSD) %
3	Fill cam [mm]
4	Fill depth [mm]
5	Overfill [mm]
6	Feed frame speed [rpm]
7	Rotor speed [rpm]
8	X_1 (Lactose monohydrate)
9	X_2 (Avicel PH_102)
10	X_3 (Lactose anhydrous)

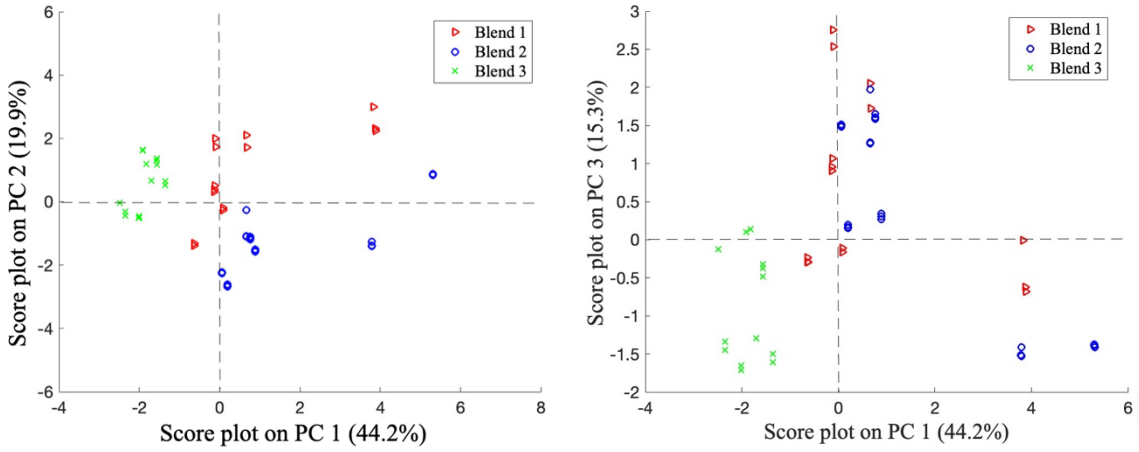

Figure 4.20. *Score plot of (a) PC1 vs PC2 and (b) PC1 vs PC3 built on PCA model based on Dataset 2 in which a single point represents an average of weight and weight RSD for a single time instant in a single run of the blend.*

Each point appearing in the score plot (Fig. 4.20) represents a synthesis of weight and weight variability at a single time instant for a run of each blend. It can be seen that blend 3 and blend 2 form a cluster with respect to PC 1 and behave in an opposite way accordingly to the first PC, while blend 1 points are more randomly distributed. No cluster can be clearly distinguished for

either PC 2 or PC 3, meaning that the observations are not properly blend dependent.

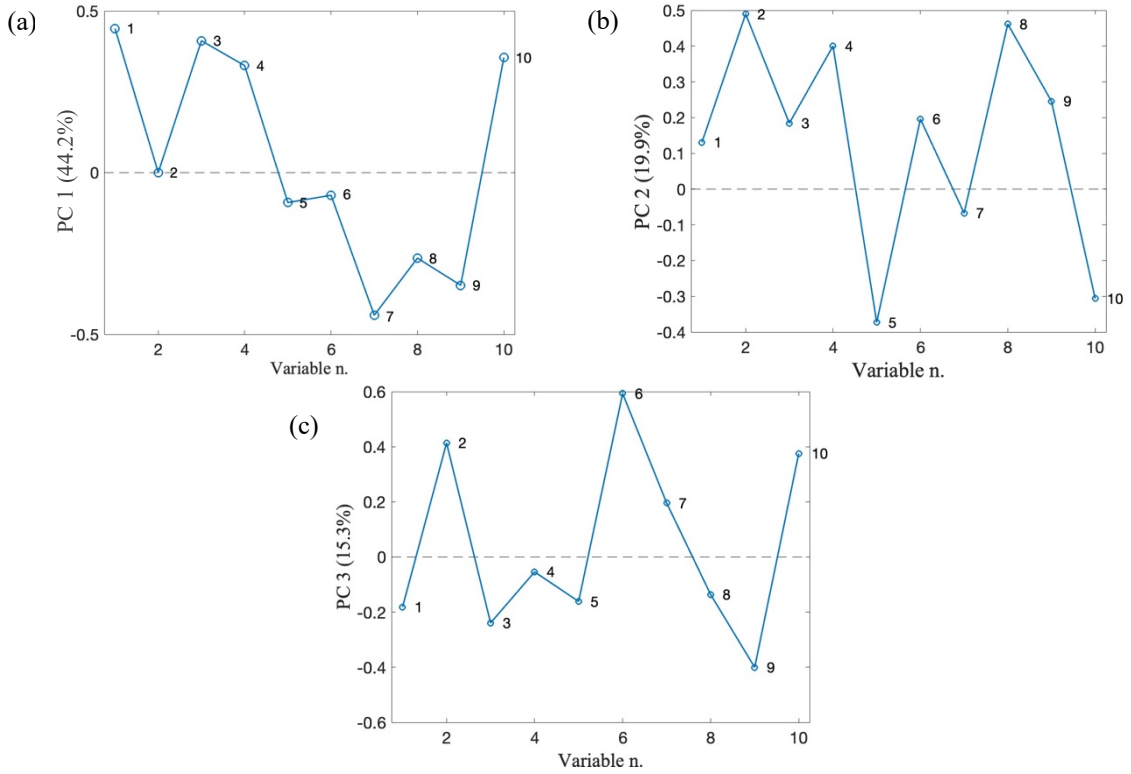

Figure 4.21. *Loading plot on (a) PC 1, (b) PC 2 and (c) PC 3 built using a PCA model based on weight data to find correlations between composition, compression settings and weight properties.*

According to the first PC, mean weight increases with fill cam and fill depth (as already known), but also with lactose anhydrous, while it decreases with higher Avicel and lactose monohydrate presence (Fig. 4.21(a)). This is confirmed by the density features of these powders, as can be seen in §4.5.2. The second PC, explaining 20% variability (Fig. 4.21(b)), suggests that there is a higher weight variability for a lower overfill, lower lactose anhydrous and higher lactose monohydrate content. Additionally, weight variability increases also with lactose anhydrous for higher feed frame speed conditions (Fig. 4.21(c)). Considering that lactose anhydrous has the largest impact on weight and that it is the component with highest presence in blend 2 (X_3=0.683), it can be concluded that blend 2 has the highest mean weight, followed by blend 1 and finally by blend 3 (adding information to what found in §4.2.2). Moreover, for the majority of the explained variability, weight variability does not increase with lactose anhydrous, while among all components the one most affecting it is lactose monohydrate. Blend 2 (X_1=0.05) is the blend less affected by weight variability. The relationship between composition and weight variability is not yet clearly defined, so further studies are needed to assess the effect of powder properties impact on flowability and weight variability. It can be anticipated that several flowability tests were carried out on free powder and feed frame-subjected samples of all three

blends to assess their flowability and how their behavior changes in the presence of the feed frame (see §4.5). From the flow function test, it can be concluded that all the blends are free flowing, but the Carr's (or compressibility) index can give some additional information.

Table 4.9. *Carr's index for free powder samples and feed frame subjected samples for all three blends under study.*

	Compressibility index (%)	
	Lubricated sample	Feed frame sample
Blend 1	21	17
Blend 2	19	9
Blend 3	19	16

Table 4.10. *Carr's index table for association of the index value with flowability properties of the powders (Shipar et al. (2014)).*

Compressibility index	**Index properties**
≤10	Excellent
11-15	Good
16-20	Fair
21-25	Passable
26-31	Poor
32-37	Very poor
>38	Extremely poor

Blend 2 is the one whose flowability is mostly improved by the feed frame presence (see Table 4.9 and 4.10), resulting to be the most flowable of the blends. A general conclusion that can be drawn is that the blend which is less affected by weight variability is also the most flowable one, indicating that a relationship between powder properties and tablets quality exists and can be exploited to obtain tablets with increased properties uniformity. In fact, blend 2 is not subjected to compaction force variations due to weight deviations. The most flowable blend is consequently not damaged by the presence of feed frame speed, on the contrary it is enhanced by it, and for any compaction force used weight properties are not affected.

4.3.4 Dynamic dependence of weight data on compression settings

Dataset 2, which provides sixty weight data for each time point considered in each run, is used to find more rigorously which are the compression settings that most influence the mean weight and the replicates weight variability inside a run. It is recalled that mean weight is the weight, averaged over time, achieved for specific setting conditions, while replicates weight variability

inside a run is intended to be the replicability of the experiment, analyzed to evaluate whether for the same compression settings the same weight is achieved in all tablets.

4.3.4.1 PLS model construction

PLS analysis is employed, building matrices with a run wise unfolding structure combining weight data at different time instants according to the strategy explained in §4.2.2. In this case, although there are 60 weights available for each time point, using all of them for the combination would result in a matrix of extremely large dimension and difficult to handle. To avoid this, 20 of those 60 weight data at t=0 are randomly selected and then combined with another 20 of 60 weight data at t=5 and with 20 weight data of t=10, obtaining a total of 8000 rows for each run. Note that up to this point there would be three weight data points for each tablet replicate, one per time point. Since for the PLS model construction it is required to have a single response data for each row, a mean weight is calculated among the three weights available for the single row, obtaining a response vector ($\mathbf{Y_1}$) whose dimension is 8000× 1. This means that we are renouncing to identify the variability of the response in time, but anyway we still try to correlate the average response over time with the variables point values at different times. For weight variability within a run, the combination procedure differs in that it first considers a weight RSD calculated on all 60 original weight data for the specific time point. Then, as for the weight, three weight RSDs would be obtained for each row and an average of these values is performed to obtain a response vector ($\mathbf{Y_2}$) whose dimension is again 8000×1.
The matrix **X** includes the compression settings varied in time, namely fill depth, feed frame speed, rotor speed, fill cam, overfill and compaction force. The dimensions of the matrices are shown in Table 4.13, from which it is possible to see also the mean weight models structure, in terms of latent variables chosen and corresponding explained variability. Given that the combination strategy provides 8000 rows for each run, the resulting matrices for PLS model will have a number of rows corresponding to the runs included, namely the ones of Dataset 2 (as shown in Table 4.11). Note that all runs of Dataset 2 are used for each blend, even if meant to achieve different target weights. This is done in order not to lose information about the actual effect of rotor speed on weight, since runs with same target weight are all at the same rotor speed. The analysis will also focus on the different behavior between runs to achieve the 250mg and 800mg weight targets, to understand if compression settings affect the mean weight and standard deviation differently for different weight targets. For a preliminary analysis of similarities among observations with respect to their weight and weight variability, a PCA analysis is performed adding to the **X** matrix built for the PLS model (as described in §4.3.4.1) the three weight and weight variability columns that resulted from the combination strategy for each time instant, without averaging their values as it was required by PLS.

Table 4.11. *PLS model construction for the three blends including number of latent variables selected, explained variance of the process variables matrix and of mean weight response.*

	Vector Y (Mean weight)	Matrix X	N° of LVs	Explained variance of X	Explained variance of Y
Blend 1	40000 × 1	40000 × 18	2	91.0%	99.7%
Blend 2	56000 × 1	56000 × 18	2	81.5%	99.3%
Blend 3	56000 × 1	64000 × 18	2	60.6%	97.8%

A unique matrix is obtained, including the information about the process and response variables, whose dimension is respectively 40000×24 , 56000×24 and 64000×24 for blend 1, blend 2 and blend 3. For blend 1 and 2, two LVs are selected explaining 91.1% for blend 1 and 84.3% for blend 2. For blend 3, three LVs are chosen and 85.8% variability is expressed.
It is possible to see from Fig.4.22 and Fig.4.23 that the variability between different runs is much more relevant than the one within runs. This indicates that the replicability of the experiment is generally good for all blends. In addition, it can be seen that PC 1 reflects the change in tooling adopted during data collection for both blend 1 and blend 2. Regarding blend 3, where significant variations in rotor speed have been applied, weight variability is seen to increase at higher rotor speed for the same feed frame speed used, as suggested by the comparison of the clusters shape of runs 1-1A, 2-2A and 3-3A in Fig.4.21. The highest variability is recorded for run 3, which has both high feed frame and rotor speed. It is noticeable also that fill depth seems to have a role in runs variability, since for almost half of the observations (45.68%) runs at lower fill depth behave differently from the others. This confirms what obtained previously in §4.3.2.

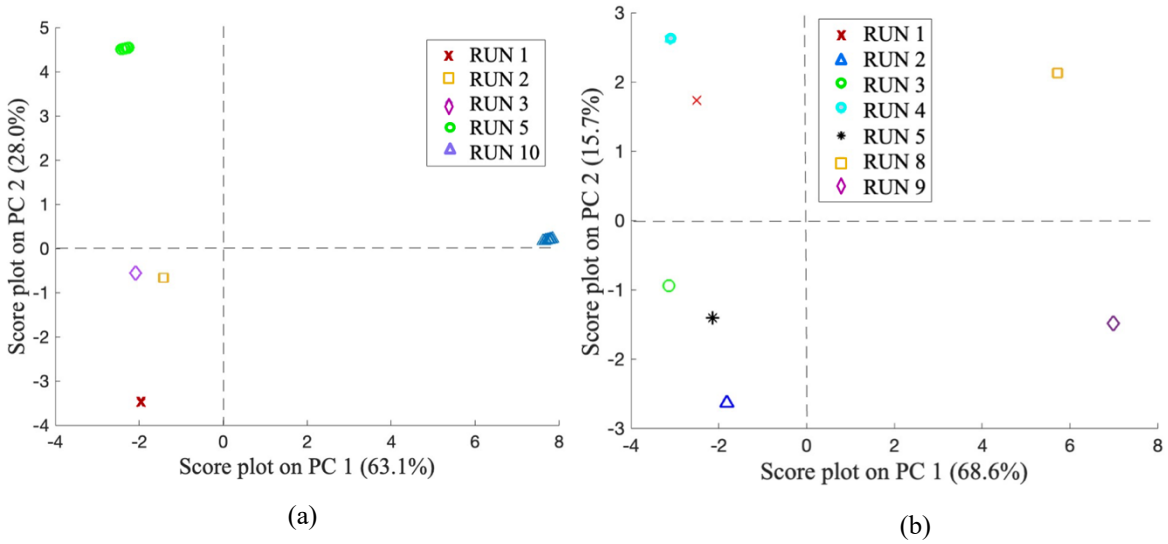

(a) (b)

Figure 4.22. *Score plot from a preliminary PCA analysis on X matrix built as the PLS one described in §4.3.5.1 including weight and weight RSD columns in the process variables matrix to assess the behavior similarities among observations for (a) blend 1 and (b) blend 2.*

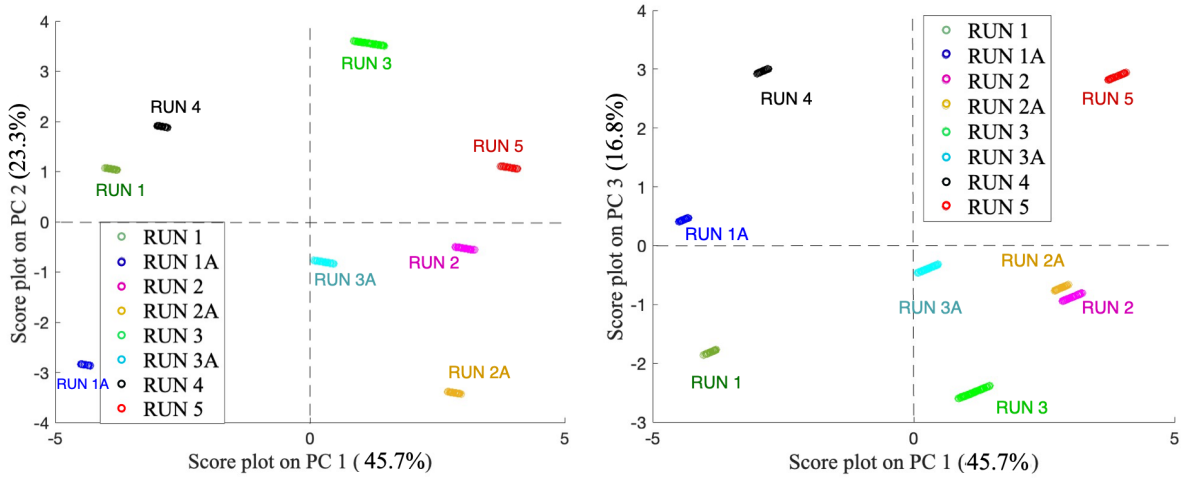

(a) (b)

Figure 4.23. *(a) and (b) Score plot from a preliminary PCA analysis on X matrix built as the PLS one described in §4.3.5.1 including weight and weight RSD columns in the process variables matrix to assess the behavior similarities among observations for blend 3.*

The following observations can be made referring to the PLS weights plot obtained for mean weight:

- for blend 1, mean weight is mainly increased by fill cam and fill depth, as well as rotor speed decreases it (Fig. 4.24(a)); also feed frame speed and overfill can respectively increase and decrease it (Fig.4.24(b)) but in a less relevant way, since their relationship with mean weight is described by the second PC, explaining a lower amount of variability (24.3%) with respect to the first one (66.7%).
- for blend 2, rotor speed as an important role on the decrease of mean weight, while fill cam, fill depth and compaction force provide an increase of it (Fig.4.24(c)).
- for blend 3, fill depth is dominant in increasing mean weight, while overfill decreases it with the same power (Fig.4.24(d)).

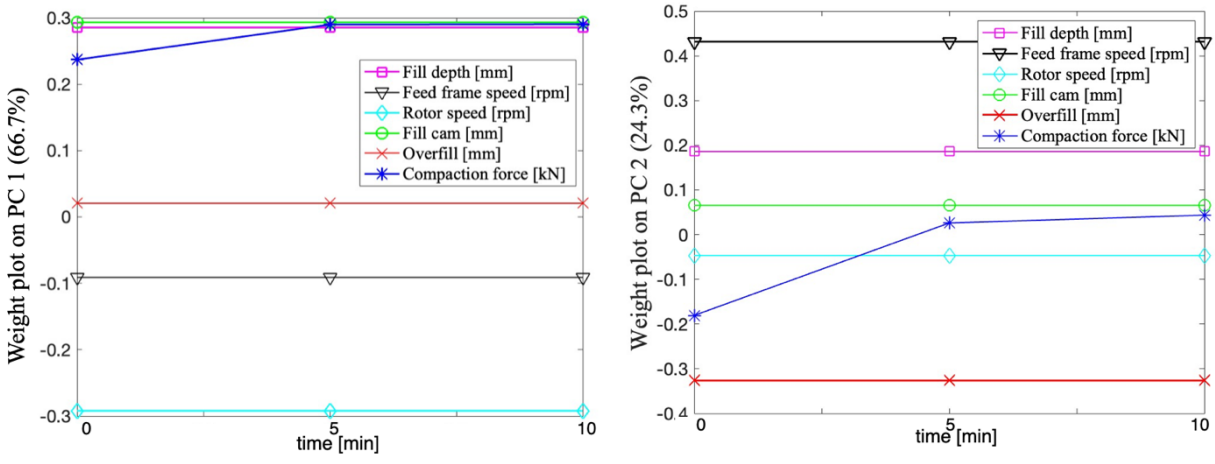

(a) (b)

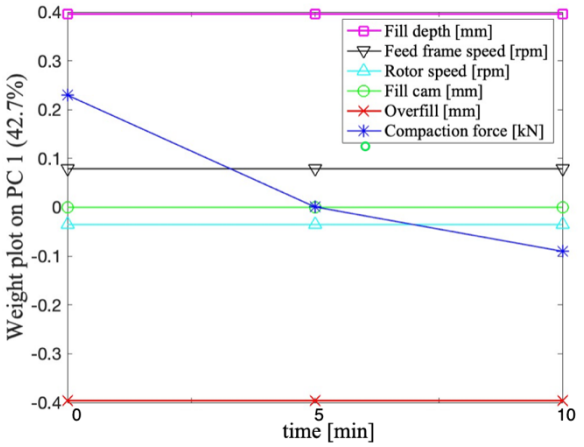

(c)

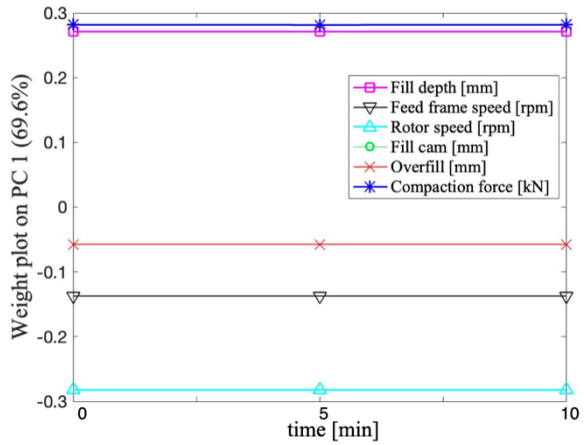

(d)

Figure 4.24. *Weight plot for PLS analysis applied to Dataset 2 of (a) the first LV of blend 1, (b) the second LV of blend 1, (c) the first LV of blend 2 (98.2% variability of mean weight) and (d) the first LV of blend 3 (92.4% variability of mean weight).*

For all blends, it is confirmed that time evolution is not significant in determining the relationship between compression settings and response variables.

In this way it is possible to know on which compression settings is more convenient to operate to achieve the target weight for each specific blend. It must be said that fill cam is a setting difficult to modify; for this reason, it is more practical to operate on the other mentioned compression settings.

Focusing now on the variability within a single run, a different model is used to study the replicability of tablets production. The process variable matrix (**X** matrix) is the same as the previous one used for PLS analysis, with the response variable which is now the weight variability of replicates in a single run, expressed in terms of relative standard deviation averaged on the mean weight along all-time instants for the single run. In Table 4.12 model structure and diagnostic are reported.

Table 4.12. *PLS model construction for the three blends including number of latent variables selected, explained variance of the process variables matrix and of weight variability response.*

	Vector Y [Weight variability]	**Matrix X**	**N° of LVs**	**Explained variance of X**	**Explained variance of Y**
Blend 1	40000 × 1	40000 × 18	3	99.5%	91.5%
Blend 2	56000 × 1	56000 × 18	3	91.7%	63.3%
Blend 3	64000 × 1	64000 × 18	3	76.8%	72.3%

The weight plots obtained by the PLS analysis are here shown, taking into account that only the most meaningful ones, explaining the majority of the variability for X and Y, are shown.

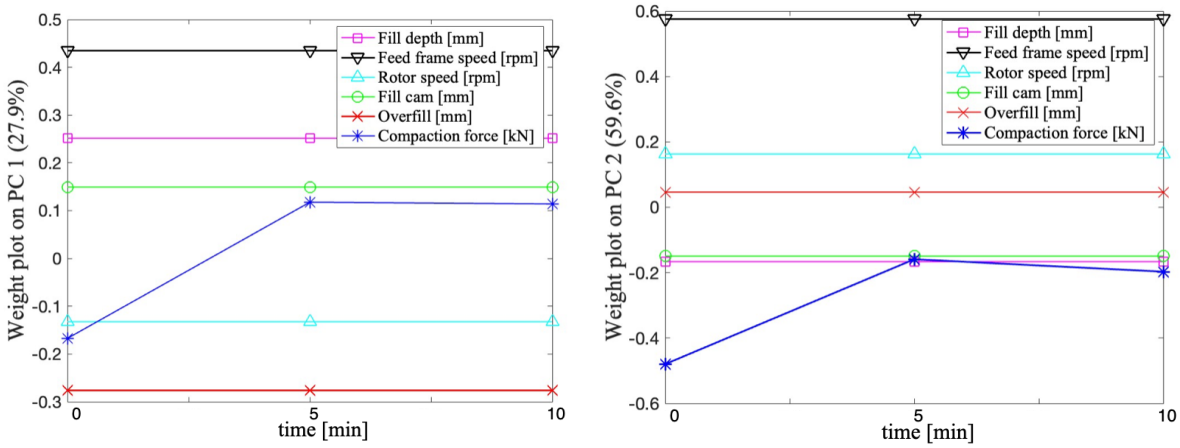

(a) (b)

Figure 4.25. *Weight plot for PLS analysis applied to Dataset 2 of (a) the first LV of blend 1 (explaining 76.9% variability of weight RSD) , (b) the second LV of blend 1 (explaining 6.5% variability of weight RSD).*

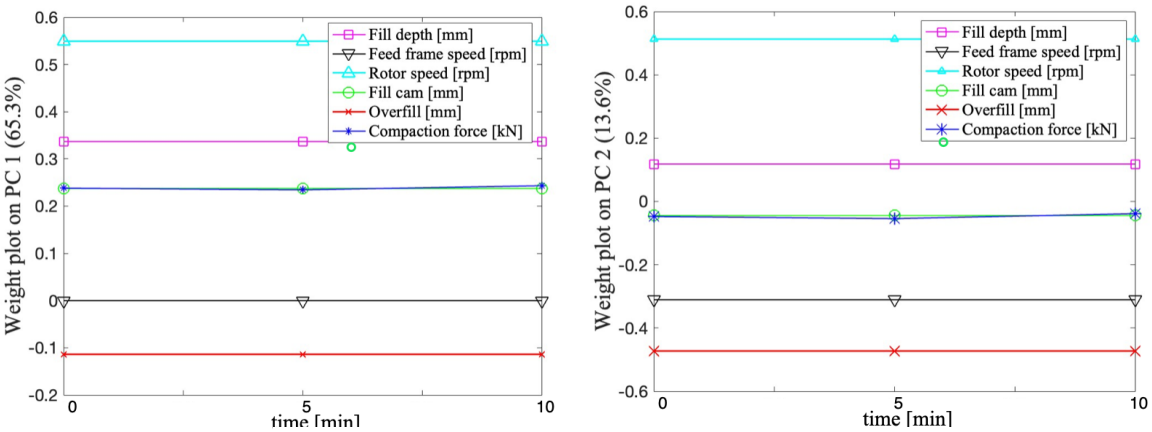

(a) (b)

Figure 4.26. *Weight plot for PLS analysis applied to Dataset 2 of (a) the first LV of blend 2 (explaining 19.3% variability of weight RSD) , (b) the second LV of blend 1 (explaining 39.6% variability of weight RSD).*

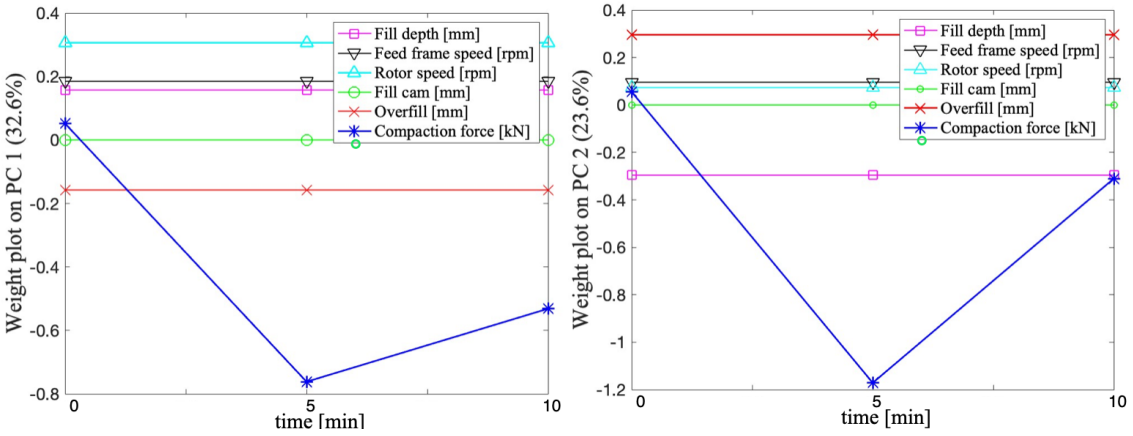

(a) (b)

Figure 4.27. *Weight plot for PLS analysis applied to Dataset 2 of (a) the first LV of blend 3 (explaining 39.5% variability of weight RSD) , (b) the second LV of blend 1 (explaining 22.7% variability of weight RSD).*

In this case, it can be derived by the weight plots that:

- in blend 1, an increase in feed frame speed cause an increase in weight variability, as explained by both the first and the second PCs of the PLS model (Fig.4.25(a) and (b)). So, working at 30 rpm instead of 45 rpm can be beneficial for replicability. Moreover, a decrease in overfill can lead to lower weight variability (Fig. 4.25(a)).
- In blend 2, an increase in rotor speed leads to an increase in weight variability (Fig. 4.26), while overfill decreases it. Since acting on overfill is difficult, modulating the rotor speed can be the main way to control also weight variability. Furthermore, for this particular blend decreasing feed frame speed is a way of increasing weight uniformity.
- In blend 3, greater weight variability results from lower compaction force (Fig.4.27). An increase in rotor speed (Fig.4.27(a)) cause an increase in weight variability, as well as greater overfill (Fig.4.27(b))., even if with less relevant contribution. For this blend, feed frame speed does not seem to have an impact on weight variability of the tablet replicates.

The main findings of this analysis are presented in Table 4.13, together with the most important results of the proposed study, with the aim of representing in a concise and effective way what was found to be characteristic of each blend:

Table 4.13. *Summarizing table reporting main findings about relationships between compression settings and tablets properties for blend 1, 2 and 3.*

	Blend 1	**Blend 2**	**Blend 3**
Weight-thickness-width-volume (values)	highly related, for given compression settings they increase or decrease together		
	greater than blend 3	greater than blend 3	smaller than blends 1-2
Compression force-hardness- TS (values)	highly related, for greater compression force also hardness and TS increase		
	smaller than blend 3	smaller than blend 3	greater than blends 1-2
Fill cam and fill depth	increase in weight		
	increase in replicates variability within a run (including weight RSD at 800mg)	/	/
Overfill	decrease in mean weight and weight variability		
Feed frame speed	Increase in weight and weight RSD *	Increase in weight and decrease in RSD	Increase in weight and not evident effect on weight RSD
	/	/	Increase in lubrication extent coefficient
Runs variability at constant feed frame speed	Poor control of compaction force on solid fraction	Strict control of compaction force on solid fraction	Not clear relationship between comp. force and solid fraction
Rotor speed (for weight)	decrease in mean weight and general increase in replicates variability within a run		
	/	increase weight RSD	increase weight RSD

* does not match knowledge from literature

4.4 Lubrication extent coefficient

Tablet formulations are typically lubricated by mixing the powder with a lubricant (in this case magnesium stearate) to improve manufacturability by reducing die-wall friction and powder adhesion to the metal components of the equipment. However, it is possible that the powder, because of overmixing (which causes excessive shear strain to be applied to the powder), reaches an over-lubrication state which damages the final tablets properties. By analyzing the compactor data available for blend 3, we want to assess whether the feed frame speed causes such an increase in lubrication.

4.4.1 Compression profiles comparison for rotary press and compactor simulator

Some powder samples, after being sheared from the feed frame in runs 2A, 3A and 5, are taken from the rotary press, are placed on the compactor simulator and compacted there, always at 6.5, 9.5, 13 and 16 kN compression force (for details, refer to §2.3) . As it can be seen from Lura et al. work (2021), the comparison among tablets properties, more specifically tensile strength vs solid fraction, is commonly used to assess the similarity between compression process followed in the rotary press and in the compactor simulator for equivalent processing conditions.

It follows that the compaction profiles obtained on the compactor simulator mimic well those of the rotary press for each feed frame speed considered (Fig. 4.28) and can therefore be used to study the over lubrication to which the compound is subjected during the real compaction process on the rotary press.

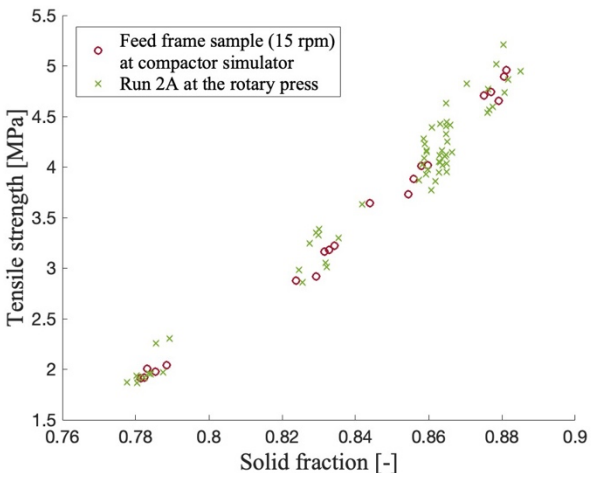

(a)

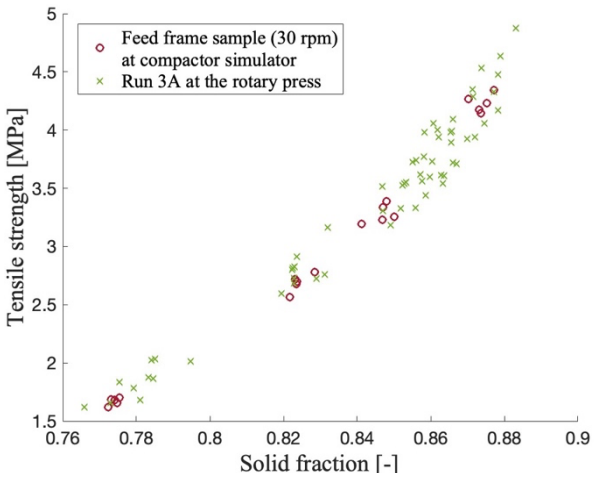

(b)

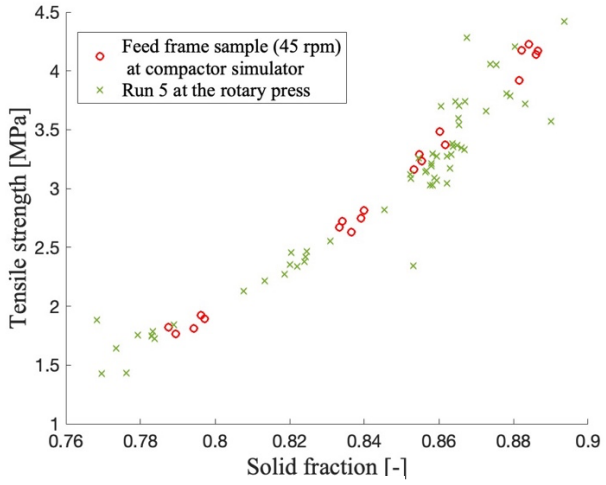

(c)

Figure 4.28. *Comparison between compression profile obtained at the rotary press and at the compactor simulator at (a) 15 rpm, (b) 30 rpm and (c) 45 rpm feed frame speed.*

4.4.2 Lubrication extent estimation for feed frame-subjected blends

Together with feed frame subjected samples, also new lubricated blends with known lubrication coefficient k are compressed at compactor simulator, obtaining the profiles reported in Fig.4.29.

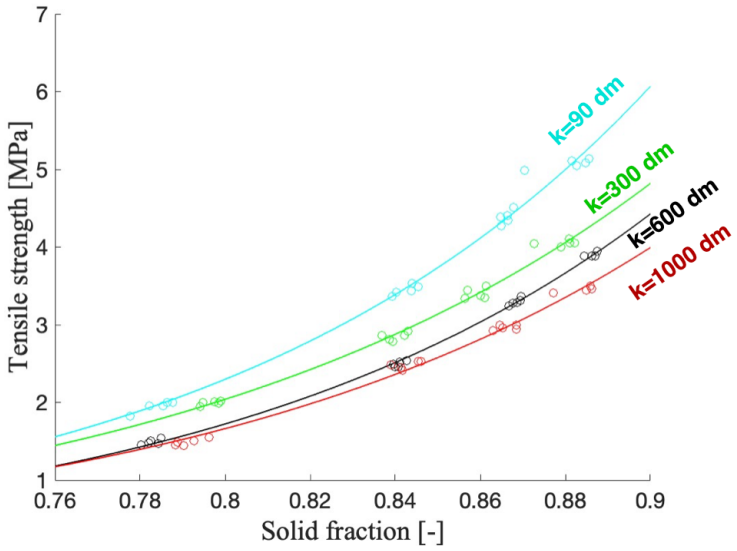

Figure 4.29. *New lubricated blends with known lubrication coefficient k (possible through blending time control) TS over solid fraction profiles after compression at the compactor simulator.*

In the above figure it can be seen that the tensile strength is lower for blends with a higher lubricating coefficient at parity of the solid fraction. This confirms what was reported in the studies of Kushner and Moore (2010), where it was found that the compactibility profiles of some powder blends based on MCC and MgSt are a decreasing function of the number of mixer

revolutions. The tensile strength over solid fraction profiles appear to be parametric to the lubrication coefficient, so that feed frame samples profiles can be projected over the new samples ones to have a qualitative description of the lubrication extent reached because of the feed frame presence. Note that the chosen fit of the experimental data is exponential, based on the knowledge of the Ryshkewitch (1953) equation relating tensile strength and solid fraction as:

$$TS = TS_0 \exp\left(b((1 - SF)\right) \tag{4.5}$$

The semi empirical model proposed by Kushner and Moore (2010) and extended by Blackwood et al. (2012) can provide an estimation of the initial lubrication extent of blend 3, before being subjected to the feed frame speed. Since the lubrication in this case is given only by the blending process, it is sufficient to calculate k_{bb} to know k:

$$k = k_{bb} = {V_b}^{1/3} \times F_{headspace} \times r \tag{4.6}$$

in which V is the bin volume, $F_{\text{headspace}}$ the fractional headspace in the bin and r the number of bin revolutions. Using the available data about the powder mass charged in the bin (m_{charged}), the bulk density of the blend formulation (ρ) and the blending time (t) and speed (s), it is possible to obtain:

$$k_{bb} = {V_b}^{1/3} \times \left(\frac{V - (m_{charged}/2) \div \rho}{V}\right) \times s \times t = 200\ \text{L}^{1/3} \times \left(\frac{200\ L - (100 kg/2) \div 0.439\ kg/L}{200\ L}\right) \times 17 rpm \times \frac{180}{60} = 128.75\ \text{dm}$$

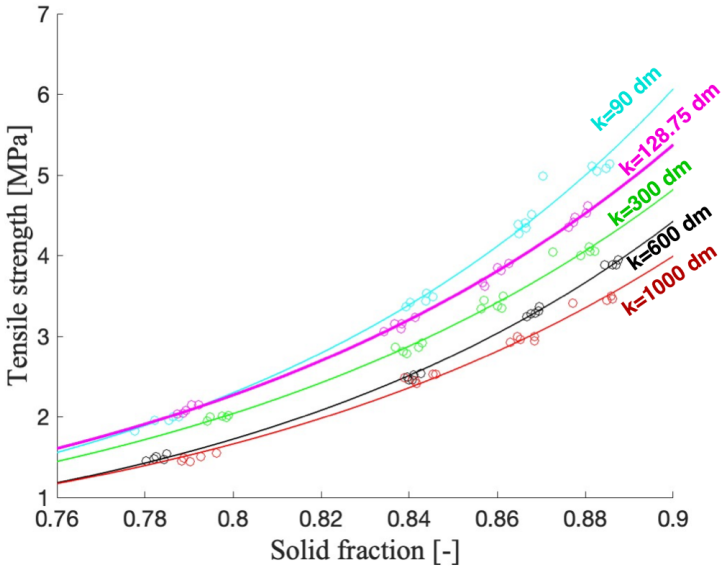

Figure 4.30 *Projection of tablets data obtained for compression of the original blend 3 (not subjected to feed frame) at the compactor simulator, together with the known-k samples ones.*

Projecting the data obtained for the original blend 3 onto the known-k samples ones (Fig. 4.30), it is confirmed that this approach is reliable to have an approximate estimate of the lubrication coefficient. The feed frame sample at 15 rpm is compressed at the simulator and its lubrication state is evaluated in Fig. 4.31(a). As the sample appears to have a lower degree of lubrication than the original, the prediction limits are found for both in order to estimate the uncertainty of the fitting used.

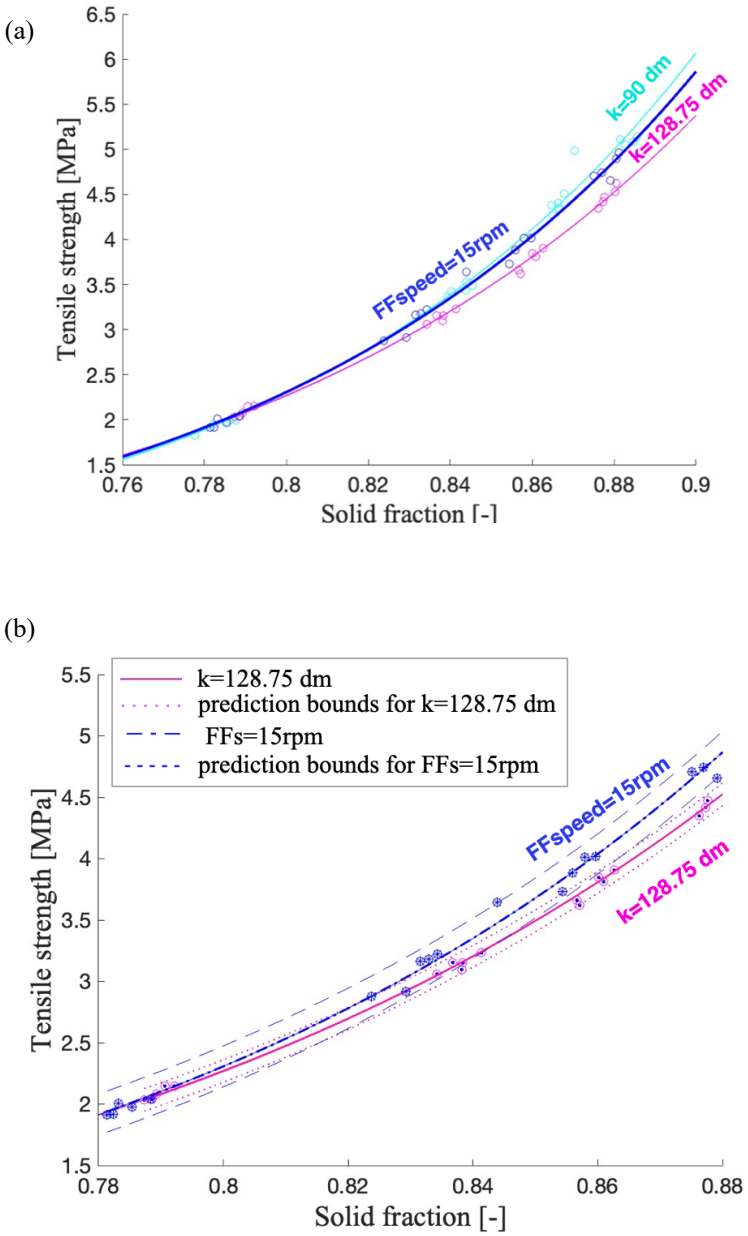

Figure 4.31. *(a) Comparison between tensile strength over solid fraction profile of feed frame sample at 15 rpm and original blend, adding in (b) the prediction bounds for both.*

The prediction bounds are found with the command *predobs* in Matlab, which is used to find the prediction intervals across the extrapolated fit range when function *fit* is employed to have a fitting of the experimental data. It can be seen in Figure 4.31(b) that the prediction boundaries of the two profiles overlap, so it can be concluded that the feed frame sample at 15 rpm behaves similarly to the original commercial mixture. Doing the same for the samples at 30 rpm and 45 rpm, it results that powder subjected to 30 rpm feed frame speed has a lubrication extent which is again similar to that of the original one, while the one at 45 rpm has a significant increase of it (Fig. 4.32(a) and Fig.4.32(b)). In fact, at 45 rpm, the lubrication extent is close to the 300 dm lubrication profile, meaning that the original k (128.75 dm) is more than doubled due to the effect of the high feed frame speed.

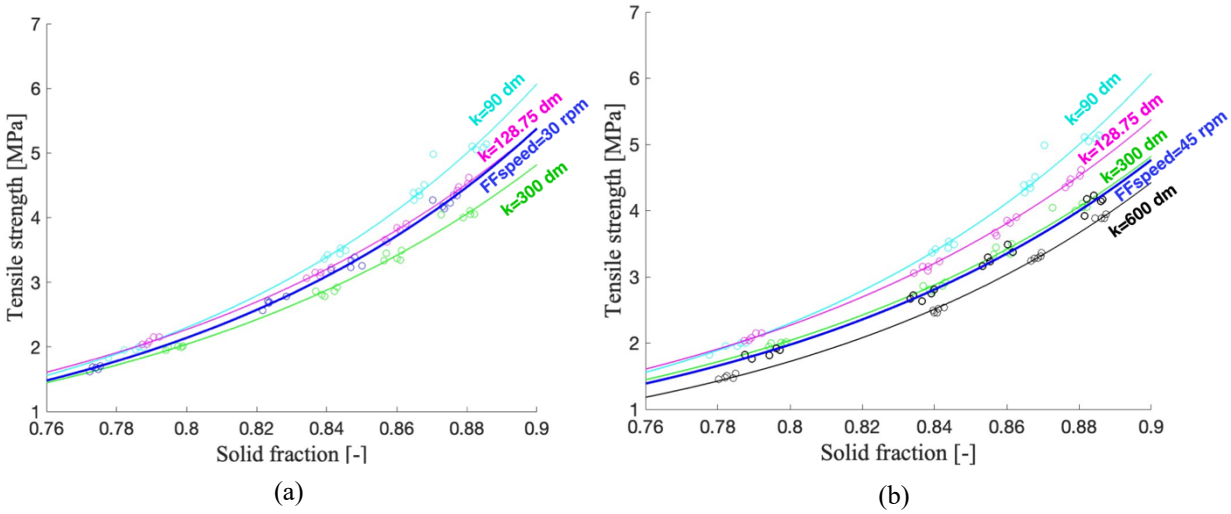

Figure 4.32 *Comparison between tensile strength over solid fraction profile of feed frame sample at (a) 30 rpm and original blend and (b) of sample at 45 rpm and original blend.*

The obtained results can be compared to the semi-empirical formula proposed by Blackwood (2012) to estimate the additional contribution given by the feed frame presence to the original lubrication state:

$$k_{ff} = v_{tip} \times \tau \tag{4.7}$$

where v_{tip} is the speed of the paddle wheel and τ the mean particle residence time in the feed frame. This contribution should be added to the blending lubrication (k_{bb}) one to have the total lubrication of the powder.

It must be noted that the results obtained in this study disagree with the semi-empirical model a priori, because the latter presumes that the powder, when subjected to the feed frame, always increases its lubrication state. Differently, here it is stated that only a feed frame speed of 45 rpm has an actual impact on the lubrication extent of the powder.

Calculating k_{ff} at 45 rpm for blend 3 using the semi-empirical model, it is obtained:

$$k_{ff} = \pi \times D_{FF} \times FF_s \times \frac{\rho_{blend} \times V_{FF}}{tablets/h \times w} = \pi \times 0.18m \times \frac{45\ rpm}{60\ s} \times \frac{0.439\ g/mL \times 0.945\ mL}{\frac{58000\ tablets/h}{3600\ s/h} \times 0.3\ g} \times 10\frac{dm}{m} =$$

=301.9 dm

which must be added to the initial k_{bb} to have the total k extent:

$$k = k_{bb} + k_{FF} = 128.75\ dm + 301.9\ dm = 430.65\ dm \quad (4.8)$$

The model seems to overestimate the lubrication contribution given by the feed frame also at the highest feed frame speed considered.

4.5 Shear cell flow data analysis

A flow function test and a wall friction test were performed on lubricated and feed frame samples of blends 1, 2 and 3 in order to evaluate their flow properties as original powders and after being subjected to certain feed frame speed. Data retrieved from the tests are employed for blends properties analysis and comparison, relating the main findings on the above mentioned shear cell flow data with the blends behavior in the rotary press.

4.5.1 Flow function test results

The ratio between the unconfined failure strength (σ_c) and the major principal stress (σ_1) for a given initial consolidation stress (I) is known to provide a flow function coefficient *ffc* which is indicative of the flowability of the powder for the specific I (§1.5.1). Taking into account all five initial consolidation stresses applied to the powder samples, it is possible to obtain a linear relationship between σ_c and σ_1, whose slope is an overall flow function value which can be used to compare the flowability state of the different lubricated blends (Fig. 4.33).

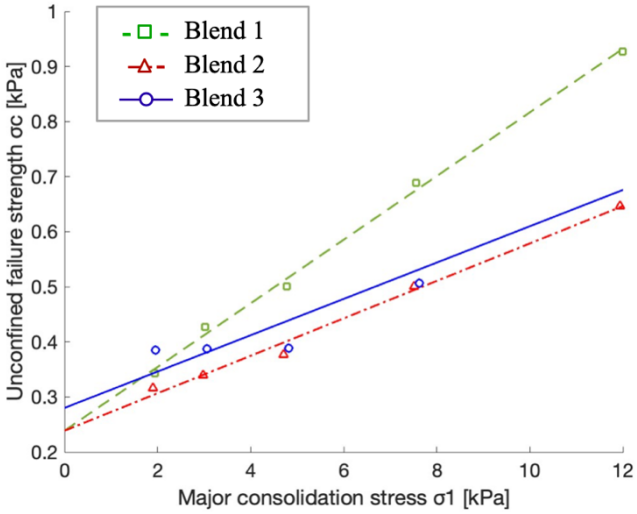

Figure 4.33 *Comparison between flow function values, given by the inverse of the slope of σ_c over σ_1, for the lubricated samples of blends 1, 2 and 3.*

When comparing the flowability values, it can be seen that blends 2 and 3 have similar flowability, while blend 1 is the least flowable of the blends (Table 4.17). In any case, it should be noted that a flow function value greater than 10 indicates a free-flowing powder behavior, and it is known by Koynov et al. studies (2015) that care should be taken in ranking materials within the free-flowing regime. For this reason, it can be concluded that all three blends have good flowability in their initial state. Considering also the powder samples subjected to the feed frame, it can be said that the presence of the feed frame does not modify the overall flowability of the blends, since the flowability values of these samples for blends 1, 2, 3 are similar to those of the lubricated blends (Table 4.14).

Table 4.14. *Details about linear fitting performed on the ratio of σ_c and σ_1 and correspondent flow function values for the lubricated and feed frame subjected powder samples of blends 1, 2 and 3*

	Linear fitting ax+*b*	R^2	Flow function value
Lubricated blend 1	0.058x+0.24	0.997	17
Lubricated blend 2	0.034x+0.24	0.991	29
Lubricated blend 3	0.033x+0.28	0.929	30
Feed frame sample blend 1	0.055x+0.25	0.992	18
Feed frame sample blend 2	0.036x+0.22	0.976	28
Feed frame sample blend 3	0.032x+0.19	0.997	31

A method proposed by Wang et al. (2016) to analyze shear cell data measured at different consolidation stresses consists in investigating the relationship between the flow function coefficient *ffc* and the cohesion τ_1 (kPa), showing that the two parameters have an intrinsic inverse correlation (power law with exponent -1). More specifically, it is proposed to refer to a dimensionless cohesion, calculated as:

$$C^* = \frac{\tau_1\,(kPa)}{I\,(kPa)} \tag{4.9}$$

This provides a classification of the flowability of different materials based on the dimensionless *C** which includes the effect of the initial consolidation stress applied.

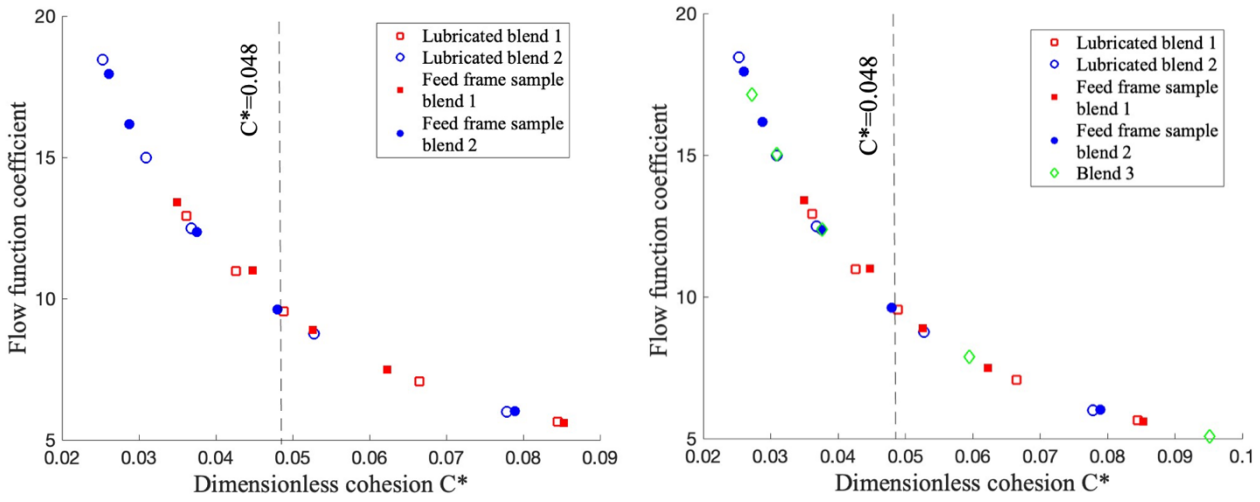

Figure 4.34 *Correlation between flow function coefficient and dimensionless cohesion for (a) blends 1 and 2 considered as lubricated or feed frame subjected samples, and (b) with addition of blend 3.*

According to the new classification, a $C^* \leq 0.048$ indicates a free-flowing powder, while for a $0.048 < C^* \leq 0.121$ the material can be considered easy-flowing (Wang, 2016). Comparing the behavior of blends 1 and 2 (Fig. 4.34(a)), it can be seen that blend 2 is a free-flowing powder for four of the five consolidation stresses applied and that the presence of the feed frame makes it more flowable, especially at 4.2 kPa. Blend 1, on the other hand, tends to have a more easy-flowing behavior and the sample subjected to the feed frame does not seem to have a better flowability than the lubricated one. For blend 3, the cohesion data available are the same for the lubricated and feed-frame exposed samples, so it is only possible to compare its overall flow behavior with the other blends. At the lower initial consolidation stress applied, its behavior is similar to that of blend 2, while at the highest consolidation level it is the least flowable of the three (Fig.4.34(b)). Blend 2 is confirmed to be the blend with the highest flowability, which is slightly improved by the presence of the feed frame. This is in agreement with the previous results, in which blend 2 was found to be a blend that can be subjected to any feed frame speed without experiencing a reduction in flowability, while maintaining high weight uniformity during tablet production.

4.5.2 Wall friction test results

The process of compaction of pharmaceutical powders and the resulting density of the tablet are mainly influenced by two major mechanisms: interparticle friction and die wall friction. For this reason, in addition to the flow function indices, descriptive of the first mentioned mechanism, wall friction test is fundamental to be considered for flowability definition in the

compression process, since it describes the friction between the powder under compaction and the die wall (Michrafi et al., 2003). In the study just mentioned, the behavior of the friction for different powders is evaluated by analyzing the friction coefficient profile over the density of the powder after compression in the die. Many indirect methods exist to calculate the friction coefficient, but it is known that, together with some geometric factors, it is mainly function of the shear stress applied during compaction. Based on this, the analysis of the bulk density profiles over shear stress applied to blend samples during the test can be sufficient to evaluate the friction behaviors of the blends (Fig.4.35).

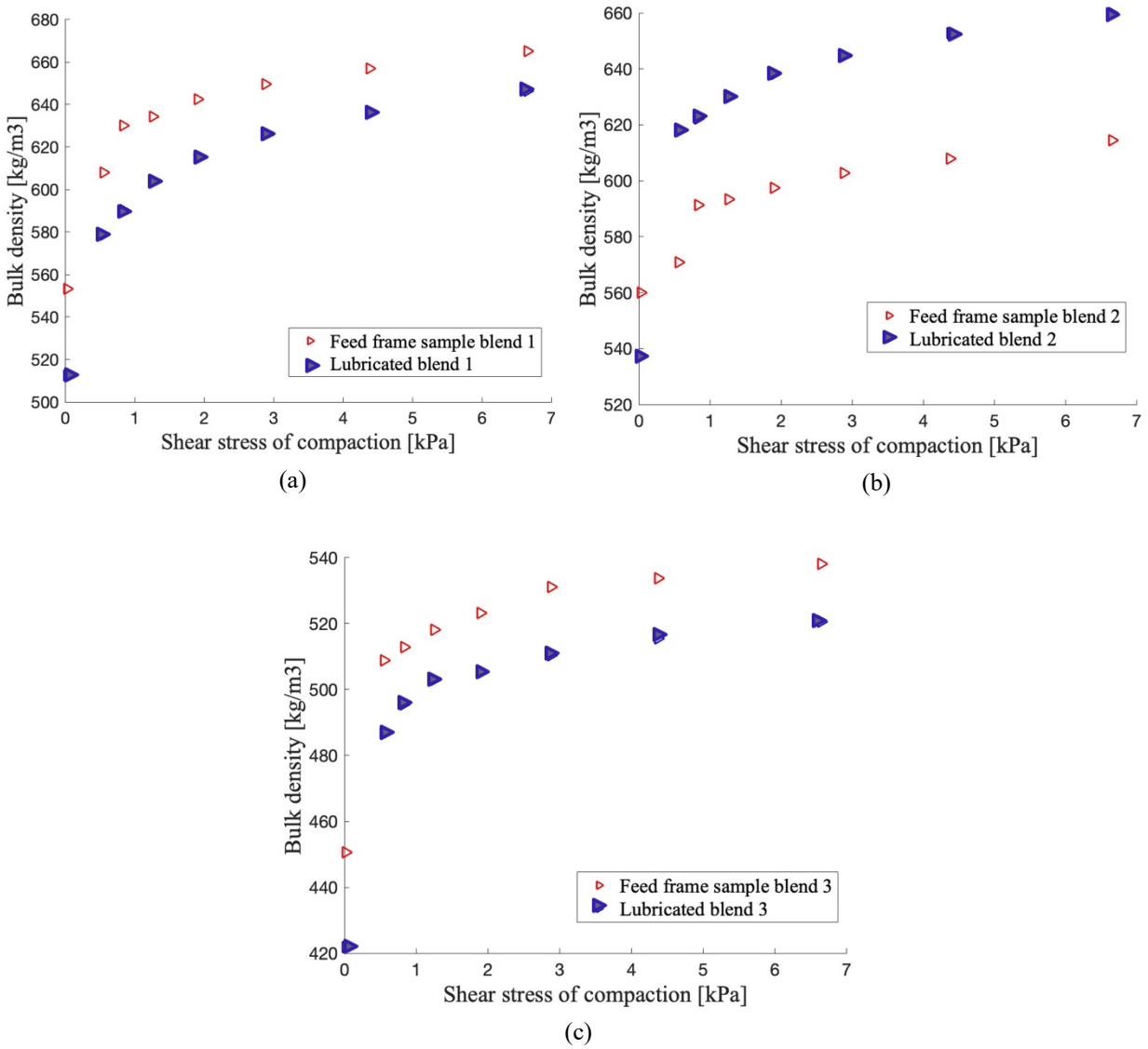

Figure 4.35 *Correlation between bulk density and shear stress of compaction for lubricated and feed frame subjected samples of (a) blend 1, (b) blend 2 and (c) blend 3.*

The density values at x=0 correspond to the freely settled bulk density of the powder ($\varrho_{B,x=0}$), before being subjected to any stress. It can then be seen that the density increases with

increasing shear stress until it reaches an approximately constant value. While the feed frame presence is causing an increase in powder densification for blend 1 and 3 with respect to the lubricated samples, blend 2 behaves in the opposite manner, decreasing the bulk density in the feed frame exposed samples for each shear stress of compaction applied and especially at the highest ones. A higher bulk density indicates that the powder is more densely packed and less prone to segregation during production processes such as compaction, but it can also result in increased wall friction which can cause flow problems such as flow stoppages and inconsistent discharge rates (Arnold et al., 2005). A further step is consequently made by using the freely settled bulk density of the powder ($\varrho_{B,x=0}$) and the maximum tapped bulk density (ϱ_T) recorded for each sample from the test to calculate the compressibility index, whose values have already been reported in §4.3.4. This index is representative of the propension of a powder to consolidate, and it is found as:

$$\mathrm{CI}(\%) = \frac{\varrho_T - \varrho_{B,x=0}}{\varrho_T} \times 100 \tag{4.10}$$

The CI values found for the studied samples confirm that blend 2 is definitely improved in flowability by the feed frame speed presence, assuming excellent flowability properties, while blend 1 and 3, although interested by an actual densification because of the feed frame, are not properly modifying their flowability features with respect to the lubricated original powder.

Conclusions

Three pharmaceutical powder blends have been subjected to the compaction process in the multi-station rotary press with the aim of investigating how compression settings affect final tablet characteristics. By performing a preliminary analysis on the available data, it resulted that two main groups of variables tend to change together for different compression settings applied. In particular, fill depth is mainly increasing weight, thickness, width and volume, while compression force affects hardness, tensile strength and solid fraction. It was also noted that variables are not changing their relationship in time, so no dynamic time dependence between data seems to be present at the typical manufacturing time scale. These considerations are valid for all three investigated blends. Focusing then on mean weight and weight variability, expressed in terms of relative standard deviation, it was demonstrated that they are differently affected by compression settings for different blends. Mean weight, even if increased by lower overfill in all blends, is greater for higher fill cam and fill depth for blend 1 and 3 and higher rotor speed for blend 2. Regarding weight variability, it is mainly increased by higher feed frame speed for blend 1, and higher rotor speed for blend 2 and 3. Regarding the latter, an increase of it can be observed also at lower compression force.

Among all the other compression settings, feed frame speed was found to be the major source of properties variability between tablets produced at the rotary press for all blends. Then, at a given feed frame speed, the main cause of variability between tablet replicates is due to wide changes in solid fraction, as shown by variations in compression force in time, in blend 1, and higher rotor speed in blend 3. This makes it more difficult to achieve adequate CQA in all tablets produced from these blends.

The results of this study only partially confirm the ability of the feed frame speed to decrease weight RSD found in the literature, as it only occurs for blend 2, while weight RSD increases with feed frame speed in blend 1. Together with the influence of feed frame speed on tablet properties, also its effect on the lubrication state of the powder is evaluated. A semi-empirical model proposed by Kushner and Moore (2010) and extended by Blackwood (2012) suggests that the presence of the feed frame always accompanies to an increase in the lubrication of the powder, progressively higher for higher feed frame speed. By using the compactor simulator data collected on blend 3, after ensuring that compactor simulator profiles were able to mimic well the rotary press ones, it was demonstrated that for the above mentioned blend the lubrication was not increased at 15 rpm and 30 rpm feed frame speed, while it was more than doubled with respect to the original blend one at 45 rpm. This means that the semi-empirical

model overestimates the effects of the feed frame speed on a powder blend, especially for lower feed frame speed values.

To conclude, the results of the flowability tests, carried out both on the free powder blend samples and on powder samples previously subjected to the action of the feed frame, indicate that all three blends have good flowability and that blend 2 is improved by the presence of the feed frame, resulting to be consequently the most flowable blend in the die filling stage. Since blend 2 was previously found to be the one characterized by the lower weight variability, it can be concluded that blends which are less affected by weight variability are also the most flowable ones, indicating that a relationship between powder properties and tablets quality exists and can be exploited to obtain tablets with increased properties uniformity. Table 4.13 summarizes the main findings of this study.

Table 4.13. *Summarizing table reporting main findings about relationships between compression settings and tablets properties for blend 1, 2 and 3.*

	Blend 1	**Blend 2**	**Blend 3**
Weight-thickness-width-volume	highly related, for given compression settings they increase or decrease together		
(absolute values)	greater than blend 3	greater than blend 3	smaller than blends 1-2
Compression force-hardness- TS	highly related, for greater compression force also hardness and TS increase		
(absolute values)	smaller than blend 3	smaller than blend 3	Greater than blends 1-2
Fill cam and fill depth	increase in weight		
	increase in replicates variability within a run (including weight RSD at 800mg)	/	/
Overfill	decrease in mean weight and weight variability		
Feed frame speed	Increase in weight and weight RSD *	Increase in weight and decrease in RSD	Increase in weight and not evident effect on weight RSD
	/	/	Increase in lubrication extent coefficient
Runs variability at constant feed frame speed	Poor control of compaction force on solid fraction	Strict control of compaction force on solid fraction	Not clear relationship between comp. force and solid fraction
Rotor speed	decrease in mean weight and general increase in replicates variability within a run		
(for weight)	/	increase weight RSD	increase weight RSD

* does not match knowledge from literature

Nomenclature

A_{r}	=	Archimedes number
C^{*}	=	dimensionless cohesion
D	=	tablet diameter
D_{FF}	=	feed frame diameter
d_{p}	=	powder particle diameter
$F_{\mathrm{headspace}}$	=	fractional headspace in the bin
I	=	initial consolidation stress applied during glow function test
k	=	overall lubrication extent coefficient
k_{bb}	=	lubrication coefficient due to blending
k_{ff}	=	lubrication coefficient due to feed frame
m	=	mass of powder in the die at given fill velocity
$m_{throughput}$	=	mass of tablets produced per unit time
m_s	=	mass of the tablet
M	=	mass of powder in a fully fill die
r	=	bin revolutions
R	=	roller radius
s	=	blending speed
t	=	blending time
TS_0	=	tensile strength at 0.85 solid fraction
V	=	die filling velocity
v_{c}	=	critical velocity
v_{tip}	=	tip speed of the feed frame paddle wheel
V	=	tablet volume
V_{b}	=	bin volume
w	=	expected tablet weight

Greek letters

δ	=	fill ratio
η	=	air viscosity
ξ	=	air sensitivity index
ρ_{blend}	=	bulk density of the blend formulation
ρ_{a}	=	air density

$\varrho_{B,x=0}$	=	settled bulk density of the powder sample in the wall friction test
ρ_s	=	solid true density
ρ_T	=	tapped bulk density of the powder sample in the wall friction test
σ_1	=	major principal stress
σ_c	=	unconfined failure strength
τ	=	mean particle residence time in the feed frame
ω	=	roller rotation rate

Acronyms

ANOVA	=	analysis of variance
API	=	active pharmaceutical ingredient
CI	=	compressibility index
CQA	=	critical quality attributes
DOE	=	design of experiment
FF_s	=	feed frame speed
ffc	=	flow function coefficient
LV	=	latent variable
MCC	=	microcrystalline cellulose
MgSt	=	magnesium stearate
PC	=	principal component
PCA	=	principal component analysis
PLS	=	projection on latent structures
RSD	=	relative standard deviation
PFT	=	powder flow tester
TS	=	tensile strength
SF	=	solid fraction

References

Abdi, H. (2007). Partial Least Squares (PLS) Regression. In: *Encyclopedia of Measurement and Statistics* (Neil Salkind, 1st Ed.), Thousand Oaks (CA).

Arnold, P.C., A.G. McLean and A.W. Roberts (1978). *Bulk Solids: Storage, Flow, and Handling* (Tunra, Ed.), Newcastle (N.S.W.), 145-160.

Baserinia, R., I.C. Sinka (2019). Powder die filling under gravity and suction fill mechanisms. *Int. J. Pharm.*, **563**, 135–155.

Beccaro, L. (2023). Accelerating pharmaceutical tablet development by transfer of compaction equipment across types and scales. *Master Thesis*, University of Padova (Italy).

Blackwood, D.O., B. MacDonald, J. Kushner IV, B. Hancock, A. Liu and K. Muteki (2012). Powder Lubrication In A Continuous Mixing Process. Presented at: *AIChE Annual Meeting Pittsburgh* 2012 (PA).

Brereton, R.G. (2018). ANOVA tables and statistical significance of models. *Journal of Chemometrics,* **33**:e3019.

Chai, Y., Yang, H., L. Zhao (2013). Data unfolding PCA modelling and monitoring of multiphase batch processes. *IFAC Proc. Vol.*, **46**, 569–574.

Dunn, K. (2023). Least Squares Modelling review. Chapter 6 in: *Process improvement using data,* 375-391.

Facco, P. (2024). Projection on Latent Structures (PLS). In: *Machine learning for process engineering* course, Industrial engineering department, University of Padova.

Geladi, P. and B.R. Kowalski (1986). Partial least-squares regression: a tutorial. *Analytica Chimica Acta*, **185**, 1-17.

Ghallager, B.N. and J.M. Shaver (2015). Introduction to Preprocessing Calibration and Application. *Eigenvector White Papers,* Manson (WA).

Hanson, A. Bryan and D.T. Harvey (2022). Learn PCA: Functions, Data Sets and Vignettes to Aid in Learning Principal Components Analysis (PCA). In: *Principal Component Analysis*. (Springer, 2nd Ed.), New York (USA).

Ketterhagen, W.R. (2015). Simulation of powder flow in a lab-scale tablet press feed frame: Effects of design and operating parameters on measures of tablet quality. *Powder Technol.*, **275**, 361-374.

Koynov, S., B, Glasser and F.J. Muzzio (2015). Comparison of three rotational shear cell testers. Powder flowability and bulk density. *Powder Technol*., **283**, 103-112**.**

Kushner, J. and F. Moore (2010). Scale-up model describing the impact of lubrication on tablet tensile strength, *Int. J. Pharm.*, **399**, 19–30.

Leung, L.Y., C. Mao, I. Srivastava, P. Du and C. Yang (2017). Flow Function of Pharmaceutical Powders Is Predominantly Governed by Cohesion, Not by Friction Coefficients. *J. of Pharm. Sciences*, **106**, 1865-1873.

Lura, A., V. Elezaj, M. Kokott, B. Fischer and J. Breitkreutz (2021). Transfer and scale-up of the manufacturing of orodispersible mini-tablets from a compaction simulator to an industrial rotary tablet press. *Int. J. Pharm.,* **602**(49):120636.

Mahto,L., Tarun De, J.Chakraborty, J. Kumar, A. Tripathi, M. Sen, and W. Ketterhagen (2024). Accelerated DEM simulation of the hopper-screw feeder and tablet-press feeder using the multi-level coarse-graining technique. *Powder Technol*., **436**, 199466.

Manokaran, M., M. Morgeneyer and D. Weis (2024). Effect of Microscopic Properties on Flow Behavior of Industrial Cohesive Powder**.** *Powders*, **3**, 324-337.

Mardia, K.V., , J.T. Kent and J.M. Bibby (1979). *Multivariate analysis*. (Academic Press, 1st Ed.), London, U.K., 224-225.

Mendez, R., F. Muzzio and C. Velazquez (2010). Study of the effects of feed frames on powder blend properties during the filling of tablet press dies. *Powder Technol.,* **200**, 105–116.

Mendez, R., F.J. Muzzio and C. Velazquez (2012). Powder hydrophobicity and flow properties: effect of feed frame design and operating parameters, *AIChE J*., **58**, 697–706.

Michrafy, A., M. S. Kadiri and J. A. Dodds (2003). Wall friction and its effect on the density distribution in the compaction of pharmaceutical excipients. *Trans IChemE*, **81**, Part A.

Mills, L.A. and I.C. Sinka (2013). Effect of particle size and density on the die fill of powders. *European Journal of Pharmaceutics and Biopharmaceutics,* **84**, 642-652.

Ohage, E., R. Iverson , L. Krummen, R. Taticek and M. Vega (2016). QbD implementation and Post Approval Lifecycle Management (PALM). *National Library of Medicine,* **44** (5), 332-340.

Özkal, S.G., M.E. Yener and L. Bayindirli (2005). Response surfaces of apricot kernel oil yield in supercritical carbon dioxide. *LWT (Lebensm.-Wiss. & Technol.),* **38** (6), 611–616.

Pellett, J. D. and G. Dalziel (2018). Accelerated Predictive Stability (APS) Applications: Packaging Strategies for Controlling Dissolution Performance. *Accelerated Predictive Stability: Fundamentals and Pharmaceutical Industry Practices*, 383-401.

Pitt, K.G. and M.G. Heasley (2013). Determination of the tensile strength of elongated tablets. *Powder Technol.,* **238**, 169-175.

Raymond, H.M. and D.C. Montgomery (2016). *Response Surface Methodology: Process and Product Optimization Using Designed Experiment*, (Wiley, 3rd Ed.), San Francisco (USA), 369-371.

Ryshkewitch, E. (1953). Compression strength of porous sintered alumina and zirconia. *J. Am. Ceram. Soc*., **36**, 65–68.

Santos, D.P., M.M. Sena, M.R. Almeida, I.O. Mazali, A. C. Olivieri and E. L. Villa (2013). Unraveling surface-enhanced Raman spectroscopy results through chemometrics and

machine learning: principles, progress, and trends**.** *Analytical and Bioanalytical Chemistry***, 415**(18), 3945-3966.

Schulze D. (2021). Flow Properties of Powders and Bulk Solids**.** In: *Powders and Bulk Solids – Behavior, Characterization, Storage and Flow*, (Springer, Ed.).

Shipar M.A.H., A- Wadhwa, C. Varughese, N. Kaur and N. Thayaparan (2014). Effect of particle size on weight and hardness variation. *Toronto Institute of Pharmaceutical Technology* 2013-2014.

Sierra-Vega, O., R.J. Romanach and R. Mendez (2019). Feed frame: The last processing step before the tablet compaction in T pharmaceutical manufacturing *Int. J. Pharm.*, **572,** 118728.

Smalheiser, N.D. (2017). Anova. *Part A: Designing your experiment*. In: *Data Literacy* (Academic Press, Ed.), 149-155.

Stranzinger, S., D. Mark, J.G. Khinast and A. Paudel (2021). Review of sensing technologies for measuring powder density variations during pharmaceutical solid dosage form manufacturing. *TrAC Trends in Analytical Chemistry,* **135**, Article 116147.

Tomba, E., M. De Martin, P. Facco, J. Robertson, S. Zomer, F. Bezzo and M. Barolo (2013). General procedure to aid the development of continuous pharmaceutical processes using multivariate statistical modeling – An industrial case study. *Int. J. Pharm.,* **444**, 25-39.

Valle, S., Li, W. and S.J. Qin (1999). Selection of the number of principal components: the variance of the reconstruction error criterion with a comparison to other methods. *Ind. Eng. Chem. Res.,* **38**, 4389–4401.

Vamathevan, J.,D.Clarck, P. Czodrowski, I. Dunham, E. Ferran, G. Lee, B.Li, A. Madabhushi, P.Shah, M. Spitzer and S. Zhao (2019). Applications of machine learning in drug discovery and development. *Nat. Rev. Drug Discov.,***18**, 463-477.

Wang, J., H. Wen and D. Desai (2010). Lubrication in tablet formulations. *Eur. J. Pharm. Biopharm*., **75**, 1–15.

Wang, Y., S. Koynov, B.J. Glasser and Fernando J. Muzzio (2016). A method to analyze shear cell data of powders measured under different initial consolidation stresses. *Powder Technol.,* **294**, 105–112.

Wise, B.M. and N.B. Gallagher (1996). Development and benchmarking of multivariate statistical process control tools for a semiconductor etch process: improving robustness through model updating. *IFAC Proc. Vol.*, **30**(9), 79-84.

Wu, C.Y, L. Dihoru and A. Cocks (2003). The flow of powder into simple and stepped dies. *Powder Technol.,* **134**, 24-39.

Yu, S. (2013). Roll compaction of pharmaceutical excipients. *PhD Thesis*, University of Birmingham.

Zakhvatayeva, A., Zhong, W., Makroo , H.A. , Hare, C. and Wu C.Y. (2018). An experimental study of die filling of pharmaceutical powders using a rotary die filling system. *Int. J. Pharm.,* **553***,* 84-96.

Zinchuk, A. V, Mullarney, M.P. and B.C. Hancock (2004). Simulation of roller compaction using a laboratory scale compaction simulator. *Int. J. Pharm*., **269**(2), 403–415.

Web sites

https://dfepharma.com (last accessed: 02/09/2024)
https://www.researchgate.net (last accessed: 10/09/2024)
https://www.fette-compacting.com (last accessed: 30/08/2024)
https://www.korsch.com (last accessed: 24/08/2024)
https://tabletingtechnology.com (last accessed: 03/09/2024)
https://store.brookfieldengineering.com (last accessed: 20/08/2024)
https://learnche.org (last accessed: 15/09/2024)
https://online.stat.psu.edu (last accessed: 23/08/2024)
https://jaeronline.com (last accessed: 30/08/2024)
https://www.ipharmachine.com (last accessed: 02/09/2024)
https://powderprocess.net (last accessed: 02/09/2024)